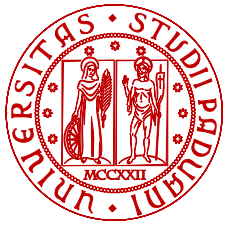

UNIVERSITÀ
DEGLI STUDI
DI PADOVA

UNIVERSITÀ DEGLI STUDI DI PADOVA

DIPARTIMENTO DI INGEGNERIA INDUSTRIALE

SCUOLA DI DOTTORATO DI RICERCA IN INGEGNERIA INDUSTRIALE
INDIRIZZO IN PROGETTAZIONE E DINAMICA DEI SISTEMI MECCANICI
CICLO XXVI

Design and development of the MotoMacchina vehicle

Direttore della Scuola:
CH.MO PROF. PAOLO COLOMBO .....

Coordinatore d'Indirizzo:
CH.MO PROF. ALBERTO DORIA .....

Supervisore:
CH.MO PROF. VITTORE COSSALTER .....

Dottorando: MASSIMILIANO CANERI

.....

Abstract

Abstract

This work concerns the design and development of a tilting four-wheeled vehicle. The peculiarities of this prototype required, first, the adoption of a fast, simple, trial and error based approach to develop case knowledge and find out possible design problems. Then, a more methodical numerical-based approach was used to find performing solutions to the very particular issues. Specific multibody models of roll, steer and suspension subsystems were self-constructed ad used in numerical optimizations. In all cases, satisfying results were achieved. In addition, the constructive design and fabrication of main subsystems were performed.

Sommario

Il presente lavoro è finalizzato alla progettazione ed allo sviluppo di un veicolo a quattro ruote rollanti. Le peculiarità del prototipo hanno richiesto, dapprima, l'utilizzo di un semplice e veloce approccio di tipo empirico, finalizzato ad accrescere la conoscenza dello specifico caso progettuale ed evidenziare possibili problemi nella fase di design. In un secondo momento, è stato usato un approccio maggiormente metodico e basato su metodi numerici, al fine di individuare soluzioni profittevoli agli specifici problemi del caso di studio. Modelli multibody specifici degli apparati di rollio, sterzo e sospensioni sono stati autocostruiti ed utilizzati nelle ottimizzazioni numeriche. In tutti i casi trattati, sono stati raggiunti risultati soddisfacenti. Infine, sono state effettuate la progettazione costruttiva e la realizzazione dei principali sottoassiemi.

Contents

Introduction

INTRODUCTION

Aim of this work

In the last few years tilting three-wheeled vehicles were proposed by major motorcycles constructors and, generally, this kind of vehicles proved to be very attractive both by a technical and a commercial point of view. The Motorcycle Dynamics Research Group (”MDRG”) of University of Padova was involved in the design and production of several prototypes of these vehicles, too. Aim of this work is to extend the frontier, in terms of knowledge and methodology, to the design of an innovative tilting four-wheeled vehicle: in particular, it is different from many other products and prototypes, because of its general layout and its driving system. In fact, its shape and dimensions are more similar to those of a small race car, rather than of a motorcycle, as common to other tilting vehicles. Moreover, it can be driven by a fully separated use of the steering and the roll systems, allowing for a completely new and unexplored driving experience. According to its particular specifications, this project required the solution of some peculiar problems, which are not fully covered by literature or common knowledge. Therefore, a series of different strategies were studied to find a solution which could satisfy the specific requirements. The dynamic behaviour, a summary of which will be presented in this work, was studied by the MDRG by using the Optimal Maneuver Method coupled by a simplified multibody model of the vehicle. This represented the first input to the design phase. One of first problems to overcome was the mutual interdependency between subsystems, which affects both the constructive and the kinematic/dynamic aspects: as a result, it was necessary to spend a great effort in the design phase, to grant a feasible and proficient overall layout and to conceive some efficient solutions to functional problems. Particular attention was dedicated to the steering and roll systems, with the aim to make this prototype not only working, but good enough to represent a first step toward a good-handling tilting four-wheeled vehicle. The study of kinematics of these subsystems was made step by step by progressively increasing the capability of the applied methodologies, until a satisfying result was obtained. In detail, a preliminary, empirical and trial and error based approach typically revealed the need of more systematic methodologies, made possible only by the self construction of fully dedicated models. Therefore, several kinematic synthesis and optimization were performed: even if such an approach could be considered too advanced for the purposes of a prototype design, it proved to be absolutely necessary to overcome some problems and allowed for the right interpretation of some aspects. Construction problems were analyzed and solved, too: main subsystems were designed and then constructed with the support of the departmental manufacturing facility and some sponsors.

Methods

The methods used during the design phase which this work is related to, were chosen and updated in consideration of the following inputs:

1. type of target
2. knowledge acquired during the development of the specific task
3. level of detail

The targets can be distinguished in:

- kinematic synthesis and optimization
- geometrical modelling (part and assembly)
- structural validation/refinement
- production of components

Particular attention was dedicated to the synthesis of mechanisms, with the target of profiting of dynamical behaviour of four-tilting wheels: information acquired by means of multibody modelling and the Optimal Maneuver Method were translated in kinematic requirements for the mechanisms to be sinthesized. An extensive study was conducted to improve the knowledge of dedicated steering, roll and suspension subsystems, and design them to fulfill all desired requirements. Such a target can be pursued by means of a kinematic modelling, which can be implemented in different CAE environments, each one granting a different methodology and flexibility. These different approaches highlighted, during the different phases of design, which aspects could be profitably solved, and which ones needed an improvement on modelling to be better analyzed. Generally, the first phase was treated in an integrated, user friendly multibody environment like LMS Virtual.Lab, allowing to fast develop a try-error approach based on common knowledge. During this step, it was possible to point out some weaknesses of starting solutions and some difficulties on their improvement without a deeper investigation, possible only by increasing the flexibility of the model used. Therefore, the first step was generally fundamental to increase the knowledge of the analyzed problem (point 2), so updating system requirements, and to redefine the level of detail (point 3) of model, necessary to definitely fulfill the updated requirements during the second step. This one was generally carried out by creating an analytical/numerical model specifically dedicated to the problem to solve, implemented in a flexible environment (Maple/Matlab) so that it could be easily addressed by an optimization algorithm, used both for analysis/comparison purposes and to obtain a profitable solution.

With regard to geometrical definition, structural validation/refinement and manufacturing targets, the main topics can be distinguished in:

- choosing an environment which allows for a flexible, parametric approach and management of several different and modular versions/configurations, and for a fast and easy re-use of geometrical models for Finite Element Analyses needed for structural validation
- performing a functional and manufacturing oriented geometrical design of assembly/components
- integrating third party components into assembly

- addressing the production of components

The chosen environment is Dassault Systèmes Catia V5, due to the following reasons:

- possibility of a high-level parametrization of model variables
- capability of a high-level associativity between different inputs/outputs
- capability of management of large assemblies
- integration of a F.E.M. module
- full integration with the geometrical model of LMS Virtual.Lab (used during the first step of kinematic synthesis)

Generally, the geometrical definition of single components was carried out in an assembly environment, i.e. each part was modelled by taking previously designed parts as a reference for the new ones: this approach allowed for automatic re-instantiation and update of new parts in case of update of the previous ones, resulting in a faster and more reliable revision process. The parts were generally modelled according to the following criteria:

- kinematic compliance
- manufacturing constraints
- structural compliance
- lightness

In detail, several manufacturing constraints resulted from the effective availability of technologies present in the departmental facility, and from the purpose of fulfilling strict financial requirements, so reducing third party production to be as limited as possible. In addition, during the assembly integration phase, it was necessary to benefit of the effective geometry of used third party components: in these cases, the reverse engineering (point cloud acquisition and post-processing) of them was carried out, by means of a ball probe/laser scanner measuring arm.

The production of components was carried out by:

- producing drawings of parts
- designing fixing supporting parts specifically dedicated to the assembly of parts/components
- supervising the assembly phase
- structural validation/refinement by means of F.E.M.
- reverse engineering of third party components, post processing and assembly integration

Finally, all used methods can be resumed as follows:

- multibody dynamic/kinematic modelling both in CAD-integrated/numeric computational software environments
- kinematic optimization

- parametric geometric design
- structural validation/refinement by means of F.E.M.
- reverse engineering of third party components, post processing and assembly integration

CHAPTER 1

The MotoMacchina Project

Aim of the MotoMacchina Project is to design and produce a vehicle that combines some aspects typical of motorcycles together with some peculiarities of four-wheeled vehicles. By introducing the capability of changing wheel camber angles, a motorcycle-like driving style can be adopted, trying to put car driving safety together with motorcycle riding fun and directional precision. In addition, the rolling chassis can provide a completely new feeling to the pilot. The reduction in the area of contact patch can lead to improvements in fuel efficiency, too.

Such a project represents a great challenge for the *Motorcycle Dynamics Research Group* of the University of Padova: first, the innovative driving system and the peculiar shape and dimensions make this prototype different from other tilting vehicles, requiring the development of fully dedicated solutions; second, the lack of consolidated design guidelines and of a dedicated technical literature force to construct a specific methodology to be adopted in the synthesis process; third, this project must undergo some quite strict technical and financial restrictions: the supporting fund only covers a third of the planned budget, so sponsor attendance is absolutely necessary. In addition, to limit costs, many components must be produced in the departmental facility: this fact limits, in some cases, the choice of the technology to be adopted, and cause a rise in lead times.

This work deals with the design and development of the first prototype. The preliminary design was made in cooperation with some Master Degree students, producing a proposal for main subsystems, first layout and the design of the chassis. A second step, performed by the author, focus on improvements in solution feasibility and functionality: a methodical approach is adopted, with the aim of developing both knowledge and performances of final solutions; in addition, the construction of main subsystems (chassis, roll system/suspensions, steer system and transmission) is performed with the methodologies cited in the introduction and by supervising the production of custom components.

1.1 The preliminary design

The main target of this design stage is to define the concept of the whole vehicle and then to traduce it in a first overall proposal.

According to a functional design approach, the first input to be considered is the set of main targets to be achieved: to design and produce a tilting four-wheeled vehicle capable of:

- proposing a completely new drive style, similar to motorcycle riding;
- profiting of dynamical advantages of motorcycles over conventional cars.

These main targets must be translated in a set of more defined requirements, concerning both the drive system and the mechanical concept, which are mutually related. In this case, they are pointed out as follows:

1. the driver should be able of separately controlling steer and roll angles, allowing for a drive strategy similar to motorcycles;
2. the chassis should roll towards the inner side of curves during cornering maneuvers, so recalling motorcycle riding feeling;
3. dynamical aspects must be studied with the aim of pointing out design guidelines more precisely.

Finally, some technical targets can be traced to address the conceptual and preliminary design phase:

(a) a drive system must be conceptually defined, to grant the fulfillment of requirement 1;

(b) a preliminary proposal of roll and steer systems must be pointed out; in particular, the roll system should satisfy requirement 2

(c) a first assembly layout must be defined, capable of housing, among others, the peculiar roll subsystem

(d) a dynamical modelling of the vehicle must be constructed, to trace design guidelines like required in 3.

The fulfillment of all of these technical targets requires the adoption of a wide range of specifically chosen methodologies. In addition, this phase is typically characterized by a lack in the knowledge of specific problems and interaction between subsystems. Therefore, a concurrent approach in the analysis and preliminary solution of problems should be used, aiming at highlighting any feasibility issue and improving the knowledge of any peculiar aspects.

According to these considerations, the preliminary design phase is performed with a diversified, concurrently adopted set of methodologies, in particular:

- geometrical design by CAD softwares, used in the preliminary definition of the overall layout and main subsystems;
- preliminary multibody modelling by means of commercial general purpose softwares, to define a first kinematic layout of the roll system;

- dynamical multibody modelling, by constructing a fully dedicated model implemented in a computational code, with the purpose of producing specific dynamical simulations and highlight general peculiarities of a test vehicle similar to the one to be designed (see 2.

As a result, a preliminary overall layout and a first technical and geometrical definition of subsystems is performed. Next paragraphs describe the main features of this first proposal, with regards to: drive system, roll system and general concept and layout.

1.1.1 Drive system

As cited, the drive system must grant to the pilot the possibility of separately actuate steer an roll movements. Since layout and weights will be typical of a small race car, the roll actuation can not be performed by simple pilot movements, and a dedicated subsystem must be adopted and controlled. Therefore, one additional command is necessary, with respect to conventional cars. In particular, it should be chosen to give to driver a feedback as fast and intuitive as possible on roll position, so granting the capability of perform fast roll maneuvers and trajectory corrections. A functional approach inspired the following solution:

- The roll movement is commanded by two pedals fixed together, capable of rotating with respect to the cockpit. A pressure on the right pedal (and the contemporary release of the left one) should induce a roll movement towards left, and vice versa.
- Throttle, brakes and friction, consequently, cannot be controlled by pedals. Therefore, the first two are integrated in a handle bar: steer, throttle and braking are so commanded like in common motorcycles, with the only exception that both levers are dedicated to brake control (front and rear wheels).
- Due to the high number of defined controls, it is chosen to adopt automatic gear shifting.

1.1.2 Roll system

The definition of this subsystem requires to study a completely dedicated solution, due to the peculiarity of this application: no guidelines are available in literature or similar implementations, therefore a synthesis methodology must be defined. At this stage, the identification of possible solutions is performed by a trial and error approach, based on kinematic analyses performed by using a commercial 2-D multibody software. The main requirement considered during this phase consists in pointing out a solution which can grant the contemporary roll movement of wheels and chassis in the same direction. Two possible solutions are identified: both feature a "roll slide" which can laterally translate with respect to the chassis, so inducing a displacement in suspension links. One solution is based on a conventional four-bar layout, the other one on an innovative six-bar linkage mechanism. Fig. 1.1 represents the layout of the latter one. A complete description of examined solutions, as well as details regarding the synthesis process, are reported in Chapter 3.

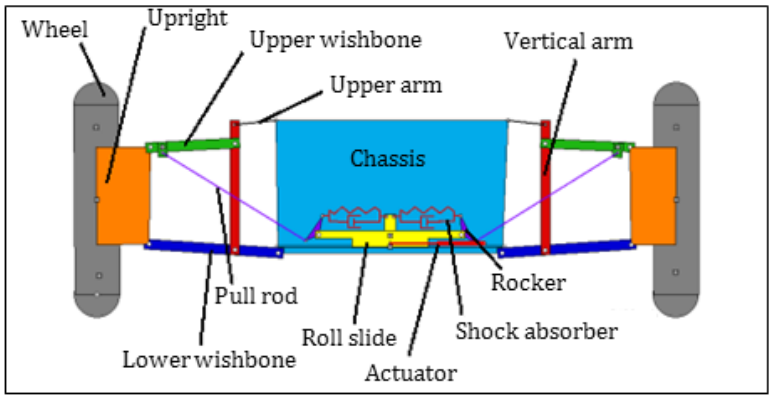

Figure 1.1: Example of roll system layout

1.1.3 General concept and layout

The general layout is inspired by the adoption of common race car proportions, together with more specific aspects, related to subsystem positioning and ergonomics. In particular:

- height of center of gravity must be contained;
- engine is positioned behind seat, to preserve a typical race car weight distribution;
- some volumes inside the chassis must be dedicated to roll system, without affecting ergonomics;
- the general layout must grant easy assembly/disassembly operations, which could be frequent due to set-up and tuning process;
- interfaces with suspension links should be rigid to grant a precise actuation of roll movements.

Especially in innovative design, tool flexibility can represent a real advantage in terms of time and results: for this reason, the parametrization of geometrical layout was studied to allow for an easy and fast modification of general component positioning and generation of different alternative solutions. Therefore, the starting geometry consists in a parametric symbolic skeleton (Fig. 1.3) to be used as a reference for components positioning and volume calculations. This approach revealed to be fundamental in iteratively setting general chassis measures and composition. In particular, Fig. 1.3 highlights the rational segmented subdivision of the chassis: the above cited roll slides are located in two volumes between two couples of plates, which provide the required stiffness to zones close to suspensions. In addition, the front roll slide is positioned in order not to limit the room dedicated to the pilot. The engine resides in the central zone. A first proposal for mechanical components was formulated taking this model as a basis: the result, based on the innovative six-bar linkage roll system, is presented in Fig. 1.4 Even if such a high detail seems to be excessive if compared with the limited knowledge of the particular dynamical aspects of this car, the concurrent approach proved to be useful in highlighting some drawbacks of the concept. In particular, even if based on a preliminary kinematic analysis performed on the roll system, the steering system has not yet been analyzed at this stage: in this first proposal, an hydraulic actuation is hypothesized both for steer and roll systems. This option revealed to be poor with regards to steer actuation: hydraulic steer systems are not commonly used in fast vehicle, since they are designed for slow maneuvers; additionally, they cannot

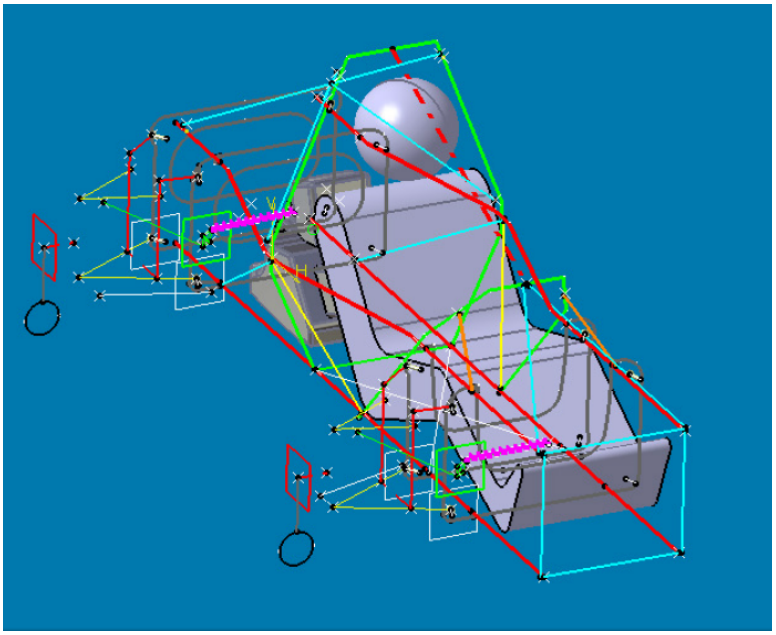

Figure 1.2: Parametric skeleton geometry

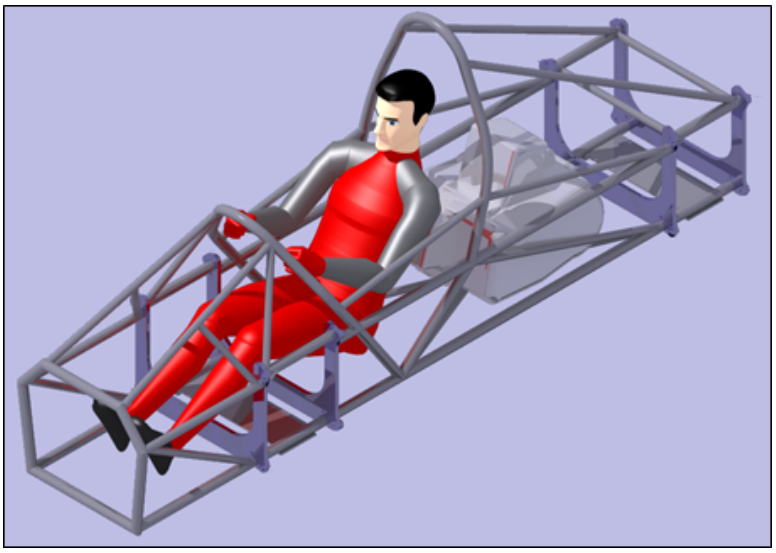

Figure 1.3: Chassis segmented structure

provide an immediate force feedback to the pilot. Therefore, this choice, with regards to the steer system, will be reconsidered in Chapter 4, by studying a conventional mechanical solution. Another critical point is roll slide position: even if it seems particularly suitable, it dramatically interacts with transmission layout: in fact, as seen in Fig. 1.5, the unique feasible position for the differential is, with this layout, the volume above the rear roll slide, and this forces two axle shaft to be very sloping. As a consequence, unbearable angles are imposed to CV-joints both in rolled and symmetrical positions, so compromising the constructive feasibility of this proposal.

The solution to these problems is pursuit by the construction of fully dedicated algorithms, inspired by the dynamical investigation described in the next chapter.

Last, some technical specifications are provided:

Figure 1.4: First assembly proposal

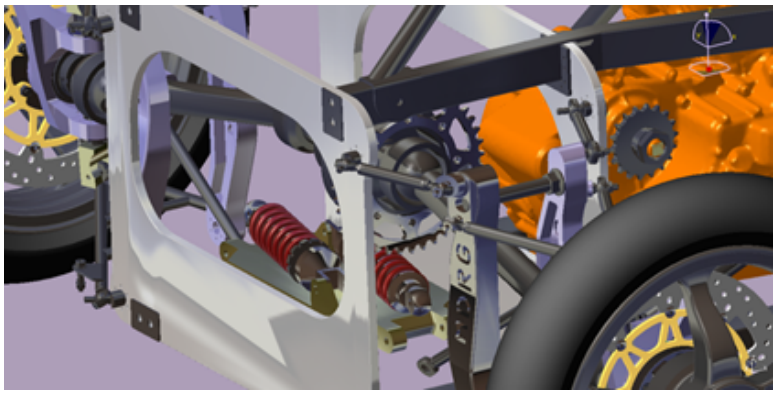

Figure 1.5: Issue in roll slide/transmission positioning

- wheelbase: $1800\ mm$
- track: $\sim 1500\ mm$
- weight: $350\ kg$ (estimated)
- COG height: $400\ mm$ (estimated)
- engine: $V\ 90°$ two cylinders, $850\ cm^3$, $56\ kW$, $73\ Nm$, automatic gear shifting.

CHAPTER 2

Dynamical Aspects

In this Chapter, the dynamical aspects which inspired the design of this vehicle will be illustrated. They are mainly related to cornering, which represents the major field in which this car differs from conventional ones.

First, a brief resume of classic two-wheeled and four-wheeled cornering is presented: tyre mechanics, transversal dynamics and steady-state cornering are described, with the aim to highlight the main differences between these two types of vehicles. Then, the same description is done for a tilting four-wheeled vehicle, with emphasis on aspects which represent the meeting points between two and four wheels dynamics. In the end, the relation between dynamical aspects and design guidelines for the present prototype is illustrated.

2.1 Mechanics of tyres

With regard to tyre mechanics, the main aspect of interest for the present case study is the lateral force generated in the contact patch. Generally, it can be produced by means of two components, the first one being generated by the sideslip angle, and the second one by the camber. Sideslip and camber angles are defined referring to Fig. 2.1 [1]: the first one is the angle between the direction of motion and the intersection between the wheel symmetry plane and the street plane; camber is the angle between the vertical plane XZ and the wheel symmetry plane, the reference frame being chosen accordingly to the SAE definition. The component of the lateral force generated by the sideslip angle is due to the distortions of the tire carcass (Fig. 2.2). Given a point P on the tire patch, it meets the street plane in the position A, then it follows the straight path AB parallel to the forward velocity V, due to the adhesion force. In B, this force is exceeded by the effect of the lateral elastic stress originated by the distortions of the carcass, and the point P slips towards the position C. An increase in the value of the sideslip angle λ produces an increase of the distorted area, so resulting in a greater lateral force modulus.

The component caused by a camber angle is schematized in Fig. 2.3, and it is related to the tire shape. Considering an ideal, completely rigid tire, it would meet the street plane by a single contact point P, which would follow the path composed by points P'. During a straight motion of the tire, the projection of its positions on the street plane would be an ellypse. In the

actual deformable tire, a greater contact patch can be noticed, which the point P belongs to; in this case, it follows the straight path composed by points P'' aligned to the segment $a - a$, due to the friction which occurs between the contact patch and the street. The deviation on the trajectory of P can be ascribed to two types of deformations: the first one, PP' in Fig. 2.3, due to weight, the second one, $P'P''$, which is due to the lateral force.

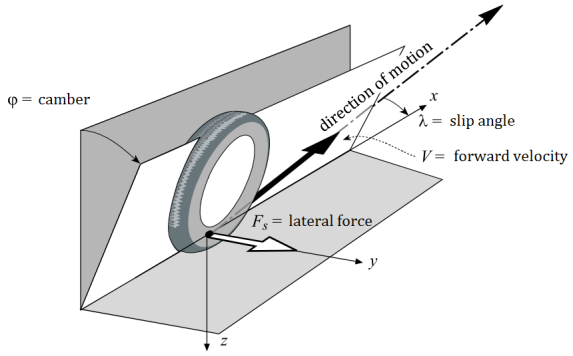

Figure 2.1: Tire angle definition

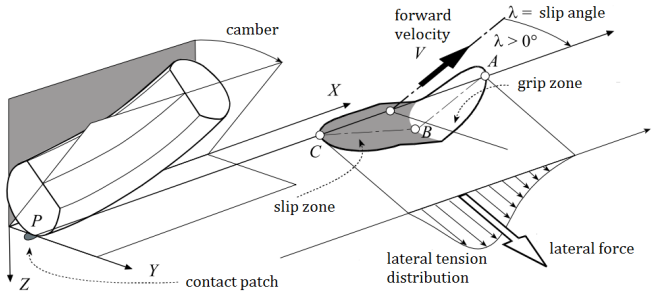

Figure 2.2: Tire sideslip force

A generalized force acting on the tire can be analytically described by the Pacejka's *Magic Formula* , which can be formulated like in Eq. 2.1 :

$$\begin{aligned} Y(x) &= y(x) + S_v \\ y(x) &= -(D)\sin(C\arctan(-Bx + E(Bx - \arctan(Bx)))) \\ X &= x + S_h \end{aligned} \tag{2.1}$$

where x represents the slip and y is the force generated; B, C, D, E are constant parameters, while S_h and S_v are the intersections of the curve with the x and y axes, respectively. The general shape of the curve of Eq. 2.1 is reported in Fig. 2.4.
According to the same formulation, the coupling of the two components of the lateral force (given by camber and sideslip angles) can be represented like in Eq. 2.2:

$$\begin{aligned} F_s = D_s N (&-\sin(C_\lambda \arctan(-B_\lambda\lambda + E_\lambda(B_\lambda\lambda - \arctan(B_\lambda\lambda)))) \\ &+ \sin(C_\varphi \arctan(B_\varphi\varphi - E_\varphi(B_\lambda\varphi - \arctan(B_\lambda\varphi))))) \end{aligned} \tag{2.2}$$

in which two sets of parameters B_λ, C_λ, E_λ and B_φ, C_φ, E_φ , related respectively to the sideslip and the camber component, appear. D_S corresponds to the parameter D of Eq. 2.1, and N is

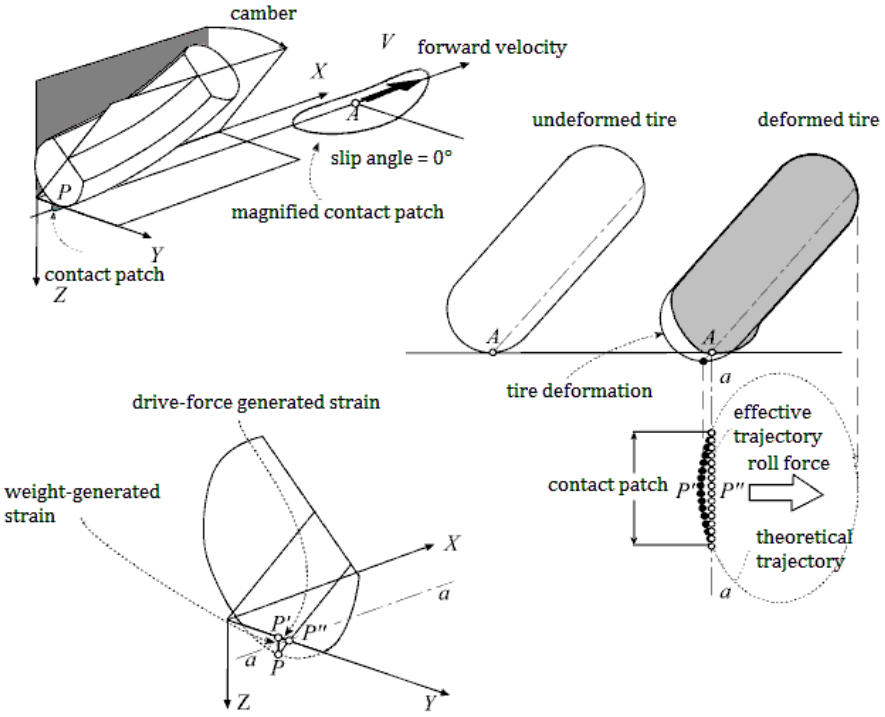

Figure 2.3: Tire camber force

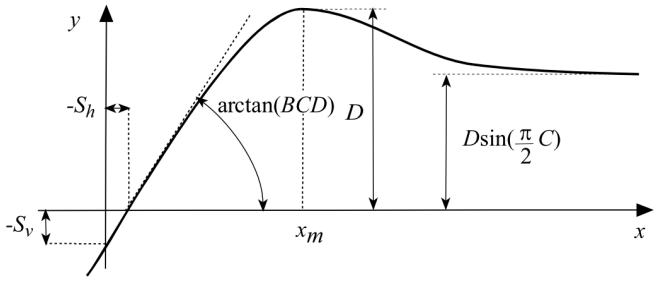

Figure 2.4: Generic Pacejka curve

the normal load applied to the considered tire.
Camber and cornering stiffnesses can be defined by Eq. 2.3 and 2.4, respectively:

$$K_\varphi = \frac{\mathrm{d}F_S}{\mathrm{d}\varphi} \tag{2.3}$$

$$K_\lambda = \frac{\mathrm{d}F_S}{\mathrm{d}\lambda} \tag{2.4}$$

where F_S is the lateral force defined in Fig. 2.1. The corresponding adimensional stiffnesses can be defined like $k_\varphi = \frac{K_\varphi}{N}$ and $k_\lambda = \frac{K_\lambda}{N}$.

In Eq. 2.2 the two components, due to sideslip angle and to camber, are fully separated. In two-wheeled vehicles' cornering, the latter one ("camber thrust") is generally the uppermost contribution. Conversely, conventional four-wheeled vehicles mainly exploit the contribution due to the sideslip angle, since camber is constrained to values of about $0.5 - 1°$ and the camber stiffness K_φ is 5 to 10 time smaller than the cornering stiffness K_λ [2]. As an example, Fig. 2.5 reports the normalized lateral force F_S/N for tires of some two-wheeled vehicles.

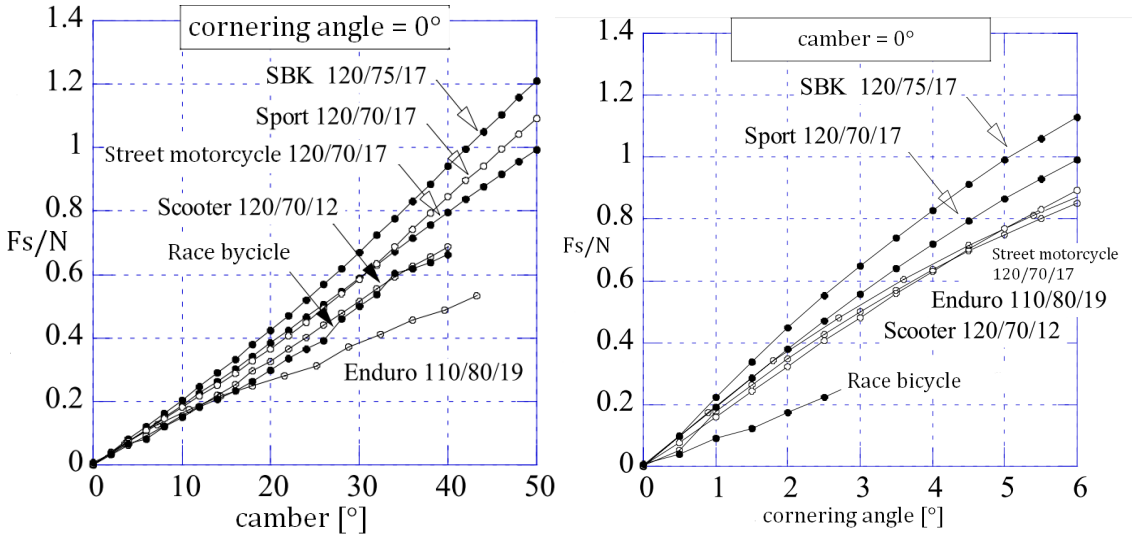

Figure 2.5: Comparison between camber (a) and cornering (b) stiffnesses for tires of two-wheeled vehicles

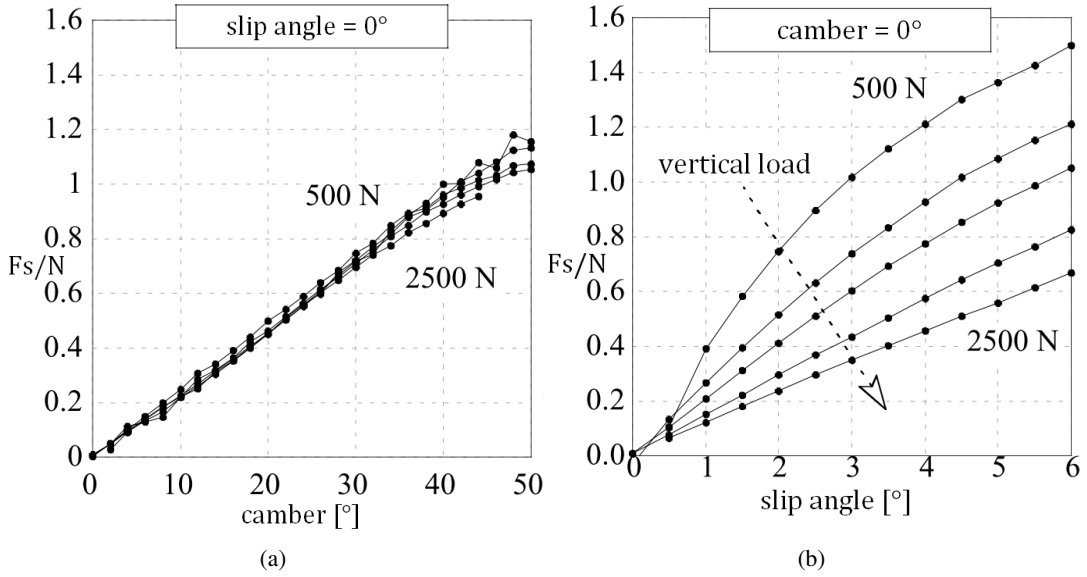

Figure 2.6: Influence of the vertical load on F_S/N for $\lambda = 0$ (a) and $\varphi = 0$ (b)

Another important aspect, with regard to the present study, is the influence of the normal load N on the adimensional stiffnesses (Fig. 2.6) and on the lateral force F_S (Fig. 2.7). The last relation typically presents a positive, decreasing gradient.

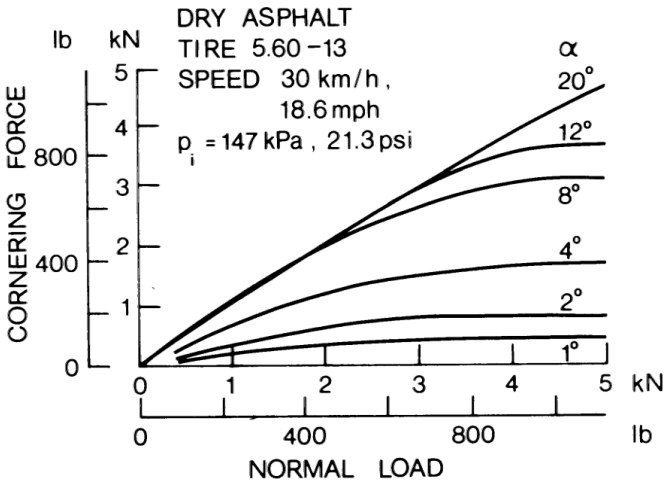

Figure 2.7: Non-linearity of the relation between F_s and N

2.2 Transversal dynamics

Transversal dynamics of two and four-wheeled vehicles are deeply different. In motorcycles, the camber angle in steady-state cornering is determined by imposing the equilibrium of generalized forces in the transversal plane YZ. The total momentum of gravity and centrifugal forces calculated with respect to the contact point must be null, thus introducing a relation between the camber φ and the forward velocity V, according to Eq. 2.5 and Fig. 2.8 [1]:

$$\varphi_i = \arctan \frac{R_c \Omega^2}{g} = \arctan \frac{V^2}{g R_c} \tag{2.5}$$

where R_c is the curve radius, Ω the yaw rate, V the forward velocity and g the gravity acceleration. The satisfaction of this equilibrium is mandatory for avoiding capsize instability.

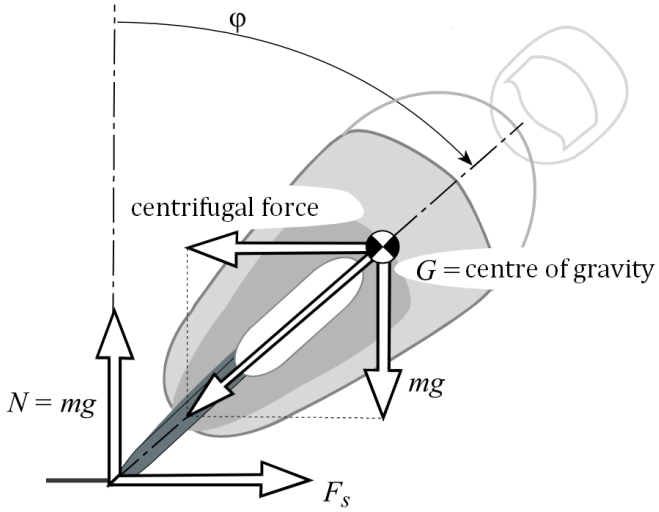

Figure 2.8: Transversal equilibrium on two-wheeled vehicles

Four-wheeled vehicles, on the contrary, are not affected by this problem; however, the centrifugal force causes a load transfer from the inner side wheels to the outer side ones, illustrated in Fig. 2.9. In this planar model, four wheels are substituted by two equivalent ones, on a single axle. F_1 and F_2 are the reaction forces originated by the centrifugal force F_C. They present a

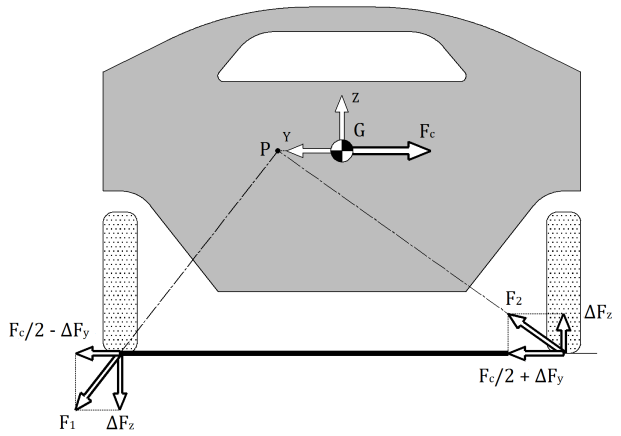

Figure 2.9: Transversal equilibrium on four-wheeled vehicles

vertical component with the same norm ΔFz, equal to the load transfer, and opposite sign. The vertical load applied to two equivalent wheels is so given by the static load component, which is equally subdivided on two wheels, and by the load transfer component Fz: $F_{1z} = \frac{mg}{2} - \Delta Fz$ and $F_{2z} = mg2 + \Delta Fz$, where mg is the total static load. Due to the different value on vertical loads, two equivalent wheels produce different lateral forces, according to the relation exemplified on Fig. 2.7: $F_{1y} = \frac{F_C}{2} - \Delta F_y$ and $F_{2y} = \frac{F_C}{2} + \Delta F_y$. It is worth noting that, given the decreasing trend of the $F_S(N)$ relation, the load transfer produces a decrease on the overall value of lateral force F_S provided by two equivalent wheels.

2.3 Steady-state cornering

The first topic to be presented is the steady-state cornering of two-wheeled vehicles. Referring to kinematic steering, the actual steer angle Δ differs from the steer angle δ measured around the steer axis Fig. 2.10). In particular, it depends on δ, on the camber angle φ, on the caster angle ϵ and on the pitch angle μ, according to the following expression:

$$\Delta = \arctan\left[\frac{\sin\delta\cos\left(\epsilon+\mu\right)}{\cos\varphi\cos\delta - \sin\varphi\sin\delta\sin\left(\epsilon+\mu\right)}\right] \tag{2.6}$$

which can be simplified, assuming small δ and μ angles:

$$\Delta = \arctan\left(\frac{\cos\epsilon}{\cos\varphi}\tan\delta\right). \tag{2.7}$$

The meaning of Δ with regard to steering kinematics is illustrated in Fig. 2.11 [1], in which the rotation δ_p of the rear frame, due to the steer angle δ_n (measured in a plane orthogonal to the symmetry plane of the rear frame) appears. R_c is the kinematic cornering radius, which can be calculated with the following expression:

$$R_C = \frac{1}{C} \tag{2.8}$$

$$C = \frac{\tan\Delta}{x_{P_f} + y_{P_f}\tan\Delta} \simeq \frac{\tan\Delta}{p} \tag{2.9}$$

where x_{P_f} and y_{P_f} define the position of the contact point P_f of the front wheel in the SAE reference frame, and C is the curvature of the trajectory. The cornering radius R_C actually

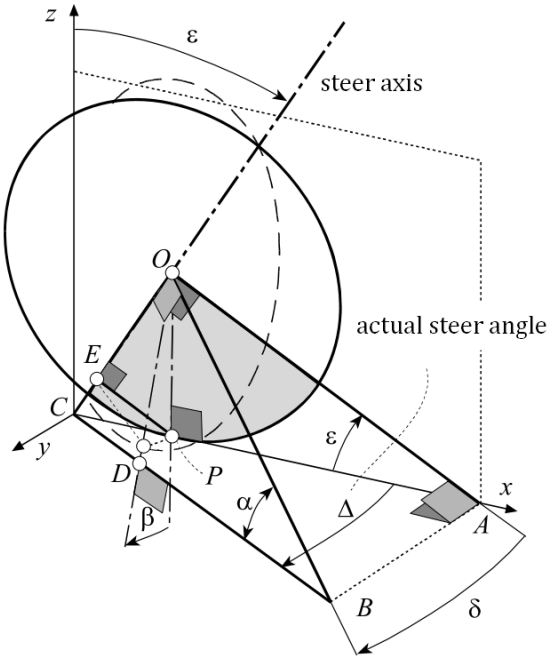

Figure 2.10: Kinematic steer angle on two-wheeled vehicles

differs from the effective one, since kinematic steering does not consider the effect of the centrifugal force, which can not be neglected if the speed is moderate or higher: Fig. 2.12 reports an example of nomogram to determine the sideslip angle needed to make the total lateral force balance the centrifugal one, and obtain a certain cornering maneuver. The diagram is valid the inertial properties of the motorcycle and the tires being fixed. On the right, the camber thrust is compared with the centrifugal force F_C which corresponds to the indicated camber angle, according to Eq. 2.5. For angles smaller than $28°$, the camber thrust is greater than the necessary lateral force: therefore, a negative sideslip angle must be used to decrease the value of the total lateral force. Conversely, for camber angles greater than $28°$, a positive sideslip angle is needed to match the magnitude of the centrifugal force. For a camber of $28°$, the camber thrust exactly matches the centrifugal force: in this case, the sideslip angle can be null. The sideslip angle needed for each value of the camber can be read on the diagram reported on the left on Fig. 2.12. The effective steer angle can definitely be described by the expression:

$$\Delta^* = \Delta + \lambda_r - \lambda_f \tag{2.10}$$

The condition $\Delta^* = \Delta$ can be achieved only when $\lambda_r = \lambda_f$; the particular case $\lambda_r = \lambda_f = 0$ corresponds to kinematic steering. The effective curvature radius of the rear frame is:

$$R_{Cr} = \frac{p}{\tan(\Delta - \lambda_f)\cos\lambda_r + \sin\lambda_r} \tag{2.11}$$

where λ_f and λ_r are the front and rear sideslip angle, respectively. The Eq. 2.11 can be simplified, assuming small λ_f, λ_r and δ angles, as follows:

$$R_{Cr} \simeq \frac{p}{\Delta + (\lambda_r - \lambda_f)} = \frac{p}{\Delta^*} \tag{2.12}$$

The meaning of Δ^* and R_{C_r} is represented in Fig. 2.13. By previous considerations it can be observed that, even if the condition $\lambda_r = \lambda_f = 0$ is not common, sideslip angles can generally be small, so making common cornering maneuvers close to the kinematic steering model.

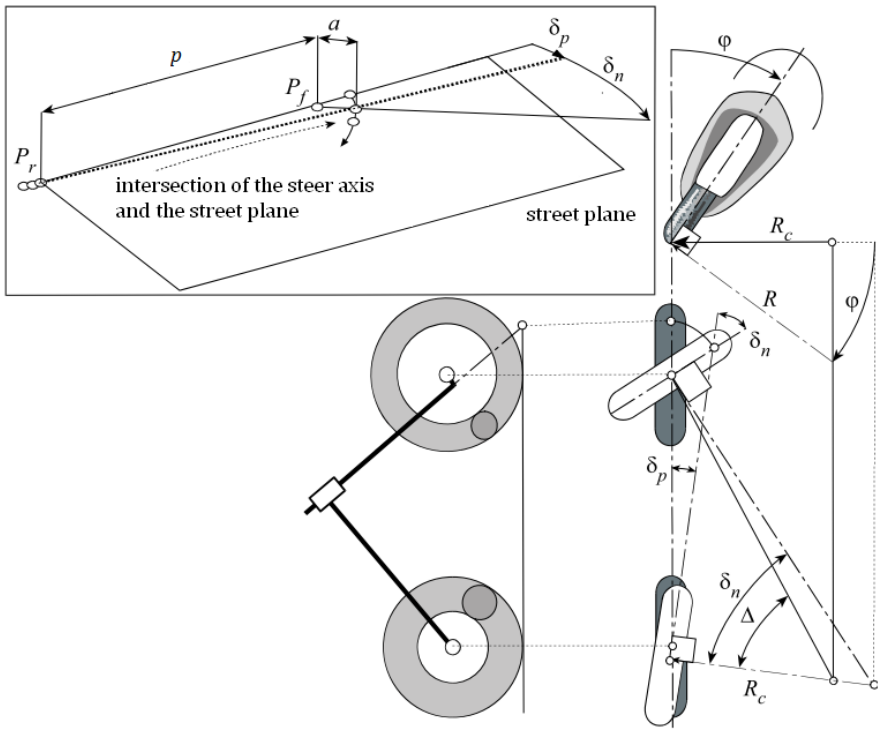

Figure 2.11: Meaning of the kinematic steer angle on two-wheeled vehicles

In four-wheeled vehicles, kinematic steering can be represented by Fig. 2.14 [3], in which p is the wheelbase of the car, t is the track and δ_o and δ_i are the steer angles of the outer and inner wheel, respectively. Since for cars, as aforementioned, camber is very small, in the definition of kinematic steering it is considered to be null. Neglecting the effect of the centrifugal force, for sideslip angles to be null, a precise relation must be satisfied, commonly known as Ackerman condition:

$$\cot \delta_o - \cot \delta_i = p/L \tag{2.13}$$

This condition ensures that both tracks of the vehicle corner around the same point without scrub: the centerlines of front wheels at the inner and at the outer track intersect each other in the point C_c, which lies on the centerline of rear wheels and corresponds to the center of cornering. In traditional cars the Ackerman condition is generally not fully satisfied. Fig. 2.15 [2] compares the Ackerman steering geometry (a) with (b), parallel steering ($\delta_i = \delta_o$), and (c), Reverse or Anti-Ackerman. The geometry (c) is generally used in race cars, to make the steer response faster by a greater steer angle on the outer wheel, which is the most solicited by the vertical load due to the lateral load transfer. Passengers cars usually adopt a geometry which lies between (a) and (b): Fig. 2.16 [4] shows an example of $\delta_o/\delta i$ relation used in practice against a theoretically correct curve (Ackerman) and a parallel steer curve. A good approximation of the Ackerman relation can be obtained by means of a steering system which follows the common rule of Fig. 2.17, which implies a rack and pinion scheme: the rack should be positioned behind the centre of front wheels, so that tie-rods centerlines intersect in the middle point of a line which joins the centres of rear wheels.

If the centrifugal force is taken into account, the dynamic equilibrium is satisfied by means of the lateral forces originated by the sideslip angles. Fig. 2.18 refers to the widely used single-track model, in which two wheels of a same axis are substituted by a single equivalent wheel: this model is very similar to the one represented on Fig. 2.13, except for the lack of

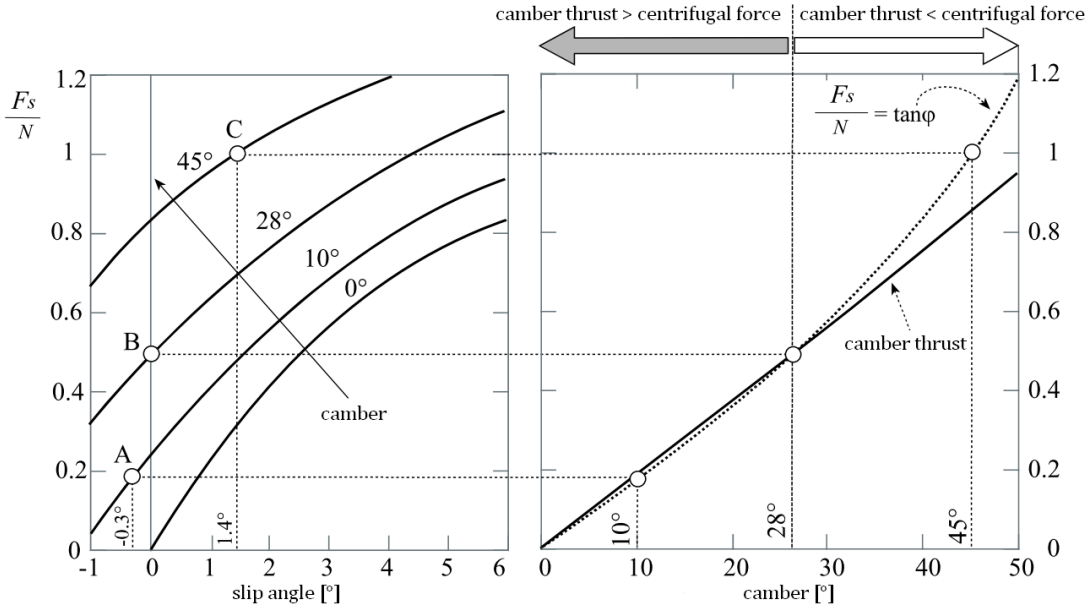

Figure 2.12: Example of nomogram for the determination of the sideslip angle

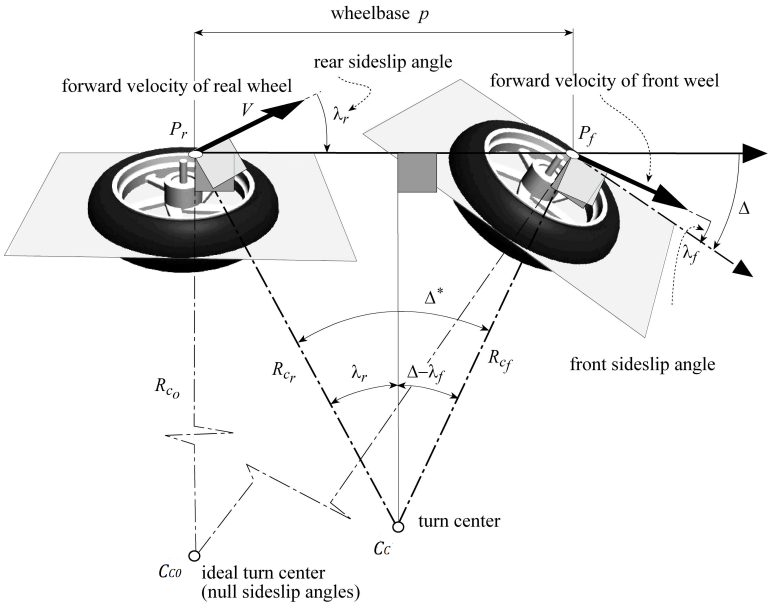

Figure 2.13: Meaning of Δ^* and R_{C_r}

camber angles. This simplified model does not illustrate the relation between the left and the right sideslip angles, however it highlights that, differently from motorcycles, the lateral force needed to balance the centrifugal one can be obtained only by sideslip angles (neglecting the small effect of camber). The normalized lateral forces to be developed at front and rear wheel, calculated by imposing the transversal equilibrium, are:

$$\begin{aligned} \frac{F_{S_f}}{N_f} &\simeq \frac{V^2}{gR_{Cr}} \\ \frac{F_{S_r}}{N_r} &= \frac{V^2}{gR_{Cr}} \end{aligned} \tag{2.14}$$

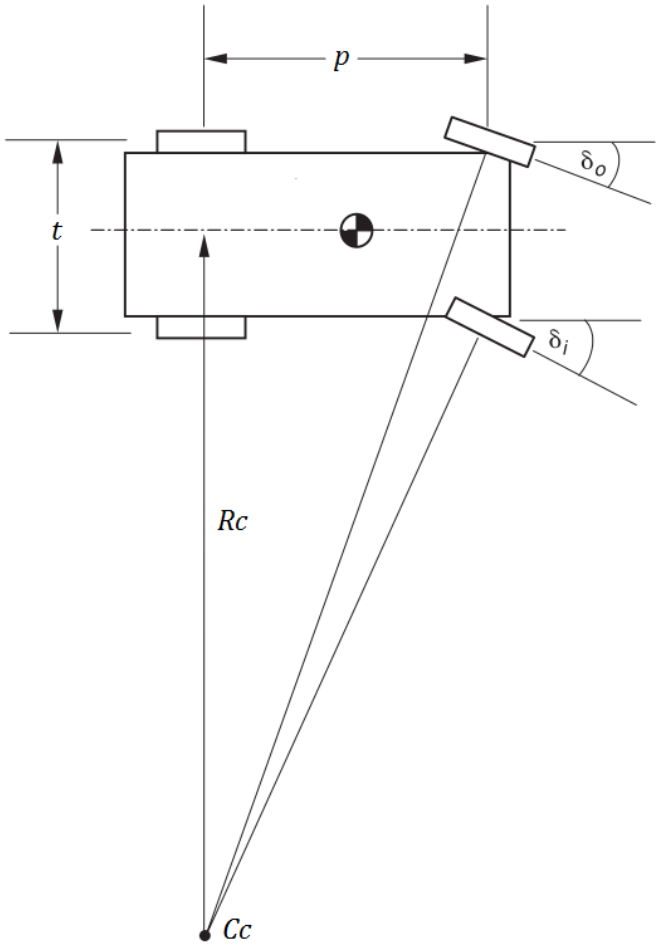

Figure 2.14: Kinematic steering on four-wheeled vehicles

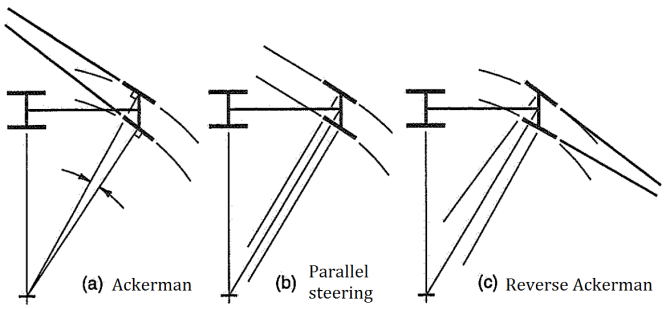

Figure 2.15: Ackerman, parallel and reverse-Ackerman steering

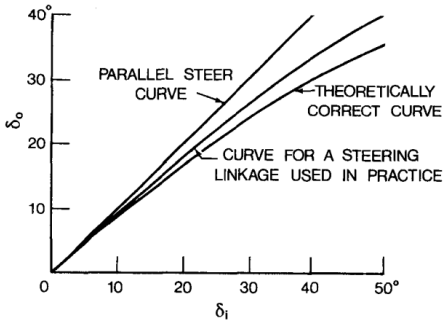

Figure 2.16: Example of $\delta_o/\delta i$ relation for different steer systems

where F_{S_f} and F_{S_r} are the front and rear lateral force, respectively, V is the forward velocity, g the gravity acceleration and R_{Cr} the effective cornering radius, while $N_f \simeq mg\frac{b}{p}$ and $N_r \simeq mg\frac{p-b}{p}$ are the normal forces applied to front and rear wheels, with p and b defined like in Fig. 2.18. At low forward velocity the centrifugal force is limited, the normalized lateral forces are small and so are the sideslip angles: only under these conditions, the cornering model can be reasonably referred to kinematic steering. This consideration will be taken into account in the definition of design guidelines.

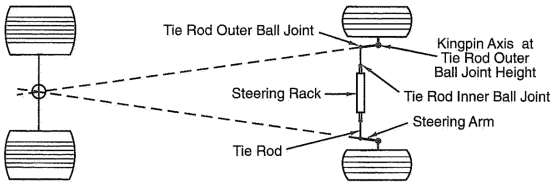

Figure 2.17: Common layout compliant with the Ackerman rule

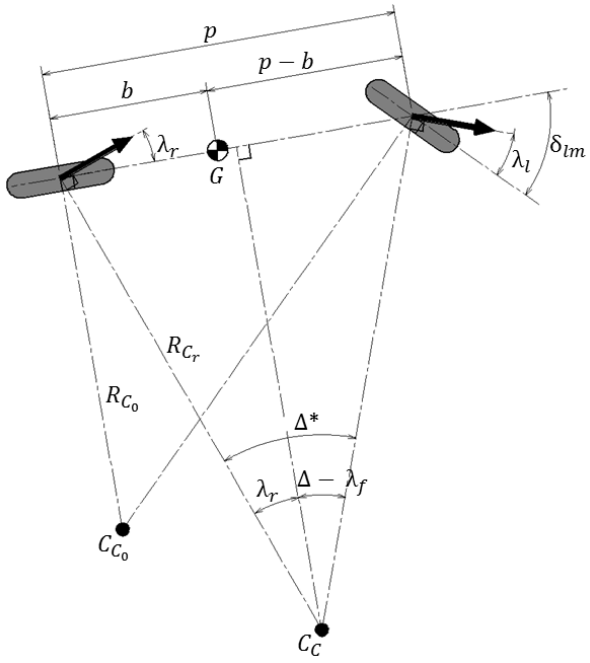

Figure 2.18: Single-track model of four-wheeled vehicles

2.4 Cornering in a tilting four-wheeled vehicle

This section introduces some aspects of cornering dynamics with regards to tilting four-wheeled vehicles, highlighting similarities and differences with respect to conventional two and four-wheeled vehicles. Then, modelling and results of some preliminary multibody simulations implementing the *Optimal Maneuver Method* are presented. In the end, the design guidelines are discussed.

2.4.1 Kinematic steering and lateral dynamics in tilting four-wheeled vehicles

During a cornering maneuver, a tilting four-wheeled vehicle exploits some aspects typical of two-wheeled vehicles, and other ones belonging to conventional four-wheeled vehicles. A curve can be performed by profiting both of camber and sideslip angles, without the disadvantage of lateral instability which affects motorcycles. Since the camber thrust is related to carcass deformations, its response time is generally smaller than the one related to the sideslip component of the lateral force [1]; in addition, the gradient of the cornering component over the sideslip angle is relatively small in typical bias-ply motorcycle tyres. Therefore, the camber can be theoretically used for a fast curve engagement phase, with a fine tuning of the cornering angle made by acting on the steer command.

The adoption of motorcycle tyres can be useful only if their characteristics are exploited, i.e. they are used as in motorcycle applications. To find a solution to this problem, first, the kinematic steering of the analyzed vehicle must be taken into account. Fig. 2.19 highlights that, differently from conventional four-wheeled vehicles, the Ackerman condition must be imposed on actual kinematic steer angles Δ like defined by Eq. 2.6, instead of angle δ: this way, the kinematic contribution of camber is taken into account. To operate at low slip angles, i.e.

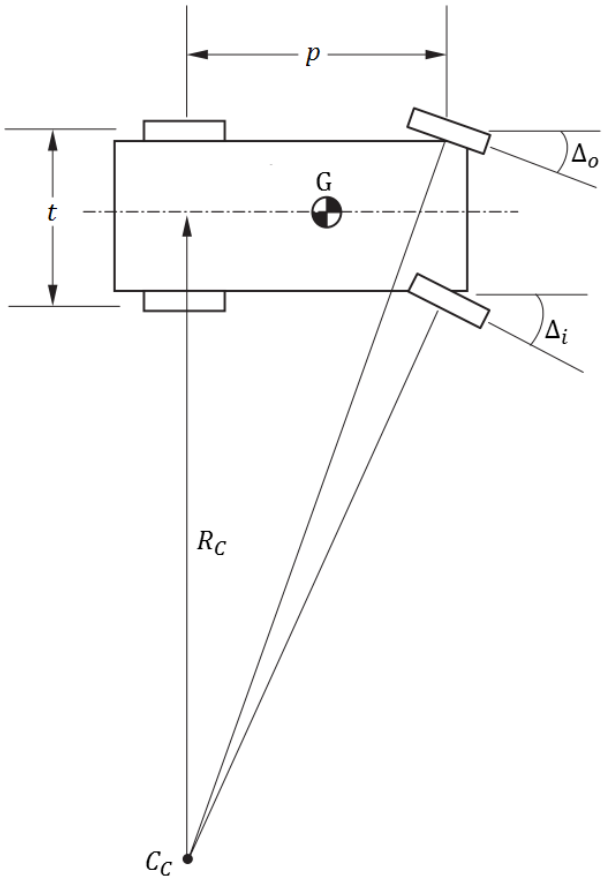

Figure 2.19: Kinematic steering for a tilting four-wheeled vehicle

the typical use condition of motorcycle tyres, scrub must be avoided: therefore, especially at low forward velocity, the Ackerman rule, applied to kinematic steer angles Δ, should be satisfied.

Transversal dynamics can be described referring to Fig. 2.20, which represents only one of two axles. Assuming that the roll of wheels (not represented) imposes a rotation and a translation of the chassis, the center of mass moves from position G to G', being $\Delta y_{G'}$ the magnitude of the lateral component of translation. This aspect is not present in conventional four-wheeled vehicles, except for the effect due suspensions. A momentum $M_g = F_g \Delta y_{G'}$ is so originated by gravity force, with reference to point G, and an equivalent load transfer ΔF_{zg} appears on the left and right wheels, with the same magnitude but opposite sign. Assuming that, if the wheels are rolled towards the inner side of the curve then the chassis translates in the same direction, ΔF_{zg} is opposite to the load transfer caused by the centrifugal force F_c, so mitigating its weakening effect on the overall lateral force. Moreover, the distribution of F_s among inner and outer wheels can be more uniform. These considerations are confirmed by the numerical results of the preliminary multibody simulations, which are described in the following section.

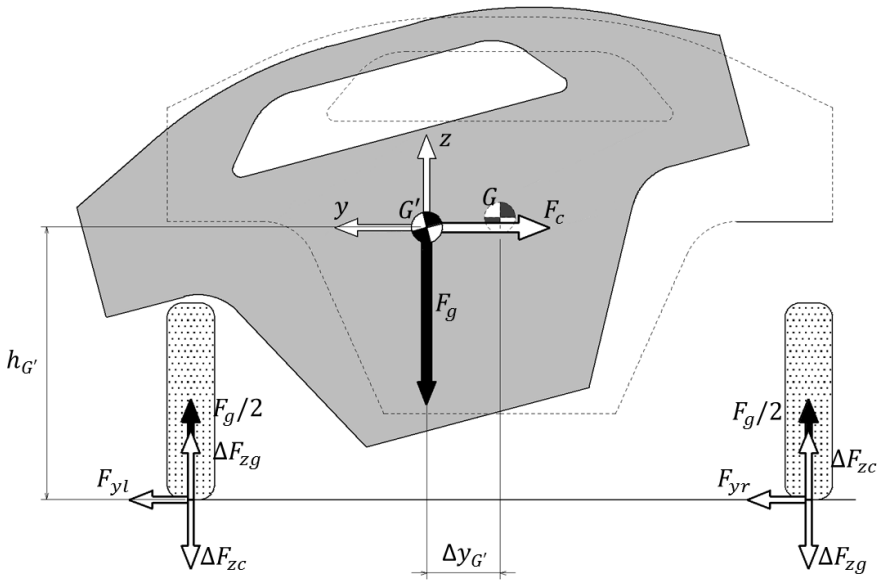

Figure 2.20: Transversal dynamics of a tilting four-wheeled vehicle

2.4.2 Multibody simulations with the Optimal Maneuver Method

This section describes the symbolic multibody modelling of a tilting four-wheeled vehicle and the numerical results given by simulations done by MDRG staff. This results are used to confirm some considerations reported in the previous paragraph and to identify the design guidelines for the first prototype.

The dynamical model was compiled in Maple language using the multibody package "MBSymba". Then, the equations of motion were numerically addressed by using the Optimal Maneuver Method and numerically solved with the dedicated Xoptima software. Fig. 2.21 represents the definition of the main geometrical features of the model and of the moving frame. The chassis is connected to the wheels by means of symbolic suspensions with linear springs with elastic modulus k_f and k_r at front and rear wheels, respectively, and without dampers. Even if the model is double-track, the steer angle δ on two front wheels is considered to be the same. The camber, too, is considered to be the same for all wheels, see Fig. 2.22(a). This simplification, even if does not match the behaviour of the final prototype, improves the flexibility of the model, allowing for faster simulations and more general results. The chassis movement due to a change in wheel camber is calculated in two steps, referring to Fig. 2.22(b): first, the tire roll movement is imposed by following expressions:

$$\Delta z_c = r_w \left(1 - \cos\varphi\right) \tag{2.15}$$

$$\Delta y_c = r_w \sin\varphi + r_t \varphi \tag{2.16}$$

where z_c and y_c are the translations of the chassis enter of mass and of the wheel center, considered to be equal, r_w and r_t are defined in Fig. 2.22(b). During this step, the starting configuration ($\varphi = 0$, red) changes in the grey one. Second, a translation equal to $-\Delta y_c$ in lateral direction is applied to the center of gravity of the chassis, so identifying the light blue one. The final displacement, by a dynamical point of view, is so defined by a vertical translation of the chassis and a lateral translation of the contact points equal to $\Delta y_{cp} = -r_w \sin\varphi$. By this scheme, it is possible to calculate the load transfer caused by a change in wheel camber, by means of two equivalent semi-tracks c_l and c_r (with reference to the moving frame T_{10}, defined

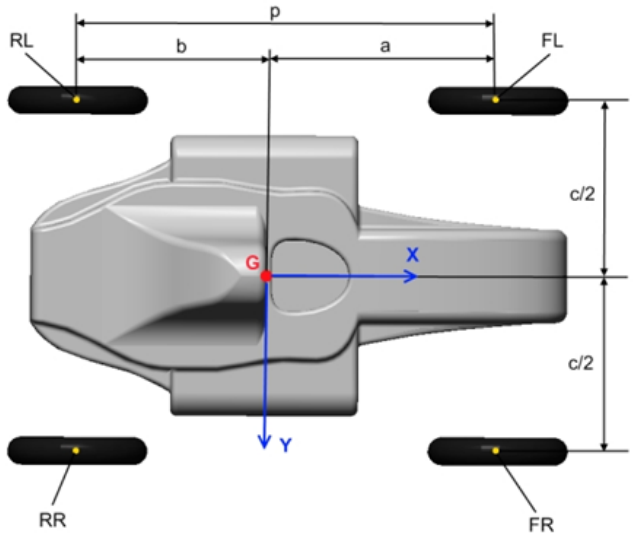

Figure 2.21: Main geometrical properties used in the symbolic multibody model

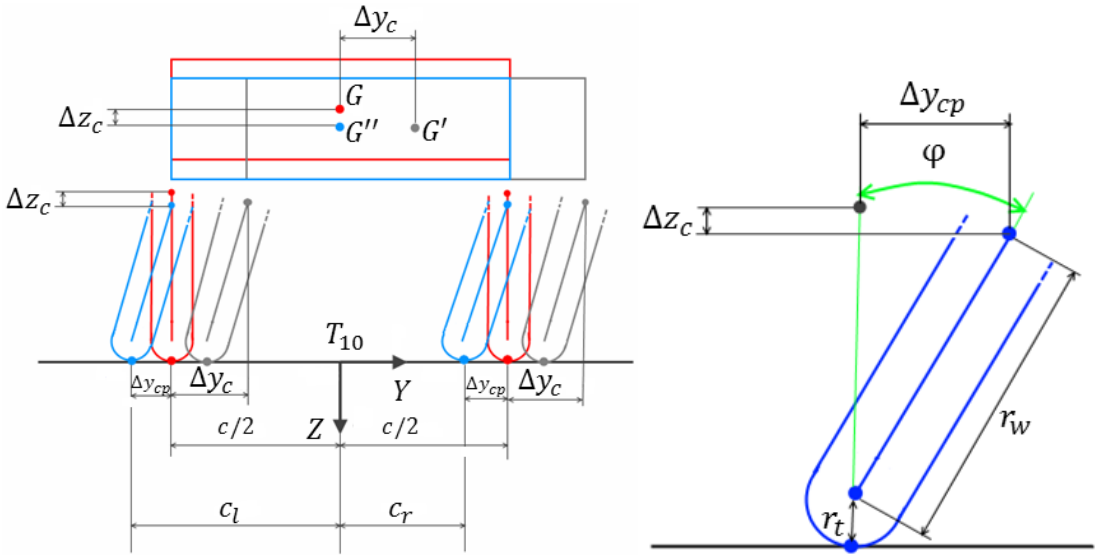

(a) (b)

Figure 2.22: Roll in the symbolic model: (a) movement of the chassis and (b) lateral translation of the contact point

like in Fig. 2.22(a)). Spring compression is calculated according to Fig. 2.23 by the equation:

$$\Delta l_s = l^{'} - l = h + z_{P_s} - \Delta z_c \tag{2.17}$$

where Δl_s is the compression of a generic spring, h is the original height (in static trim) of the link point between the spring and the chassis, and z_{P_s} is its height in the actual configuration. The whole multibody model features 3 degrees of freedom ("DOF"), i.e.
the position of its center of mass in the XY plane and its yaw angle, all referred to a global frame (where Z is the vertical axis). Therefore, the state-space description adopts three variables:

- $u(t)$, longitudinal velocity of the chassis
- $v(t)$, lateral velocity of the chassis

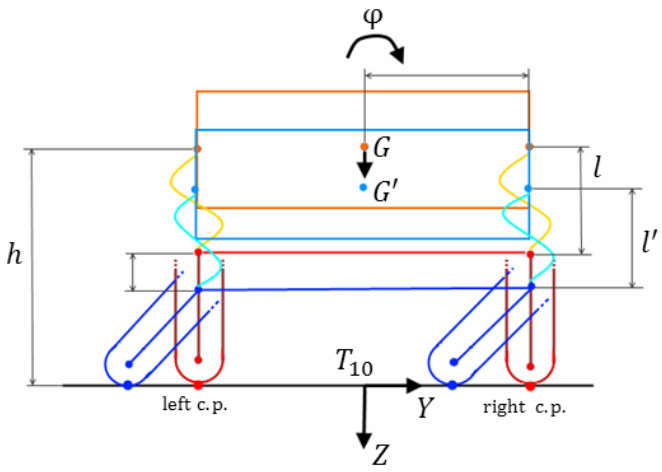

Figure 2.23: Main geometrical properties used in the symbolic multibody model

- $\dot{\Psi}(t)$, yaw rate of the chassis.

The input variables are:

- Front longitudinal force (brake force)
- Rear longitudinal force (traction and brake forces)
- Steer angle δ
- Camber φ .

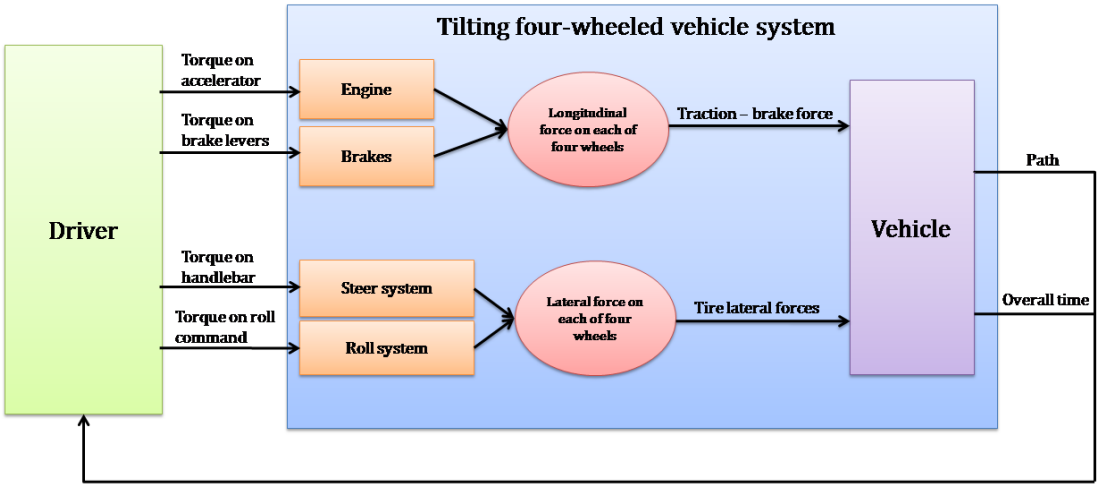

Figure 2.24: Functional scheme of the Optimal Maneuver Method control

The control of the vehicle is managed by the Optimal Maneuver Method (Fig. 2.24). A virtual driver acts on vehicle subsystems through commands (accelerator, brake levers, handlebar, roll pedals); longitudinal and lateral forces develop between wheels and street plane, according to inputs provided by the driver and to vehicle dynamics. The output of the system are the path generated and the overall maneuver time. The inputs provided by the driver are generated with

the objective of minimizing a function of the following type:

$$\int_0^L J\left(x\left(s\right), u\left(s\right)\right) ds \tag{2.18}$$

where:

- $J =$ chosen performance index
- $s =$ curvilinear abscissa along the chosen path
- $x =$ state vector of the overall system
- $u =$ driver commands (as above listed)
- $L =$ length of the chosen path.

In the present case study, the performance index is the time to cover the chosen path: therefore, the objective is to produce an overall maneuver which is as fast as possible. The optimization problem is subject to some conditions:

1. the trajectory must lay inside path borders
2. the grip of four wheels must be assured
3. camber and its rate must not exceed imposed limits
4. steer angle and its rate must not exceed imposed limits
5. longitudinal forces must not exceed imposed limits.

The infringement of each of these conditions causes a penalty on the overall performance. The minimization of the objective function 2.18 is conducted by a numerical optimization algorithm. The conditions 3 and 4 can be used to impose some limits due to the physical capabilities of the driver. If this aspect is neglected, the pure vehicle performances can be investigated; otherwise, the car can be analyzed by and handling point of view. The present analysis focuses on the second of two approaches, with the aim to obtain results closer to the experimental ones. For a deeper description of the model see [5].

Two types of simulations are conducted on the described model: the first type is aimed to compare the performances of the same vehicle, with and without the use of camber. The second type of simulations are aimed to point out some guidelines on the drive strategy, with particular regards to the relation between camber and sideslip.

Fig. 2.25 quantifies the contribution of wheel roll usage on the speed: the scale represents the percentage increment in speed of a tilting vehicle over a conventional one, having the same characteristics, along a 90° curve 2.25(a) and a U-turn 2.25(b). An important aspect is to note that the height of the center of gravity ("COG") of the tested model is typical of a circuit race car, being equal to $290\ mm$ with respect to the street plane. The overall advantage is quantified in $0.68\ \%$ and $1.13\ \%$, in maneuver (a) and (b), respectively: this value is very modest. However, the overall scenario changes as the height of the COG increases: Fig. 2.25 compares the percentage speed increment given by the introduction of the roll usage, along a complete circuit, with COG $290\ mm$ height (a) and $500\ mm$ height (b), the latter one being closer to a passenger car. The arise of the COG causes an increase from $1.41\ \%$ to $5.64\ \%$ on the advantage of the tilting vehicle over the conventional one: in fact, the entity of the lateral load transfer

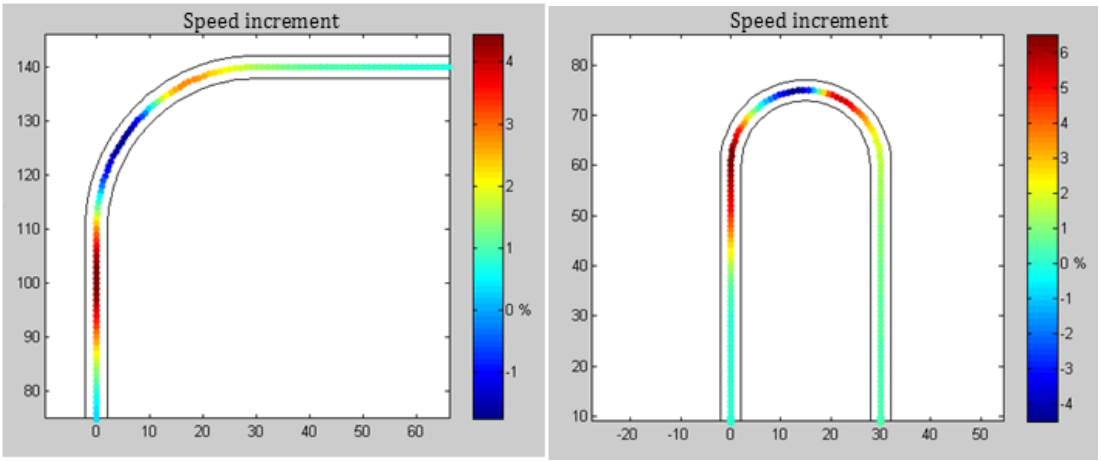

(a) (b)

Figure 2.25: Comparison of overall speed between tilting and conventional vehicle: (a) 90° curve and (b) U-turn

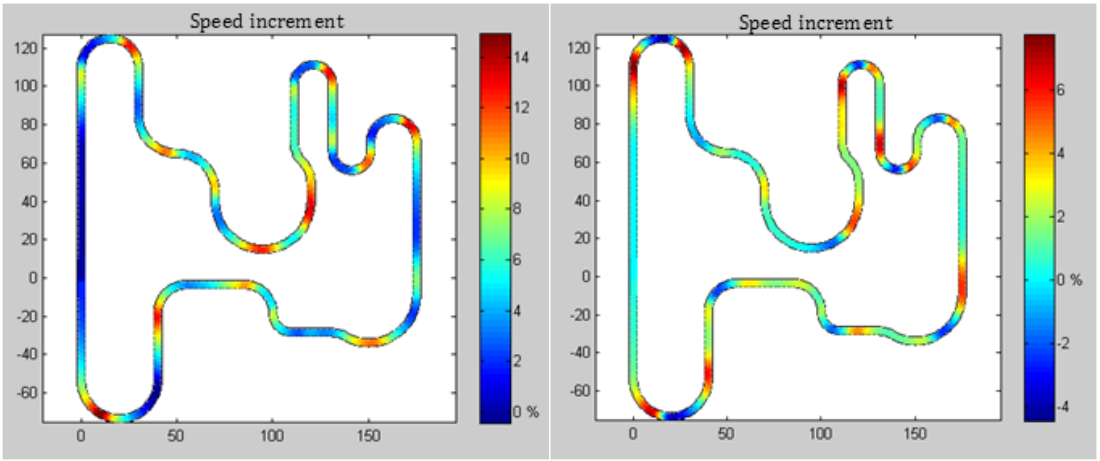

(a) (b)

Figure 2.26: Comparison of overall speed between tilting and conventional vehicle: (a) CoG at 500 mm curve and (b) CoG at 290 mm

due to the centrifugal force is proportional to the height of the COG, and so is the negative effect on the overall lateral force F_S: as above discussed, the load transfer originated by the roll movement can be used to contrast this effect. It can be concluded that, in general, the actuation of the roll movement increases the average speed of the vehicle, and this effect is greater for a vehicle with a higher COM.

A second performance index is the drift angle, i.e. the angle between the effective velocity of the vehicle, and its longitudinal component. Fig. 2.27 depicts a general result: the use of the roll movement is addressed by the algorithm so that it causes a general decrease of the drift angle, especially during the curve engagement phase. Along some curve segments, the drift angle can be negative.

Third, Fig. 2.28 compares the distribution of the lateral force over the four wheels, in a conventional vehicle (a) and in the tilting one (b), during a $90°$ curve: in the second one, this distribution is significantly more uniform, confirming the mitigating effect of the roll over the load transfer. The aforementioned second type of simulations offer an interpretation of the right

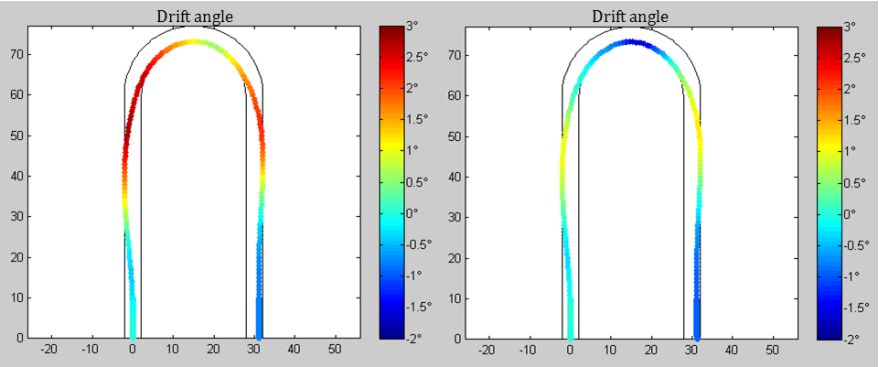

Figure 2.27: Drift angle on a conventional four-wheeled vehicle (left) and on the tilting one (right) during a U-turn

usage of camber and steer: Fig. 2.29 depicts a typical trend, consisting in the anticipation of camber with respect to the sideslip angle, in this case along a U-turn. The dominant usage of the first is apparent, too. Fig. 2.30(a), on the contrary, illustrates the small mitigating effect of the roll over the sideslip angle, by comparing the same vehicle with and without roll capability. Fig. 2.30(b) shows a similar sideslip angle for a conventional vehicle with the same properties but with car tires. It can be concluded that the use of tires is similar to motorcycles: the curve engagement is done, first, by imposing a roll angle with predominant magnitude with respect to the sideslip angle; additionally, the drift angle is limited, especially in curve engagement. On the contrary, the magnitude of the sideslip angle needed to perform a given maneuver, even if smaller than camber, is not significantly reduced by roll.

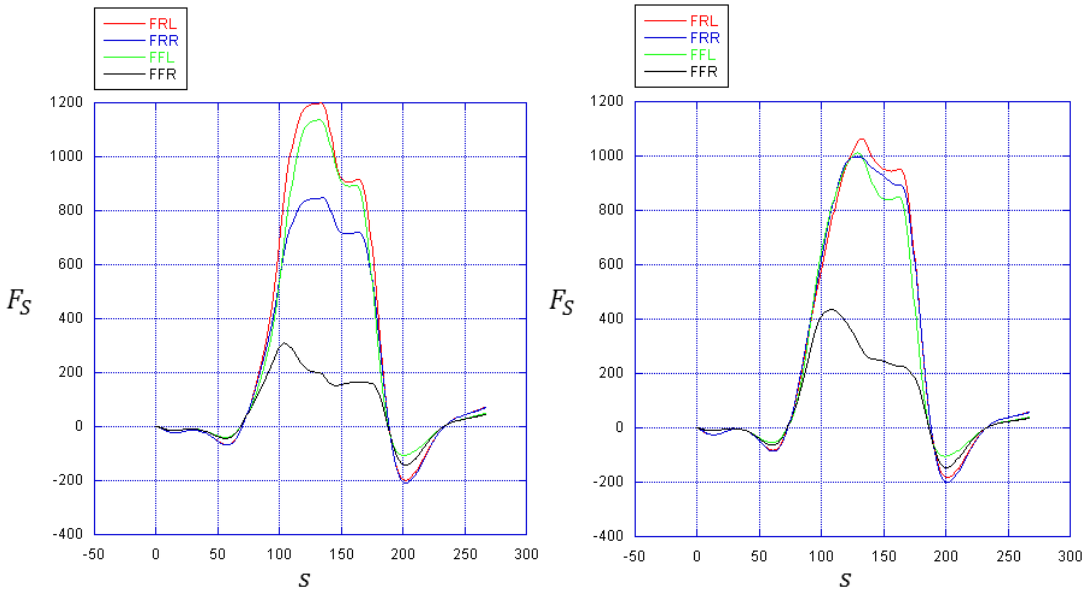

Figure 2.28: Lateral force distribution on four wheels along a 90° curve: conventional four-wheeled vehicle (a) and tilting one (b)

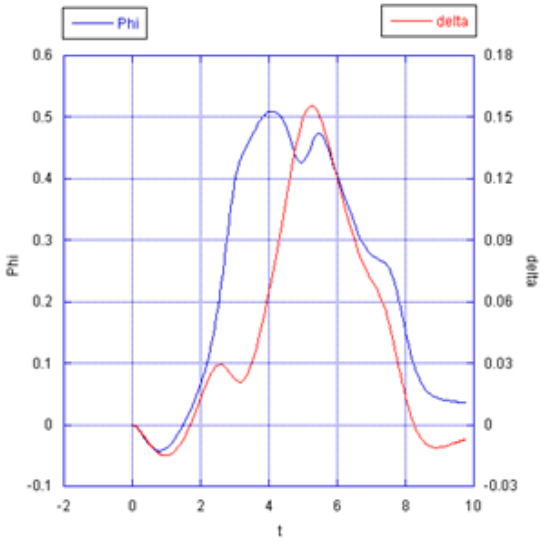

Figure 2.29: Phase shift between roll and steer along a U-turn

2.4.3 Design guidelines

The numerical results presented in the previous section can be schematized as follows:

1. The roll capability allows for an overall speed improvement, especially if the height of the COG is relevant.

2. Drifting does not seem to be a profitable strategy to improve the overall speed in the tested tilting four-wheeled vehicle.

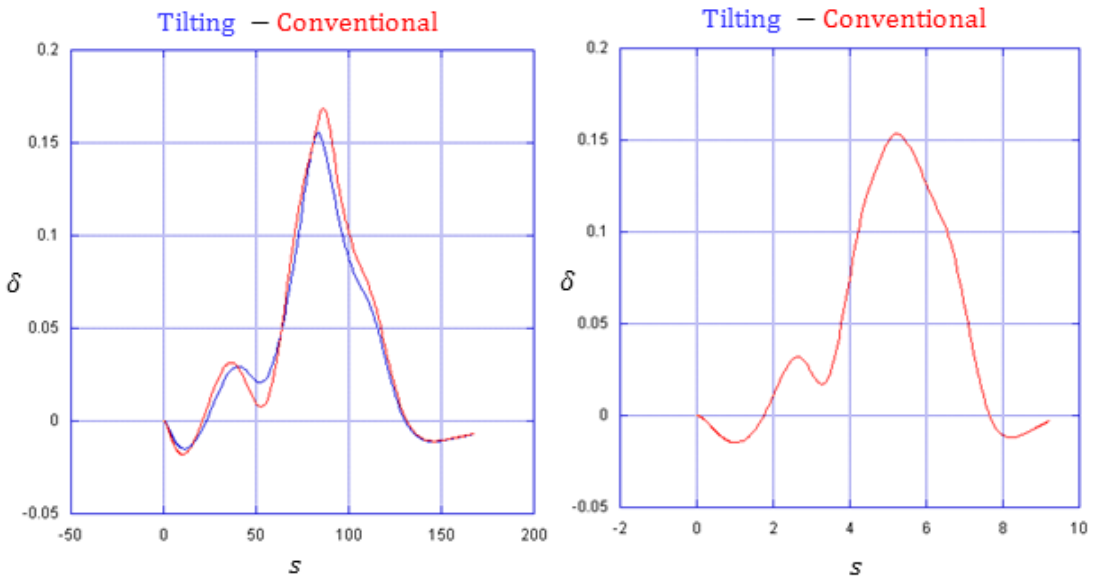

(a) (b)

Figure 2.30: Sideslip angle on a U-turn maneuver: comparison of tilting four-wheeled vehicle and conventional one with the same tires (a) and conventional vehicle with car tires (b)

3. The lateral force distribution over the four wheels is significantly more uniform in the tilting vehicle.

4. A phase shift between camber and sideslip angles is a profitable strategy to obtain good performances, with a roll actuation which anticipates the imposition of the steer angle.

5. The introduction of the roll does not reduce significantly the magnitude of the steer angle needed to perform a given maneuver. However, camber entity is generally greater than sideslip, similarly to motorcycles.

Two main guidelines can be defined accordingly:

(a) Points 1 and 3 highlight the importance of balancing the discussed negative effect of the lateral load transfer due to the centrifugal force, by inducing a lateral translation of the COG, towards the inner side of curve, through the roll movement. A contemporary reduction in COG height can further enhance this positive effect. Therefore, the first guideline is to design a roll subsystem which can maximize the lateral translation of the chassis during the roll phase and, at least, does not induce a rise in COG height.

(b) Points 2, 4 and 5 highlight the great importance of roll in the drive strategy, pointing out some similarities with motorcycle riding: camber is generally greater in tested maneuvers, and systematically shifted in time with respect to the sideslip angle. Drift is not particularly used. Steer angles are not significantly reduced by the roll capability. Therefore: the steering system must grant angles of magnitude similar to conventional four-wheeled car; it must be coupled with the roll system as less as possible, to allow for time shifts between angles δ and φ, and to exhibit a predictable behaviour to produce a good handling; additionally, to obtain a tire usage which is similar to motorcycles, it should respect, within a certain tolerance, the Ackerman condition, thus avoiding scrub at low forward velocity.

CHAPTER 3

The roll system

In this Chapter, the process of kinematic synthesis of the roll system will be described. The guidelines discussed in Chapter 2 define one of functional requirements of the mechanism:

- to maximize the lateral translation of the center of gravity of the chassis during the roll phase, and not to introduce significant rises in its height.

During the concept phase, two other requirements were pointed out:

- the roll movement of the chassis must be in the same direction of wheel camber, so providing a roll feedback similar to motorcycles
- the change in track must be minimized to limit the scrub during the roll phase.

The definition of the mechanism to be constructed was done by following steps:

1. Some alternative topologies were preliminary compared with a commercial multibody code, so pointing out the most promising ones, according to functional requirements. This phase also highlighted the need of a more flexible and customizable procedure to improve results.
2. The best options produced in the previous step were implemented in dedicated multibody models to overcome the limits of commercial software.
3. An optimization was performed on custom models, allowing for a numerical comparison between alternatives and, at the same time, the choice of the best performing mechanism.

Each of these steps is described in the following sections.

3.1 Preliminary analysis

Targets of this phase are the selection of the more promising topologies for the mechanism to be designed in detail, and the acquisition of first non quantitative information with regards to possible problems. Since this phase is carried out by a user-driven, trial and error approach, the analysis method must grant:

- low testing time
- simple and intuitive definition and representation of outputs
- easy update of tested mechanism.

This way, a large amount of tests can be done, providing a sufficiently huge amount of information to be dynamically interpreted by a heuristic approach. Therefore, the methodology was defined in the following keypoints:

(a) Definition of a trial topology by a commercial two-dimensional, multibody code, with drag-and-drop capabilities in geometrical definition and kinematic simulation. Trial values are imposed to linkage lengths.

(b) Analysis of the mechanism by means of visual inspection.

(c) Manual change in values assigned to design variables (member lengths) to set-up a new candidate from the same topology.

(d) Comparison among tested solutions.

(e) Change in topology and iteration of the test.

The following paragraphs describe the solutions tested by this procedure. For each mechanism a brief description is done, highlighting advantages and disadvantages.

3.1.1 Four-bar linkage suspension with rolling upright

The first tested topology (Fig. 3.1) features a conventional four-bar linkage suspension, and an upright composed by two parts: the first one, which is tilting, is connected by a rotational joint to the second one, and this one is connected to pull rod and wishbones. The roll movement is actuated by a roll slide, which can move in lateral direction with respect to the chassis, which it is connected to by means of a translational joint. Camber is imposed to uprights through a roll arm. The main drawback of this topology is that wheels and chassis roll in opposite direction within a reasonable range of linkage lengths (Fig. 3.2). For this reason it is discarded.

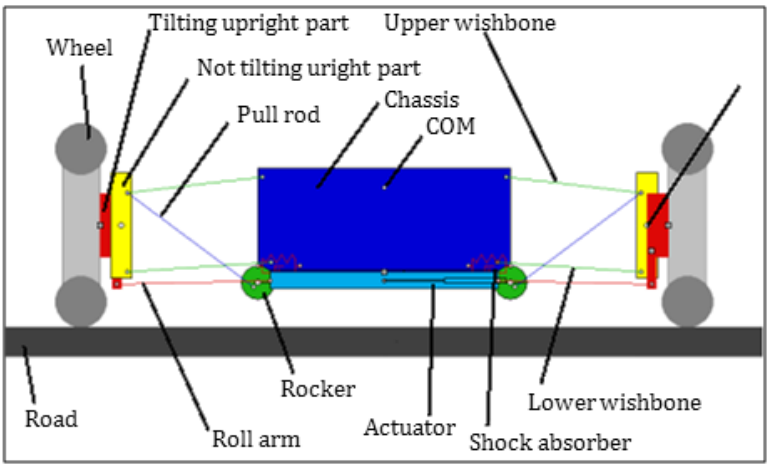

Figure 3.1: Mechanism with rolling upright: topology

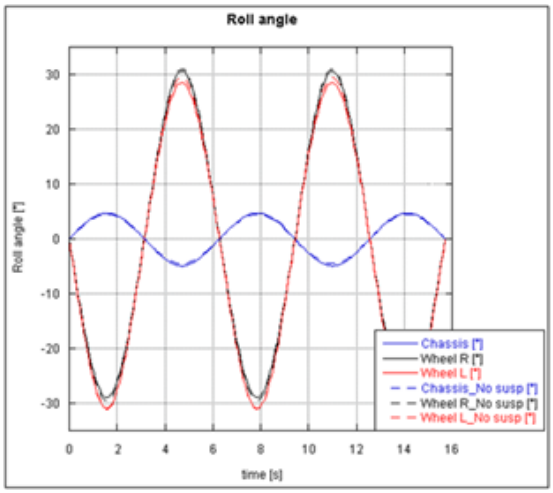

Figure 3.2: Mechanism with rolling upright: wheels and chassis roll

3.1.2 Four-bar linkage suspension with variable wishbone length

An alternative to the previous scheme is obtained by imposing wheel camber with a wishbone (upper or lower) with variable length (Fig. 3.3). Unfortunately, this topology exhibits the same result of the first one with regard to chassis roll direction. In addition, the construction is considered significantly complex. Therefore, this solution is discarded, too.

3.1.3 Four-bar linkage suspension with moving wishbone linking points

A third step is made analyzing the system of Fig. 3.4, which features a roll slide connected to inner joint of wishbones, on which it imposes a lateral translation. Also this system is affected by the problem of the opposite direction of chassis and wheels roll.

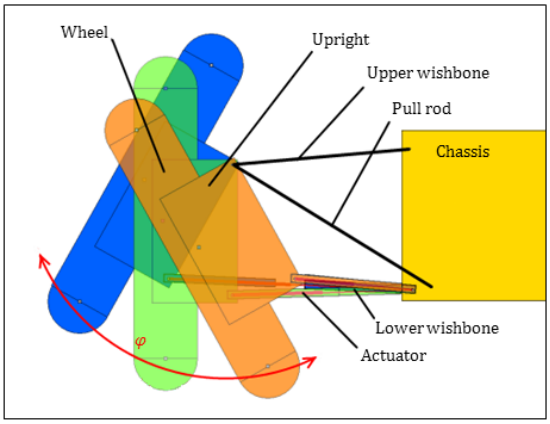

Figure 3.3: Roll actuated by a change in wishbone length

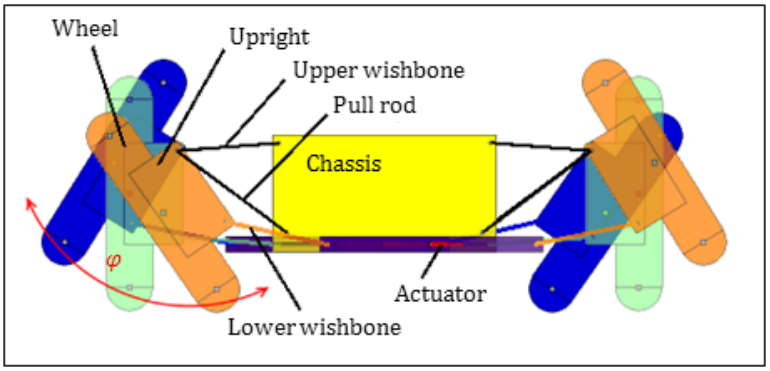

Figure 3.4: Roll actuated by a translation of wishbone inner joint

3.1.4 Four-bar linkage suspension with variable pull rod length

In this case, the roll is actuated by means of a change in pull rod length (Fig. 3.5). This topology does not suffer of the problem which afflicts the previous ones, however the roll movement is delayed by an excessive compression/extension of shock absorbers which are directly connected to pull rods. Moreover, the system seems to be particularly prone to COG rise.

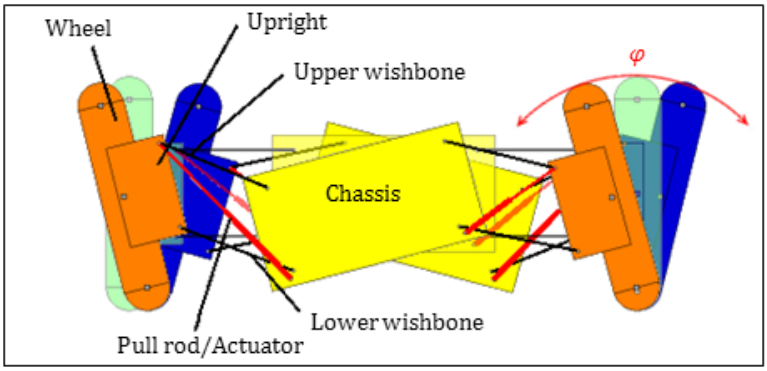

Figure 3.5: Roll actuated by a change in pull rod length

3.1.5 Four-bar linkage suspension with moving rocker

In the scheme of Fig. 3.6 the roll is actuated by lateral translation of rockers, which are carried by a roll slide. The camber is transmitted to the uprights by means of pull rods (or push rods). This mechanism offers indeed an advantage in construction due to its simplicity, and proves to perform well according to chosen functional requirements: in fact, finding a combination of member lengths so that chassis and wheel camber have the same sign is not difficult; results in terms of changes in COG height and track, as well as the magnitude of chassis lateral displacements, are quite changeable depending on the particular set of dimensions chosen. In general, in tested configurations, the shock absorbers do not result particularly solicited during the roll phase, so overcoming the problem detected on the previous solution. Therefore, this scheme deserves to be investigated in a deeper extent, to find out a solution which possibly performs well according to all of the defined criteria.

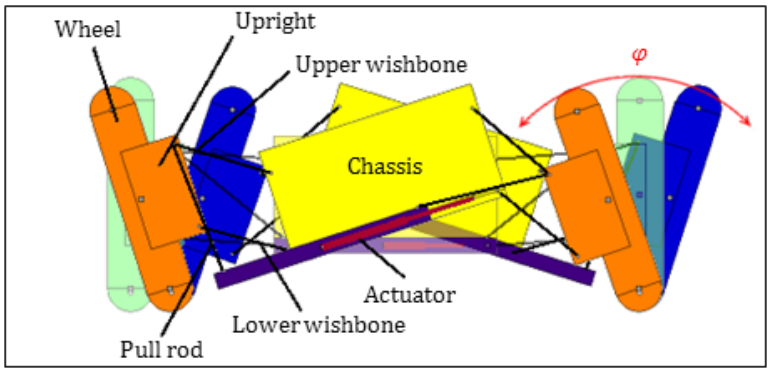

Figure 3.6: Roll actuated by rocker lateral translation

3.1.6 Six-bar linkage suspension with moving rocker

The concept of this topology comes from the purpose of improving the solution with four-bar linkage and moving rocker: this mechanism basicly features a greater number of design variables which can be changed in the pursuit of a better performing solution. Fig. 3.7 illustrates the layout of this solution: the roll movement is actuated by the same scheme of the previous solution, composed by a roll slide, a rocker and a push/pull rod. On the contrary, the suspension presents a vertical arm, which connects the lower and the upper wishbone, and is connected to the chassis by an upper arm. The tests performed on this solution produces results similar to the previous one. However, the purpose of exploiting the improvement opportunity given by a greater number of design variables suggests to study in deep this solution, by developing a more powerful synthesis strategy.

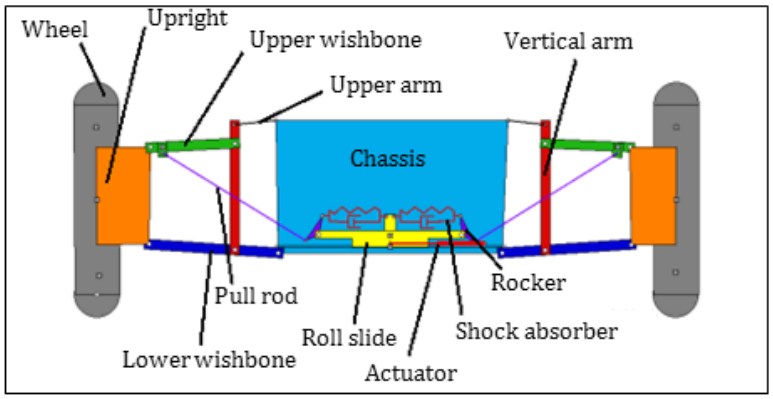

Figure 3.7: Six bar linkage with roll actuated by rocker lateral translation

3.1.7 Roll system: preliminary results

The described test method revealed some limitations due to its simplicity and its heuristic, trial and error approach: it was not possible to deduce apparent trends in performance indexes over the changes in values assigned to design variables. This can be motivated by the strong non-linearities related to system topologies and the considerable amount of design variables. On the contrary, the comparison between the six presented solutions proved to be useful to address a deeper synthesis process and to highlight some aspects to be taken into account. The solutions of Par. 3.1.5 and 3.1.6 are the best performing in the tests effectuated: among both of them, it was possible to find different candidate solutions with chassis and wheels rolling towards the same direction, and without a significant increase in COG height; additionally, both mechanism types do not present particular constructive problems. One more advantage: in tested mechanisms, rockers are not very solicited by roll actuation: this fact suggests that, with a targeted tuning, the interaction between roll and bump/rebound movements can be substantially limited. However, the suspensive performances were not analyzed during this preliminary test, and the two solutions proved to be able to produce different behaviours depending on the set of lengths assigned to members, regarding, for example, the entity of COG displacements and their sign. These reasons motivate the choice to find a new synthesis process capable of comparing the two topologies of Par. 3.1.5 and 3.1.6 by means of defined numerical indexes , and, at the same time, of finding out among them a best performing candidate mechanism (defined by a set of member lengths).

3.2 Dedicated multibody modelling

In the previous section a preliminary synthesis process was presented; as described, the simplicity of the test model and the heuristic approach limited quality and completeness of results. This suggested to set-up a different, more targeted synthesis strategy, with the aim to compare in quantitative terms the two selected topologies, by pointing out which one is able to produce the most complete set of best performing individuals, according to the design guidelines defined in Chapter 2. Among these individuals, it will be possible to choose the best trade-off to be constructed. The implementation of this second step of synthesis process requires the definition of a multibody model to solve kinematics of candidate mechanisms: this section focus on its definition. According to the overall purpose, the functional design of the multibody model can be done to pursuit the following functional requirements:

- it must be oriented to numerical results, so that it can be addressed by an optimization algorithm;
- it must be flexible enough to allow a custom definition of convenient performance indexes;
- it must be sufficiently fast in providing results, so that it can be used in large iterations.

On the contrary:

- the flexibility on topology definition is not needed: two different models must be fully dedicated to two topologies to be optimized, so simplifying their numerical definition;
- there is no need of a user friendly interface;
- there is no need of immediate, real time testing.

According to the listed requirements, the model is implemented in Matlab code, in order to profit of its native numerical capabilities, ease of programming, and concentrate on the mechanical problem. Moreover, a method must be chosen to define the kinematic of mechanisms: due to its ease of implementation in numerical codes and of constraint management, and to the reduced amount of variables needed in mechanism description, which results in a faster solving, the *Natural Coordinate Method* is used. Before describing the two models, a brief theoretical resume is made.

3.2.1 The Natural Coordinate Method

The modelling of a multibody system requires the selection of a method of kinematic definition. Among the three main options, i.e. the *Relative coordinates*, the *Reference point* and the *Natural Coordinates* Methods, the latter one is chosen. This choice is motivated by the following comparison. The Relative Coordinates Method defines ”the position of each element in relation to the previous element in the kinematic chain by using the parameters or coordinates corresponding to the relative degrees of freedom allowed by the joint linking these elements” [6]. This results in a reduced number of dependent coordinates (equal to the number of DOF's in case of open chains), which furthers the numerical efficiency of the method. In addition, the degrees of freedom allowed by joints are directly considered in the mathematical formulation, and so easily controlled by laws imposed by motors/actuators. On the contrary, by a mathematical point of view, the matrices which are generated by constraint equations derived by the vector closure condition of kinematic loops: therefore, a pre-processing phase is required. The corresponding matrices, although small, are full, and this aspect disadvantages the computational time. Last, since the absolute position of each body is a function of the positions of other elements, its evaluation requires a post-processing elaboration. Therefore, this method is considered to be not as flexible as required. The Reference Point Coordinates Method overcomes this difficulty by directly defining the absolute position and orientation of each body by specifying the Cartesian coordinates of its COG and all necessary angles, referenced with respect to a Global Frame. One more positive aspect is that each joint type is described by a precise equation type. In addition, constraint equations are defined at a local level, since they consider only the coordinates of bodies connected by the sole joints they refer to: as a result, matrices that appear in the equation of motion are sparse and can be fast managed by dedicated algorithms. A drawbacks reside in a larger number of variables than in relative coordinates method, so resulting in a loss of computational efficiency. The Natural Coordinate Method represents a good trade off between computational efficiency and model simplicity: each body is described at least by

two points (*basic points*) in planar problems, located in joints, whose Cartesian coordinates define both position and orientation of the body. Angular variables are no further needed. In spatial problems, a combination of three points/unit vectors must be adopted for each body. Since, in mechanisms, basic points are shared by at least two bodies, a reduced number of variables is needed, resulting to be an average between the number of relative coordinates and of reference point coordinates. A basic point must be located at each rotational ("R") joint: this guideline simplifies the definition of constraint equations, since in every R joint congruency is automatically imposed by the sharing of the basic point between two bodies. Additional constraint equations are derived from:

1. Rigid body condition
2. Some kinematic joints

As an example, the constraint equations of the system of Fig. 3.8 [6] can be expressed:

$$\begin{cases} (x_1 - x_A)^2 + (y_1 - y_A)^2 - L_2^2 = 0 \\ (x_2 - x_1)^2 + (y_2 - y_1)^2 - L_3^2 = 0 \\ (x_2 - x_B)^2 + (y_2 - y_B)^2 - L_4^2 = 0 \\ \dfrac{x_3 - x_1}{x_2 - x_1} - \dfrac{y_3 - y_1}{y_2 - y_1} = 0 \\ (x_2 - x_1)(x_{3-x_B}) + (y_2 - y_1)(y_3 - y_B) - L_3 L_4 \cos\phi = 0 \end{cases} \tag{3.1}$$

The first three equations impose the rigid body conditions to members 2, 3 and 4 of Fig. 3.8, respectively, while the fourth imposes the point 3 to be aligned with points 1 and 2. The fifth equation imposes the angle between bodies 3 and 4 to be constant.

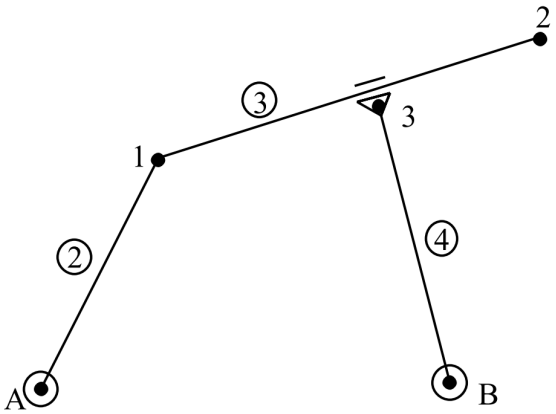

Figure 3.8: Example of mechanism solved with Natural Coordinates

For a deeper theoretical description of the Natural Coordinates Method see [6]. Any further comment necessary to understand the details of its application to the specific case study is demanded to the following description of the multibody model. The Natural Coordinates Method is chosen because of the reasonable number of variables needed in the problem definition, together with the ease of formulation of constraint equations.

3.2.2 Roll system modelling

As cited, both the four-bar and the six-bar suspension systems were modelled by implementing equations given by the Natural Coordinates Method in Matlab code. The modelling of the six-bar linkage mechanism will be described first, being the four-bar linkage construction straightforward. Since the layout is exactly the same both on front and rear axle, only one of them needs to be modelled to fully define the kinematic problem. Basic points are chosen according to Fig. 3.9. The R-L suffixes which appear on point designation simply indicate the side of points, therefore in the following they will be sometimes omitted, thus indicating homologous points on both sides. Fig. 3.11 reports the definition of the global frame: the position of the origin can conveniently be fixed in the longitudinal symmetry plane of the mechanism, so simplifying the definition of basic point positions; however, it does not influence the computational phase. Points LA, LB, RA and RB define the chassis, members $\overline{BC}$ are the upper arms, $\overline{BD}$ the vertical arms, $\overline{AE}$ are the lower wishbones, $\overline{BFH}$ are the upper wishbones, $\overline{FHE}$ are the uprights, while members $\overline{WR}$ represents the wheel radius; $\overline{HI}$ are the push/pull rods and, in the end, member $LI - RI$ is the roll slide. It is worth noting that points R represents the contact points between wheels and road plane: therefore, this model uses a wireframe wheel representation, so neglecting the radius r_t of the toroid section. The model is completed by introducing two unit vectors Lw and Rw to define the orientation of wheel axis (Fig. 3.10).

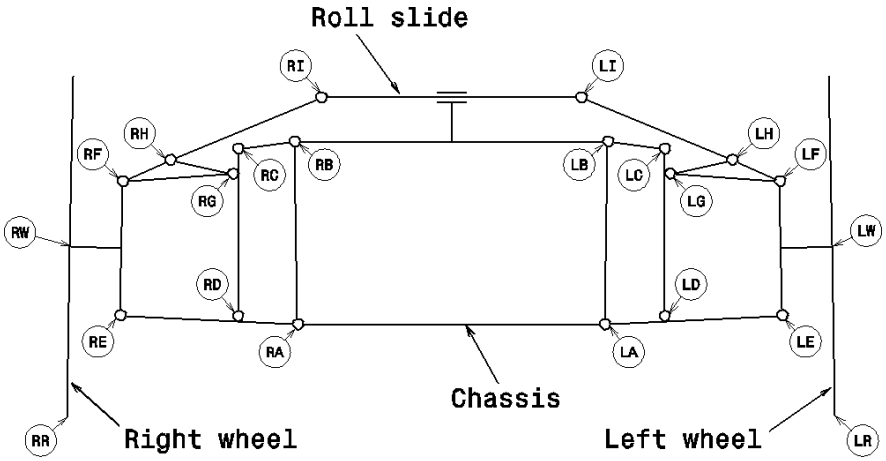

Figure 3.9: Six-bar linkage mechanism: basic points

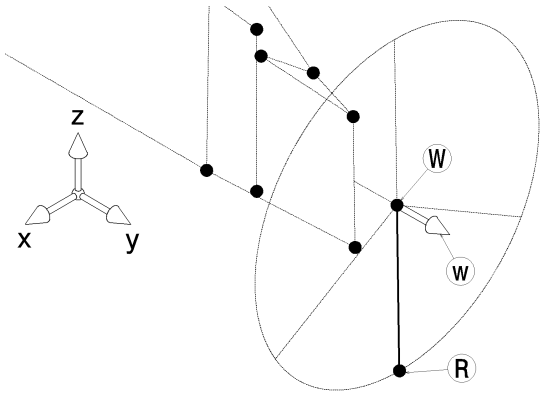

Figure 3.10: Definition of wheel axis by unit vectors

Even if the mechanism is not planar by a constructive point of view (i.e. the x coordinate is

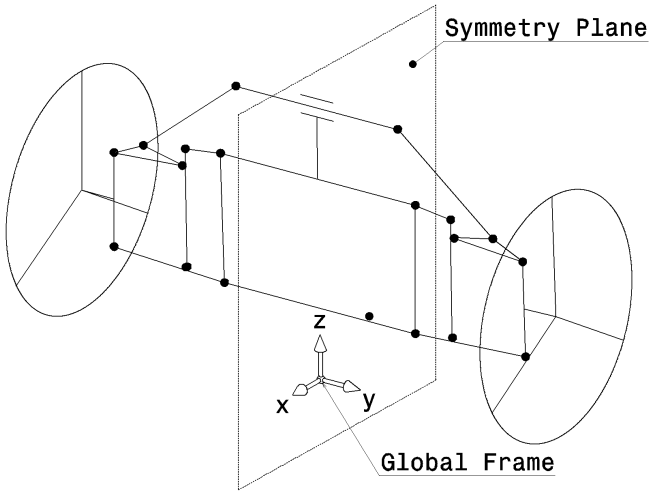

Figure 3.11: Six-bar linkage mechanism: definition of the global frame

not the same for all points), it can be considered as two-dimensional with regard to kinematics, since all displacements lie in a plane normal to the X direction: this leads to a considerable simplification in the numerical modelling, since all constraints can be expressed by considering only the y and z coordinates, for each basic point. By this hypothesis, the whole system features one single DOF, like easily confirmed by Grubler's rule.

The kinematic of the mechanism can be solved by defining two sets of equations: the first one is composed by constraint equations, which assures the congruency in each mechanism position; the second one contains the motion requirement equations, used to define the position to be reached by the mechanism. Given a generic mechanical system $P = \{\alpha_1, \ldots, \alpha_m\}$, described by m natural coordinates $\{\alpha_1, \ldots, \alpha_m\}$, the system of constraint equations is generally defined as follows [7]:

$$\begin{cases} \phi_1(\alpha_1, \ldots, \alpha_m; l_1, \ldots, l_n) = 0 \\ \vdots \\ \phi_{m-d}(\alpha_1, \ldots, \alpha_m; l_1, \ldots, l_n) = 0 \end{cases} \tag{3.2}$$

where $\alpha_1, \ldots, \alpha_m$ are the m natural coordinates necessary to define the system, $l_1, \ldots, l_n$ are the geometric dimensions of the bodies used to impose rigid body conditions, and d is the number of degrees of freedom. The general form of motion requirement equation is:

$$\begin{cases} \psi_1(\alpha_1, \ldots, \alpha_m; r) = 0 \\ \vdots \\ \psi_k(\alpha_1, \ldots, \alpha_m; r) = 0 \end{cases} \tag{3.3}$$

where $r = r(s) = \{r_1(s), \ldots, r_i(s)\}$ is a vector used to define i contemporary motion requirements, for a certain number of system states s. Fig. 3.12 depicts how the solution process of the kinematic problem is numerically implemented in this study: given a generic mechanical system in its initial position $P(0) = P_0 = \{\alpha_1(0), \ldots, \alpha_m(0)\}$, described by the set of values $\{\alpha_1(0), \ldots, \alpha_m(0)\}$, a new system position P_r must be found which respects both congruency (ϕ equations) and motion requirements (ψ equations). The solution is seek by iteratively imposing an i^{th} trial displacement field $\Delta P_{r_i} = \{\Delta\alpha_{1_i}(r), \ldots, \Delta\alpha_{m_i}(r)\}$, thus obtaining an i^{th} candidate configuration $P_{r_i} = P_0 + \Delta P_{r_i} = \{\alpha_{1_i}(r), \ldots, \alpha_{m_i}(r)\} =$

$\{\alpha_1(0) + \Delta\alpha_{1_i}(r), \ldots, \alpha_m(0) + \Delta\alpha_{m_i}(r)\}$. Then, trial values $\{\alpha_{1_i}(r), \ldots, \alpha_{m_i}(r)\}$ are imposed in equations ϕ and ψ, so calculating errors ϵ_ϕ and ϵ_ψ. It must be noted that the system composed both by constraint and motion requirement equations contains $m - d + k$ conditions, while the total amount of variables is m. Therefore, only if $k = d$ and the motion requirements can be exactly and at the same time achieved by mechanism, then the whole system can be exactly solved. Generally, $k \neq d$ and/or desired motion requirements cannot be exactly produced by the mechanism. Therefore, by a theoretical point of view, only constraint equations must be equally satisfied (so preserving congruency), while, with regards to motion requirement equations, the error ϵ_ψ should be minimized. Since the resolution of the kinematic problem is numerically implemented, the respect of ϕ equations is not exact: this problem must be solved by introducing a conveniently small threshold value $\epsilon_{\phi thr}$ and imposing the criterion:

$$\epsilon_\phi < \epsilon_{\phi thr} \tag{3.4}$$

that *must* be satisfied for configuration acceptance. The ϵ_ψ error is used in a similar condition,

$$\epsilon_\psi < \epsilon_{\psi thr} \tag{3.5}$$

but in this case the threshold value $\epsilon_{\psi thr}$ is greater, since the target is less strict, i.e. to minimize an error in system position. However, the numerical value of $\epsilon_{\psi thr}$ must be carefully chosen on the basis of the accuracy needed in system motion control and of computational time considerations. Referring again to Fig. 3.12, Eq. 3.4 and 3.5 are used to compose the acceptance criteria $f < f_thr$ which appears in the boolean block: only if it is fully satisfied, the trial displacement field $\Delta P_{r_i} = \{\Delta\alpha_{1_i}(r), \ldots, \Delta\alpha_{m_i}(r)\}$ and the candidate configuration it defines, P_{r_i}, can be accepted as the solution P_r to the kinematic problem. Otherwise, another $P_{r_{i+1}}$ configuration must be tested. To avoid infinite loops, a maximum value i_{max} must be imposed

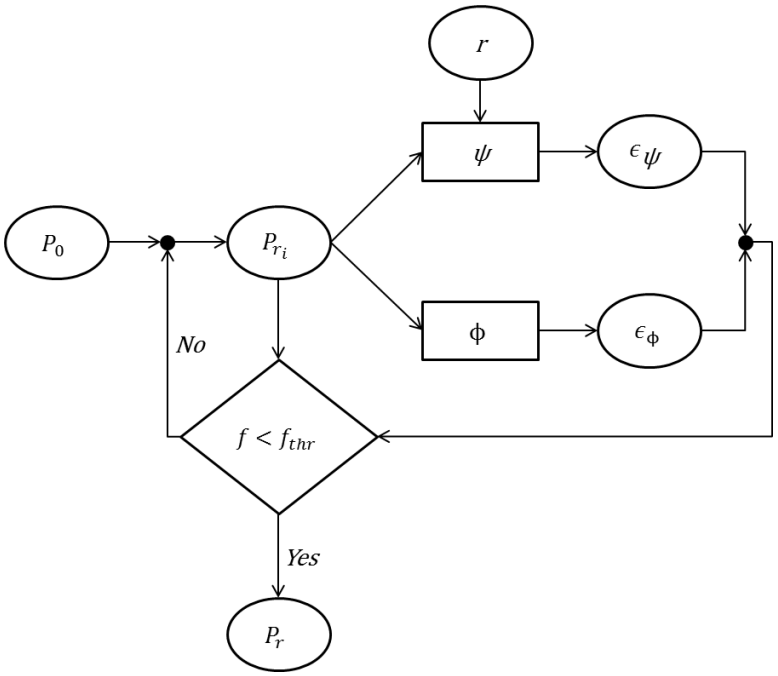

Figure 3.12: Solution algorithm to kinematic problem

to iterations. One last comment on the algorithm of Fig. 3.12 is due: in its final implementation, some of congruency constraints are extracted from ϕ equations and directly implemented in the definition of the displacement field $\Delta P_{r_i} = \{\Delta\alpha_{1_i}(r), \ldots, \Delta\alpha_{m_i}(r)\}$. As a consequence,

not all components of ΔP_{r_i} are independent. Additionally, these extracted conditions are intrinsically and identically satisfied, so producing a better solution with a minor computational effort.

In the mechanism of Fig. 3.9, $m = 48$, since each one of 22 basic points and 2 unit vectors (Fig. 3.10) is described by two coordinates (in case of unit vectors, they represent two Cartesian components). As already cited, $d = 1$, therefore a total amount of 47 constraint equations are necessary. In the present case, the rigid body condition for all members of the six-bar linkage, push/pull rod, upright and $\overline{WR}$ member, is formulated as follows:

$$(y_P - y_Q)^2 + (z_P - z_Q)^2 - [(y_{P_0} - y_{Q_0})^2 + (z_{P_0} - z_{Q_0})^2] = 0 \tag{3.6}$$

where P, Q indicates the actual positions of basic points of a generic body, and P_0, Q_0 their starting positions. It is interesting to note that in Eq. 3.6, the explicit member length (as used, for example, in Eq. 3.1), is replaced by the sum of quadratic differences between the coordinates of two basic points in their starting positions. By this alternative definition, the specification of initial point positions is sufficient to impose the rigid body constraint, instead of member length. A total amount of 22 conditions are imposed as in Eq. 3.6 and represented by bold lines in Fig. 3.13.

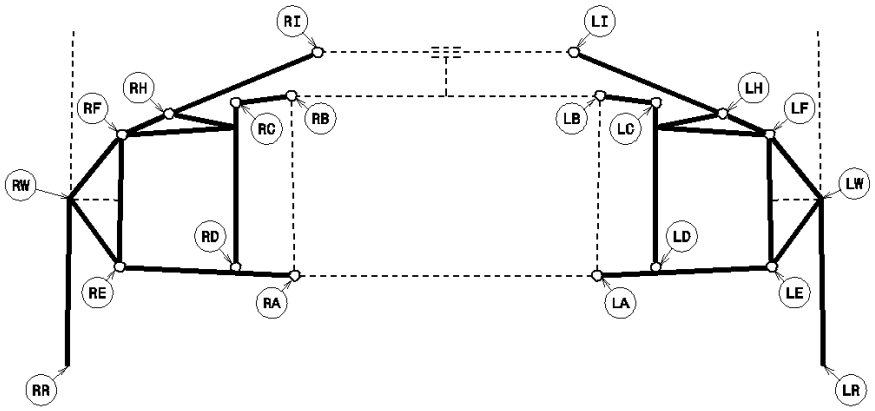

Figure 3.13: Rigid body conditions imposed by Eq. 3.6

Two different types of equation must be imposed to unit vectors to preserve the congruency of the wheel assembly: since they are defined as a couple of components, $w = [w_y, w_z]$, the first condition must preserve the norm; this can be done by using the dot product:

$$w \cdot w_0 - 1 = 0 \tag{3.7}$$

where w and w_0 are the unit vector in the actual and in the starting configuration, respectively. The second type of equations to be imposed concerns the (planar) orientation of unit vectors: the angle they form with members $\overline{EF}$ and $\overline{WR}$ must be constant during movements (i.e. wheel spin axis must retain its orientation with respect to upright, and be constantly normal to wheel radius); again, the dot product provides the right formulation:

$$\begin{aligned} &w \cdot (F - E) - w_0 \cdot (F_0 - E_0) = 0 \\ &w \cdot (W - R) = 0 \end{aligned} \tag{3.8}$$

with the usual notation. A total of 6 constraints are produced by Eq. 3.7 and 3.8.

Then, the vertical component of contact points must not change:

$$z_R - z_{R_0} = 0 \tag{3.9}$$

imposed on both sides. A total of 30 constraints is imposed. Other 17 positions are needed: they are included, as above mentioned, in the definition of the field displacement.

First, points D and G, which are aligned to lines $\overline{AE}$ and $\overline{CD}$ respectively, undergo to the following formulation:

$$\begin{aligned} D &= (1-\rho_D)A + \rho_D E \\ G &= (1-\rho_G)D + \rho_G C \end{aligned} \tag{3.10}$$

with:

$$\begin{aligned} rho_D &= \frac{D_0 - A_0}{E_0 - A_0} \\ rho_G &= \frac{G_0 - D_0}{C_0 - D_0} \end{aligned} \tag{3.11}$$

where subscript 0 indicates, as usual, initial positions. By this imposition, actual coordinates of points D and G on both sides of mechanism intrinsically respect congruency of vertical arm and lower wishbone, as above highlighted. Since Eq. 3.10 are in vectorial form, each of them imposes two scalar conditions, for a total of 8, considering points D and G on both sides.

The chassis congruency is respected by introducing two direction cosines u_{y_c} and u_{z_c}, which represent the rotation of the chassis body around x axis, and a vertical displacement Δz_c, which are used to define the displacements of basic points A and B, on both sides, as a roto-translation:

$$\begin{cases} y_P = y_{P_0} u_{z_c} - z_{P_0} u_{y_c} \\ z_P = \Delta z_c + y_{P_0} u_{y_c} + z_{P_0} u_{z_c} \end{cases} \tag{3.12}$$

where y_P and z_P are two components of the generic point P of the chassis. Therefore, three additional parameters u_{y_c}, u_{z_c} and Δz_c allow for the introduction of 8 conditions, to which the one representing the unitary Euclidean norm of director cosines must be added (this one implemented in the ϕ equations):

$$u_{y_c}^2 + u_{z_c}^2 - 1 = 0\,. \tag{3.13}$$

Last conditions concern basic points I: their distance with respect to the chassis must be constant, so assuring, by a mathematical point of view, the respect of the prismatic joint which connects the roll slide to the chassis. In addition, the rigid body condition of the roll slide must be imposed. To embed this positions on the displacement vector, one more variable is introduced, Δy_{rs}, which represents the lateral translation of the roll slide with reference to the chassis. Consequently, four equations are definitely needed to assure the congruence of the whole mechanism, and the are expressed in the form:

$$\begin{aligned} y_P &= (y_{P_0} + \Delta y_{rs}) u_{z_c} - z_{P_0} u_{y_c} \\ z_P &= \Delta z_c + (y_{P_0} + \Delta y_{rs}) u_{y_c} + z_{P_0} u_{z_c} \end{aligned} \tag{3.14}$$

where P, again, is considered to be a generic basic point. Eq. 3.14 produce the four condition needed, and, as already stated, they are identically satisfied. The four-bar linkage modelling is straightforward: Fig. 3.14 illustrates basic points choice. In this case, the total amount of natural coordinates is 40, taking into account two unit vectors which define wheel axis orientation. The modelling of wheels, chassis and roll slide is identical to six-bar linkage case. G basic points are aligned to A and B, and this condition is imposed with a vectorial expression alike Eq. 3.10 and 3.11: in this case, only 4 conditions are produced instead of 8, due to the suppression of D basic points. With respect to the previous case, other 4 conditions are missed in ϕ equations, since only 18 members are constrained instead of 22.

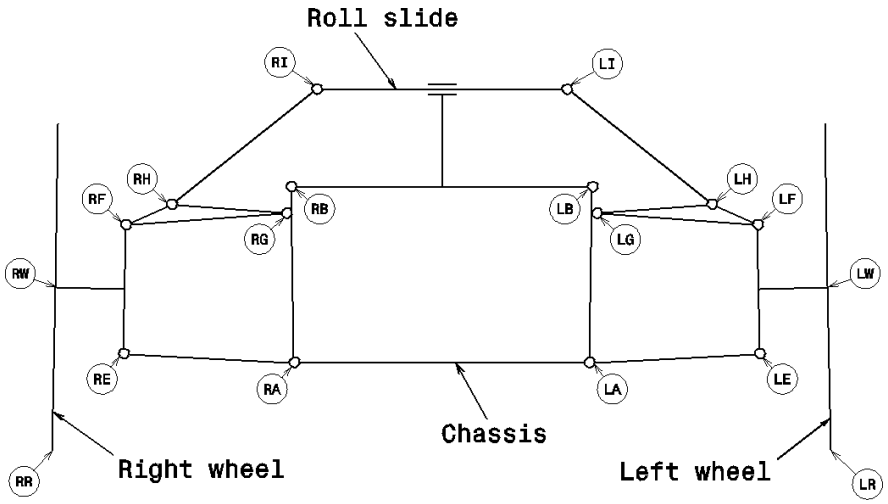

Figure 3.14: Four-bar linkage mechanism: basic points

3.3 Roll system optimization

This section describes the numerical optimization carried out on four and six-bar linkage mechanisms. The target of this phase is to compare two topologies in a deeper extent than during the preliminary analysis described in Section 3.1, pointing out, in quantitative terms, which of them can produce the most performing mechanisms with regards to design guidelines presented in the introduction to this Chapter. First, a general description of the adopted optimization scheme will be presented, then its particular application to the present case study.

3.3.1 Adopted optimization scheme: general description

The scheme of Fig. 3.15 represents the kinematic optimization phase adopted in this work. The

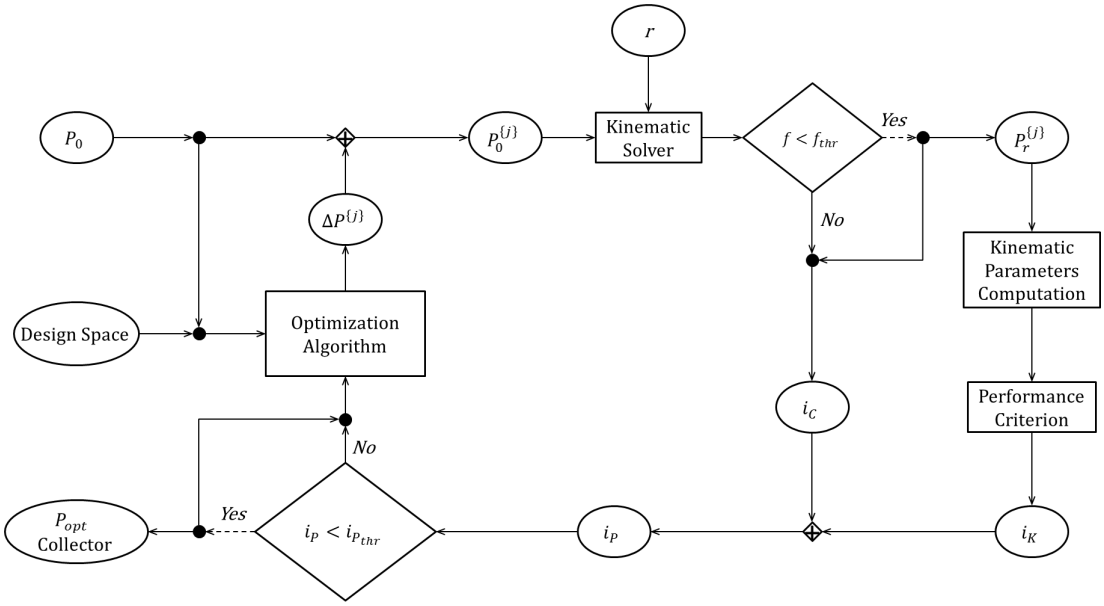

Figure 3.15: Kinematic optimization scheme

key block of this diagram is the Optimization Algorithm that, managing the starting mechanism

configuration P_0 and the chosen Desin Space ("D_S") as inputs, must provide a set or a unique P_{opt} solution as an output, on the basis of a defined Performance Criterion (P_C). In detail, P_0 represents a first, imposed trial mechanism in an initial state (or configuration) $r = 0$, which is defined by $\{\alpha_1(0), \ldots, \alpha_m(0)\}$, i.e. a vector composed by the values of natural coordinates of basic points, evaluated in the state $r = 0$. This mechanism is used by the Optimization Algorithm to generate, at each iteration j, a new candidate mechanism $P_0^{\{j\}}$ in its initial configuration, by varying a set of basic point positions by adding the vector $\Delta P^{\{j\}} = \{[\Delta\alpha_v]\}$; therefore, $P_0^{\{j\}} = \{[\alpha_v + \Delta\alpha_v], [\alpha_w]\}$, where basic point coordinates are symbolically grouped in a modified subset ("v" subscript) and in an unchanged one ("w" subscript). The number of elements and the composition of vector $[\Delta\alpha_v]$, which defines how many and which basic points can be transformed, is established by the Design Space, D_S. Please note that if only basic points positioned in rotational joints are translated, the local congruency of the new mechanism is automaticly satisfied. $P_0^{\{j\}}$ and the motion requirement vector r, that must be chosen according to optimization targets, are used as inputs to the Kinematic Solver described in Par. 3.2.2 (Fig. 3.12), which imposes the transformation $\Delta P_r^{\{j\}} = \{\Delta\alpha_1^j(r), \ldots, \Delta\alpha_m^j(r)\}$ to $P_0^{\{j\}}$ to satisfy the chosen motion requirements through the configuration $P_r^{\{j\}}$. It is essential to distinguish vectors $\Delta P^{\{j\}}$ and $\Delta P_r^{\{j\}}$: both imposes translations to basic points but the first one *generates a new mechanism*, the second one is used to *move it*. An important consideration must be committed to outputs of the Kinematic Solver block. The scheme of Fig. 3.15, unlike it is depicted in Fig. 3.12, represents the boolean block $f < f_{thr}$ out of the Kinematic Solver: this choice is aimed to distinguish its output on the basis of the reported acceptance criterium. In detail: if a solution $P_r^{\{j\}}$ which respects motion requirements is found within the an acceptable range of iterations, both $P_r^{\{j\}}$ and its conformity index i_C are produced as outputs, otherwise only the index i_C can be used to address the following optimization steps. Since the first event could not verify, the corresponding arrow in Fig. 3.15 is dotted. One further comment on Kinematic Problem solution: Motion Requirement equations defined by r, as specified in Par. 3.2.2, generally cannot be exactly satisfied by a theoretical point of view, being this condition achieved only under particular conditions; therefore, $P_r^{\{j\}}$ is usually regarded as the solution which identically satisfy constraint equations ϕ and at the same time minimizes the error ϵ_ψ in ψ solution. Then, ϵ_ψ is used to address the optimization algorithm in the search for the best mechanism. In the present case, a quite different approach is used: the number of motion requirement conditions exactly matches the number of system DOF's; in addition, the imposed requirements, as described in the following paragraph, are not strict but, on the contrary, they must be exactly matched. Therefore, a solution to be suited for final selection may identically satisfy both ϕ and ψ equations. By a numerically point of view, this implies to choose similar values, of even the same, for threshold error values ϵ_ϕ and ϵ_ψ. On this basis, addressing the Optimization Algorithm is a bit more complex than usual, and is done by using two different indexes:

- conformity index i_C, which represents the capability of $P_0^{\{j\}}$ of producing the imposed motion requirements, which is mandatory;
- kinematic performance index i_K, which results from a defined Performance Criterion applied to conveniently chosen Kinematic Parameters, which are calculated from $P_r^{\{j\}}$ configuration.

Therefore, index i_C is used to evaluate candidate mechanism compliance, so to select only the suitable ones: if the condition $f < f_{thr}$ is not respected, i_C will be conveniently set to a very high value (in relative terms) and will cause the solution to be rejected. Otherwise, if $P_r^{\{j\}}$

exists, $i_C = \epsilon_\phi + \epsilon_\psi$ and i_K will be added to obtain an overall performance index i_P. Finally, if the computed i_P is smaller than a defined $i_{P_{thr}}$, $P_0^{\{j\}}$ is stored as an optimal solution in P_{opt} Collector, otherwise it is discarded. If a multi-objective optimization is performed or a global optimal solution is seek, i_P is used to address the Optimization Algorithm in the search for other optimal solutions inside the Design Space: in both cases, P_{opt} Collector contains a set of best performing solutions but, in the case of the multi-objective optimization, the output will be composed by the array of not fully dominated solutions, while in the other case only the best solution will be chosen.

3.3.2 Specific implementation

This section describes the specific implementation of the general optimization scheme (described in Par. 3.3.1) to the roll system. The choice of a starting configuration, a Design Space, a Performance Criterion and an Optimization Algorithm must be carried out. First, targets must be considered; as already cited, they are defined according to dynamical aspects (Chapter 2) and to the preliminary kinematic analysis (Section 3.1) as follows:

- to maximize the lateral translation of the center of gravity of the chassis during the roll phase, and not to introduce significant rises in its height
- the roll movement of the chassis must be in the same direction of wheel camber, so providing a roll feedback similar to motorcycles
- the change in track must be minimized to limit the scrub during the roll phase.

In addition:

- this analysis must be suitable to compare four and six-bar topologies in quantitative terms.

The last requirement is considered in the choice of the specific Optimization Algorithm, and will be later discussed. Other three targets must be translated in a suitable kinematic performance index i_K: this can be achieved by imposing to candidate mechanisms a series of movements which can be quantified through kinematic parameters, used in the definition of i_K. This means a vector $r =$ of motion requirements has to be chosen to drive mechanism displacements by constraining the unique DOF it features, i.e. by means of one condition that makes the system of equations $\phi + \psi$ iso-constrained. The way the system movement is commanded can be chosen by a pertinent definition of this equation: i.e. any of the variables which constitute the multibody model described in Par. 3.2.2 can be constrained to impose the motion. Alternatively, the imposition can be also made on indirect parameters. Since functional requirements are related to system behaviour during the roll phase, the calculation of conveniently defined kinematic parameters can be done in a finite number of system states, well distributed during a roll maneuver, i.e. each one corresponding to a different rolled position. It is worth noting that imposing the states by explicitly controlling one of variables used in the multibody model could lead to a bad performance assessment: in fact, the only reasonable choices consist in imposing a value to roll slide translation, or to chassis roll angle. In both cases, their relation with wheel roll angles apparently changes when a new candidate mechanism $P_0^{\{j\}}$ is tested: therefore, different candidates would be tested with the same, controlled roll slide translation or chassis roll angle, but with different wheel camber angles. A more rational choice is therefore to adopt a state vector r which commands the mean camber of wheels, so testing different mechanisms in very similar dynamical conditions. For this reason, the system state is imposed on an indirect

parameter which corresponds to camber mean value. First, camber of two wheels must be defined:

$$\begin{aligned} \varphi_L &= \arcsin z_{Lw} \\ \varphi_R &= \arcsin z_{Rw} \end{aligned} \tag{3.15}$$

where z_{Lw} and z_{Rw} are the components of left and right wheel unit vectors along z axis. Please note Eqns. 3.15 directly depend on already defined parameters, therefore they do not introduce any additional constraint. The motion requirement can be definitely imposed as:

$$\varphi_m = \frac{\varphi_L + \varphi_R}{2} = r_s \tag{3.16}$$

where r_s is an element of the motion requirement vector, and corresponds to one of the states (i.e. one of mean camber angle values) in which the kinematic parameters will be calculated. In the present application:

$$r = [6^\circ; 12^\circ; 18^\circ] \, . \tag{3.17}$$

By this choice mechanism performances are evaluated at three mean angles φ_m well distributed along the full camber field $[0^\circ; \sim 20^\circ]$.

Kinematic parameters to be used in the Performance Criterion are defined directly considering the functional requirements above reported: first two parameters are the lateral and vertical components of chassis COG (defined with reference to Global Frame of Fig. 3.11); the third one is track length; then, left and right parts of track c_l and c_r; the last one is chassis camber. COG position is not directly defined in the already described multibody model, therefore it must be introduced by means of two additional natural coordinates; the congruency will be automatically respected, since COG position is calculated after the kinematic problem is solved, by the following vectorial expression:

$$COG = \rho_{COG} \frac{LB + RB}{2} + (1 - \rho_{COG}) \frac{LA + RA}{2} \tag{3.18}$$

with:

$$\rho_{COG} = \frac{z_{COG_0} - z_{LA_0}}{z_{LB_0} - z_{LA_0}} \tag{3.19}$$

where the first subscript indicates the basic point to be considered, the second one that it must be evaluated in the starting configuration (please note that all values which compares in the definition of ρ_{COG} are known). Track length is evaluated as:

$$track = y_{LR} - y_{RR} \tag{3.20}$$

while its left and right part are:

$$\begin{aligned} c_l &= y_{LR} - y_{COG} \\ c_r &= y_{COG} - y_{RR} \, . \end{aligned} \tag{3.21}$$

Finally, chassis camber is defined as:

$$\varphi_c = \arcsin u_{y_c} \, . \tag{3.22}$$

The Performance Criterion is formulated as follows: first, a conveniently high penalty is set on all cost components if the sign of φ_c is opposite to the sign of the imposed $\varphi_{mean}(s)$, in order to exclude configurations that do not satisfy one of the cited functional requirements. Then, to measure changes in track and COG position, other kinematic parameters are evaluated in the three states above cited, and in the starting configuration, conventionally set in static trim.

Therefore, a vectorial cost function with three components can be constructed. The first one is given by:

$$c_{1roll} = \text{sign}\left[\Delta y_{COG}\left(s\right)\right]\left(\frac{c_l}{c_r}\right)^2 \tag{3.23}$$

where s indicates the state and $\Delta y_{COG}(s) = y_{COG}(s) - y_{COG}(0)$; as usual, the state 0 corresponds to the initial configuration. y_{COG} is the component along y axis given by Eq. 3.18. The first factor on the right side of Eq. 3.23 is inserted to have positive values for c_{1roll} when lateral translation and wheel camber point to opposite sides of curve. The second cost component is:

$$c_{2roll} = \text{sign}\left[\Delta z_{COG}\left(s\right)\right]\sum_s \left[\Delta z_{COG}\left(s\right)\right]^2 \tag{3.24}$$

with $\Delta z_{COG}(s) = z_{COG}(s) - z_{COG}(0)$ and the usual symbolism. Again, the sign function is inserted to control the sign of the cost component: positive values are produced when COG height rise during a roll maneuver. The third component is defined:

$$c_{3roll} = \left[\Delta track\right]^2 \tag{3.25}$$

where $\Delta track = track(s) - track(0)$ as usual. Finally, the vectorial cost function is:

$$c_{roll} = \left[c_{1roll}; c_{2roll}; c_{3roll}\right] \ . \tag{3.26}$$

Please note all components are defined in quadratic form to augment sensitivity during computation, especially in low c values area. Finally, conformity of candidate mechanisms is taken into account by introducing an "if" condition: in case of congruency violation during the solution of the kinematic problem, all c components are conventionally posed equal to c_{max}, which is a conveniently high constant value fixed on the basis of some dedicated trial optimizations, run with the target of determining a reasonable range for all of cost components.

The definition of a pertinent Design Space is fundamental to obtain profitable results by the optimization phase. As aforementioned, D_S defines how many and which basic points can be transformed during candidate mechanism generation. In addition, D_S defines a possible range for each component of the vector $\Delta P^j = \{[\Delta\alpha_v]\}$ that must be constrained, thus forcing each natural coordinate which defines the candidate mechanism $P_0^{\{j\}}$ to lie in a convenient volume of the physical space, so respecting constructive restrictions. Therefore, the optimization to be run is of constrained type. The D_S is chosen to be, in the case of the six-bar linkage, a 12 dimension space, composed as follows:

$$\begin{aligned} D_S = \{&[y_{LA}]\,;[z_{LA}]\,;[y_{LB}]\,;[z_{LB}]\,;[y_{LC}]\,;[z_{LC}]\,;[\rho_D]\,;[\rho_G]\,;[y_{LH}]\,;[z_{LH}]\,;[y_{LI}]\,;[z_{LI}]\} \end{aligned} \tag{3.27}$$

where brackets indicate that some constraints are imposed to each dimension by defining an upper and a lower max transformations, $\Delta\alpha_+^{\{j\}}$ and $\Delta\alpha_-^{\{j\}}$, with reference to the first candidate definition: i.e., each of ranges that appear in Eq. 3.27 will be defined as:

$$[\alpha^{\{j\}}] = \left[[\alpha_0^{\{j\}} - \Delta\alpha_-^{\{j\}}]; [\alpha_0^{\{j\}} + \Delta\alpha_+^{\{j\}}]\right] \tag{3.28}$$

where α indicates a generic natural coordinate.

The presented definition of D_S could lead to a misleading interpretation: only basic points on the left side seem to be transformed; points on the right side are actually transformed, but their positions are related to left side points positions, since mechanism symmetry with reference to XZ plane must be preserved in static trim. Therefore, a total amount of 24 natural coordinates are indeed transformed during candidate mechanism $P_0^{\{j\}}$ generation, but D_S features, as stated,

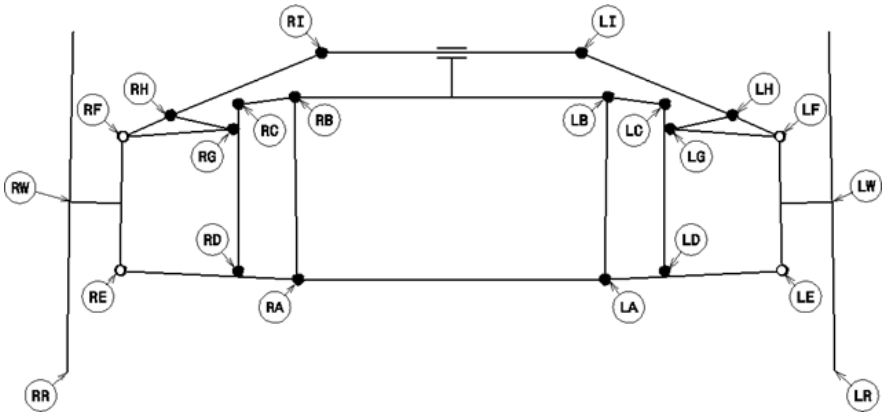

Figure 3.16: Design Space points for six-bar linkage

12 dimensions. Table 3.1 reports basic point coordinates and ρ_D and ρ_G values for the starting configuration, together with upper and lower limits on superscript and subscript. Black points on Fig. 3.16 correspond to D_S.

	LA	**LB**	**LC**	**LH**	**LI**	ρ_D	ρ_G
y [mm]	295^{310}_{290}	301^{310}_{290}	410^{410}_{390}	540^{540}_{510}	200^{250}_{180}	$0.34^{0.4}_{0.3}$	$0.86^{0.88}_{0.82}$
z [mm]	194^{210}_{194}	545^{550}_{530}	510^{510}_{495}	510^{540}_{510}	680^{740}_{680}		

Table 3.1: P_0 basic points and their limits for six-bar linkage mechanism

In four-bar linkage optimization, design space variables are reduced to 8: the Design Space D_S is reported in Table 3.2, and involved points are depicted in Fig. 3.17. Limits of homologous points are set to be equal in six and four-bar linkages, in order to have a fair comparison between two topologies. Points E and F do not undergo to optimization, in order to respect some constructive constraints related to upright design.

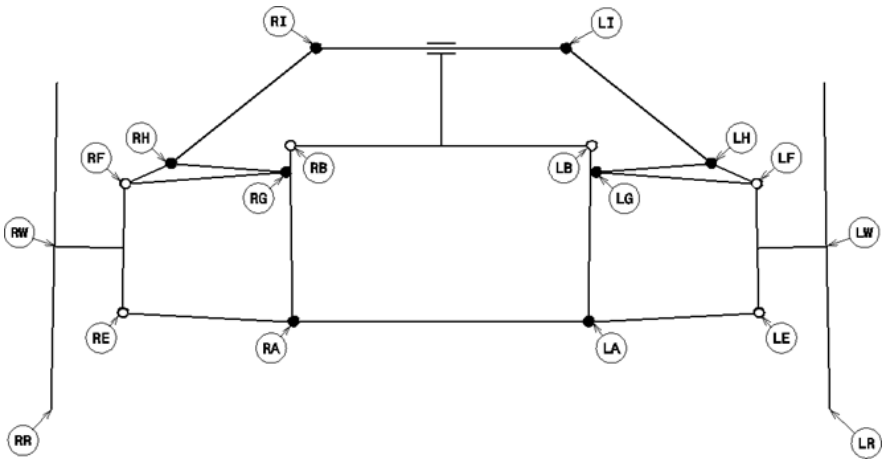

Figure 3.17: Design Space points for four-bar linkage

	LA	LB	LH	LI
y [mm]	295^{310}_{290}	301^{310}_{290}	540^{540}_{510}	200^{250}_{180}
z [mm]	194^{210}_{194}	545^{550}_{530}	510^{540}_{510}	680^{740}_{680}

Table 3.2: P_0 basic points and their limits for four-bar linkage mechanism

The last step to run optimizations is the choice of the specific Optimization Algorithm. The purpose of this phase is not only to point out a profitable solution, but also to compare which of two topologies is to be generally considered the best performing one in relation to the present application. The problem to be solved is characterized by a 12-dimensional and a 8-dimensional design space, and the performance criterion is expressed by a 3-dimensional vectorial function: due to the presence of more than one objective and of reasonable non-linearities, more than one optimal solution is expected to exist. Therefore, the best topology is not expected to produce a single, best performing candidate mechanism, but to provide the best set of well performing solutions, each of them differently ranked with regards to three objectives. The algorithm to be used must provide an overall feedback of the general behaviour of two topologies with regards to defined objectives, by producing a set of not fully dominated candidates; in addition, it must be capable of searching for global minima, without stopping inside basins of attraction. For the present case study, the *Multi-objective Genetic Algorithm* "gamultiobj" natively implemented in Matlab is used, since it is considered to be the best trade-off in terms of:

- capability of producing a set of not fully dominated solutions, by automaticly searching for the Pareto Front;
- capability of avoiding to stop inside basins of attraction;
- ease of implementation, by natively supporting the use of vectorial performance criteria.

For a complete description of the algorithm see [8].

3.3.3 Results

This section describes the results of the optimization phase, focusing on the comparison between four-bar and six-bar linkage performances according to the defined criteria. Due to the larger number of design parameters, 12 against 8, of six-bar linkage solutions are expected to overtake four-bar mechanisms in performances, however, only the analysis of results can confirm and quantify the difference in behaviour of two topologies. The performance criterion is computed in three different states, defined by mean roll angle Δ_{mean} values of $6°$, $12°$ and $18°$. Fig. 3.18 compares the Pareto fronts obtained by the optimization of both four and six-bar linkage mechanisms, while Fig. 3.19, 3.20 and 3.21 are the projections on three coordinate planes. The genetic algorithm produced a 63 point Pareto front for six-bar linkage, and a 42 point front for four-bar linkage. As expected, the first topology is capable of producing the wider population of optimal candidate mechanisms, and four-bar individuals are generally dominated by a large set of six-bar mechanisms, according to the defined performance criteria. A few exceptions are represented by four-bar individuals in the lower zone of Fig. 3.19, capable of providing smaller changes in track length, during a roll maneuver. On the contrary, the six-bar linkage topology reveals to be capable in producing best candidates both according to c_{1roll} and c_{2roll} indices, related to lateral and vertical displacements of the center of gravity.

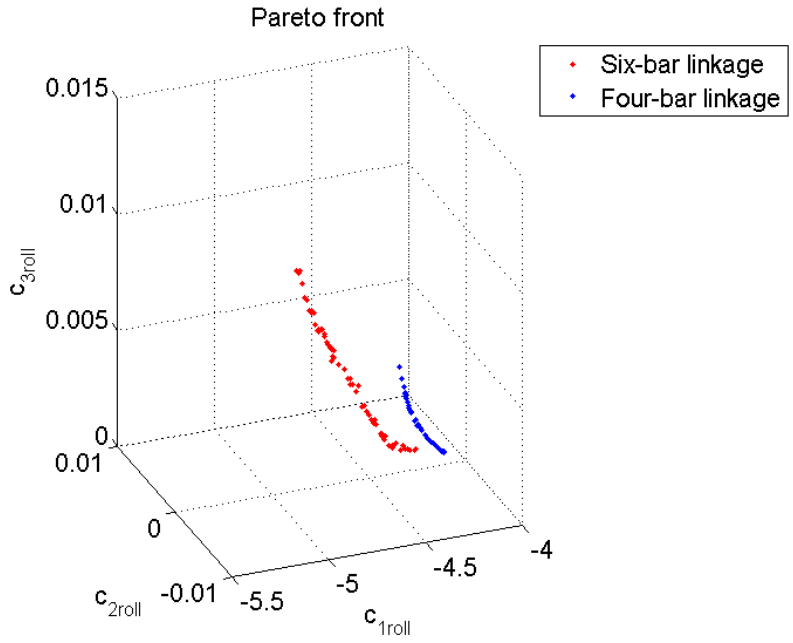

Figure 3.18: Pareto front for four and six-bar linkage mechanisms

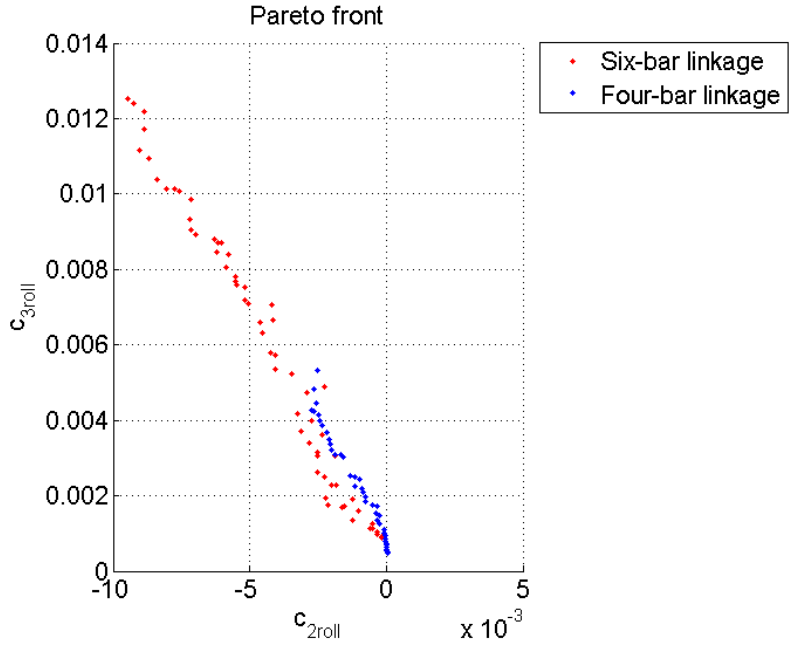

Figure 3.19: Pareto front projection on $c_{2roll} - c_{3roll}$ plane

Fig. 3.19, 3.20 and 3.21 depict how the internal points of the red front perform better than most four-bar candidates. However, due to the small number of operative points tested (i.e. the set of states used in performance computation), the components of the objective function c_{1roll}, c_{2roll} and c_{3roll} must be regarded as synthetic performance indices: therefore, the behaviour of remarkable candidates should be studied at a deeper extent before choosing the solution to be developed. Some solutions of both topologies are tested by performing a full roll maneuver in the range $0 - 20°$, with a resolution of $1°$, and calculating following kinematic parameters:

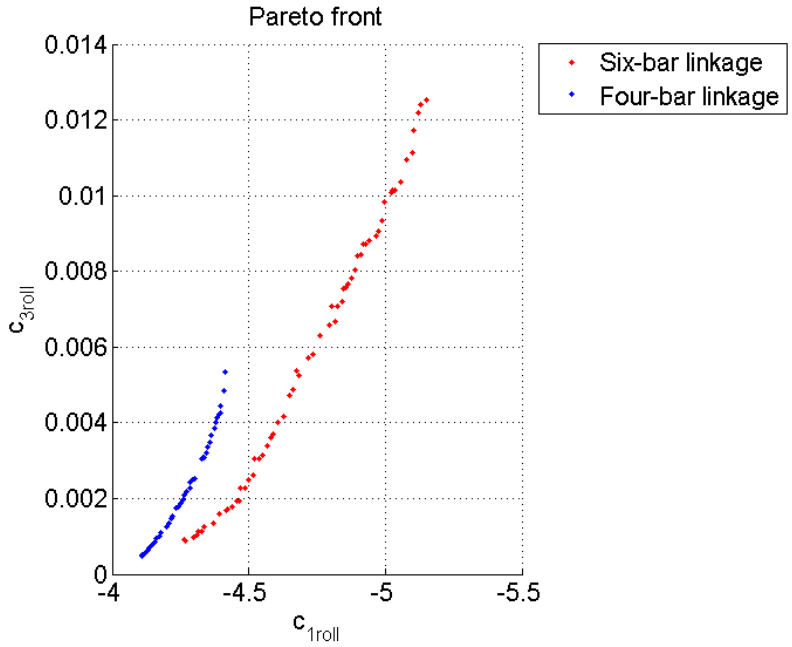

Figure 3.20: Pareto front projection on $c_{1roll} - c_{3roll}$ plane

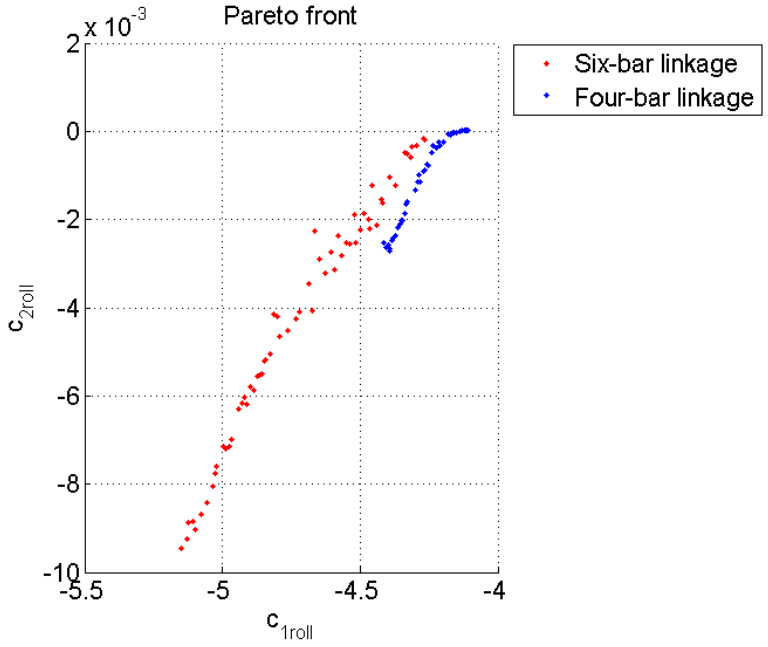

Figure 3.21: Pareto front projection on $c_{1roll} - c_{2roll}$ plane

chassis roll angle φ_c, COG vertical component z_{COG}, $\frac{c_l}{c_r}$ ratio (an increment of which must be regarded as a positive effect, since the chassis is imposed to roll like in a right turn engagement) and track. Fig. 3.22 - 3.26 compares the best scoring four and six-bar mechanisms according to c_{3roll} objective: the four bar individual indeed presents a smaller change in track during the roll maneuver, however the six-bar linkage is preferable according to other parameters: in particular, chassis roll angle is greater and, above all, Fig. 3.26 (b) presents a decrease in z_{COG} instead of the (small) increase featured by the four-bar mechanism (Fig. 3.26 (a)).

Fig. 3.27 - 3.31 compares two topologies positioned at the opposite extremity of relative Pareto curves, with respect to previous cases. Again, the change in track is the only parameter in which the four-bar linkage solution is preferable: in this case, however, a comparison based on track length curve is misleading, because these presented solutions are the worst performing ones according to these parameter. On the contrary, the six-bar solution stands out on all other parameters. A confrontation can be made between candidates that present similar maximum change in track: Fig. 3.32 indicates the choice of two mechanisms, while Fig. 3.33 - 3.37 show relative performances. The four-bar mechanism is penalized in c_{3roll} score (Fig. 3.32) because of the adopted definition of this cost component, which depicts an overall behaviour along the entire roll maneuver: the slightly higher track value at maximum roll angle and the greater slope of the curve are the reasons of this result. However, even if the definition of c_{3roll} is arbitrary, this index should not be redefined: in fact, being it computed in quadratic terms, and higher value of track change at max φ_{mean} is more penalizing than mid states, producing an effective comparison according to this performance criterion. In this case, as expected, the six-bar linkage is to be preferred according to all indices.

Finally, a solution must be chosen: due to overall superior performances, it is based on the six-bar linkage layout. The mechanism selected for development is shown in Fig. **??** - **??**: this choice is made in order to obtain a good trade-off amon all performance indices.

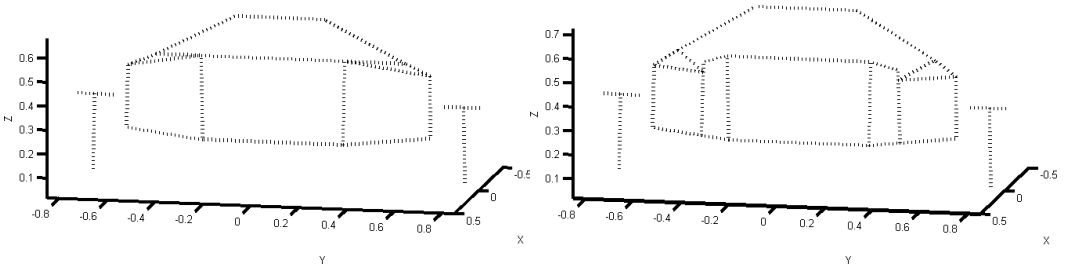

(a) (b)

Figure 3.22: Best c_{3roll} score: (a) four-bar and (b) six-bar linkage mechanism

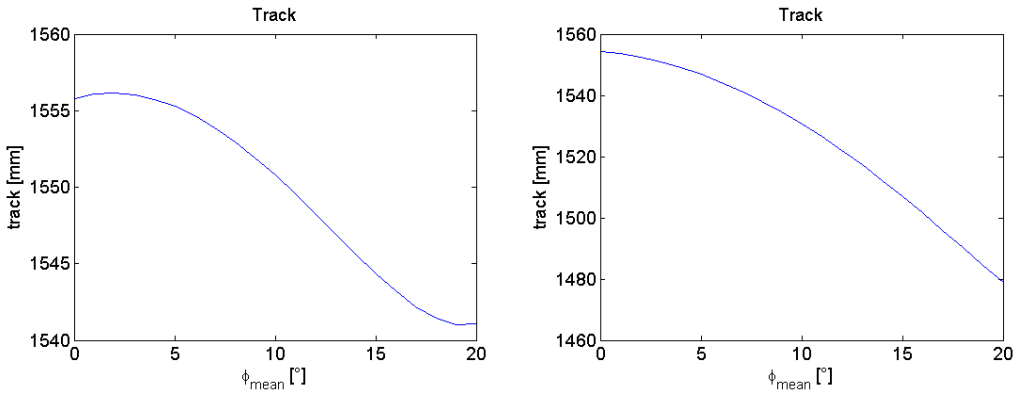

(a) (b)

Figure 3.23: Best c_{3roll} score: track over φ_{mean} for (a) four-bar and (b) six-bar linkage mechanism

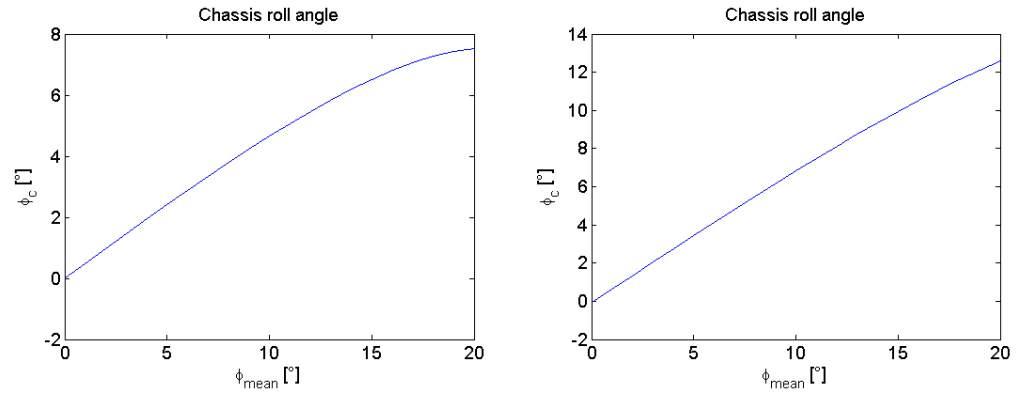

(a) (b)

Figure 3.24: Best c_{3roll} score: chassis roll angle over φ_{mean} for (a) four-bar and (b) six-bar linkage mechanism

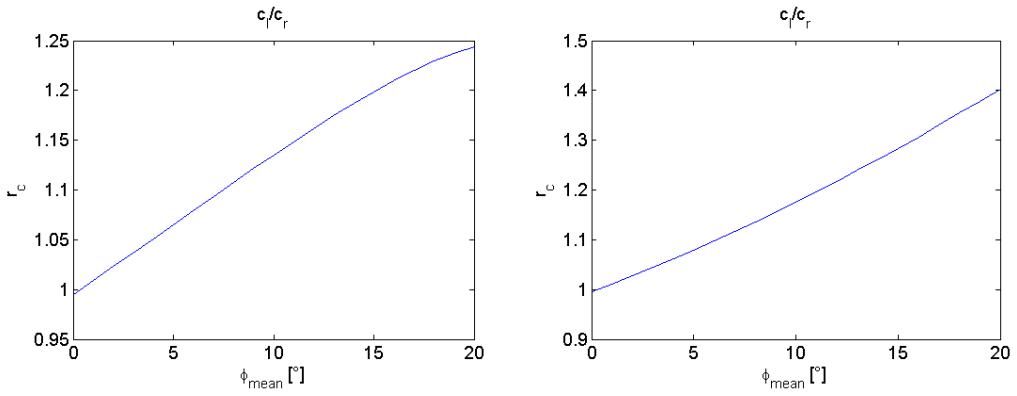

(a) (b)

Figure 3.25: Best c_{3roll} score: $r_c = \frac{c_l}{c_l}$ ratio over φ_{mean} for (a) four-bar and (b) six-bar linkage mechanism

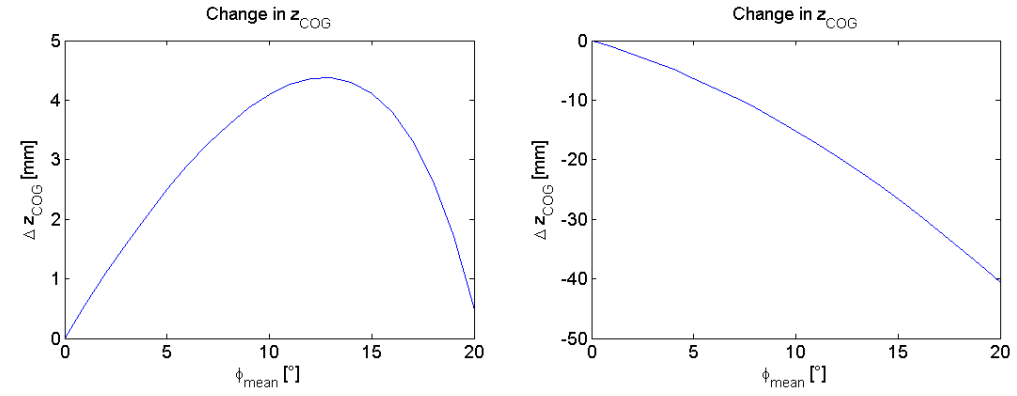

(a) (b)

Figure 3.26: Best c_{3roll} score: change in z_{COG} over φ_{mean} for (a) four-bar and (b) six-bar linkage mechanism

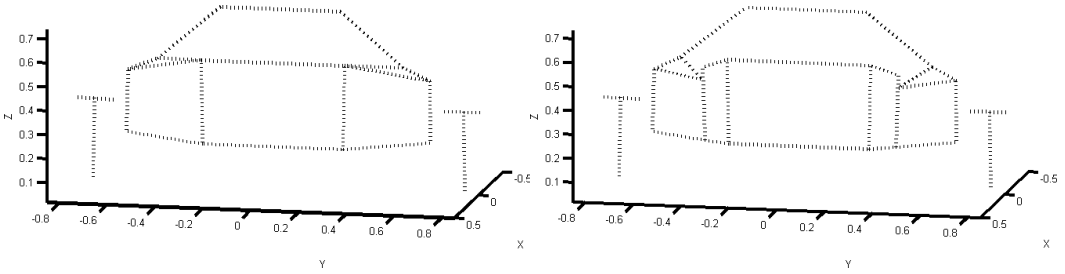

(a) (b)

Figure 3.27: Worst c_{3roll} score: (a) four-bar and (b) six-bar linkage mechanism

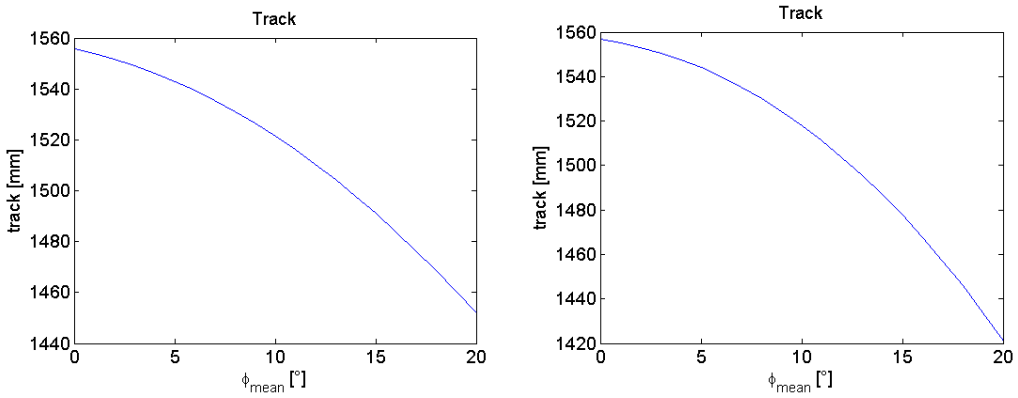

(a) (b)

Figure 3.28: Worst c_{3roll} score: track over φ_{mean} for (a) four-bar and (b) six-bar linkage mechanism

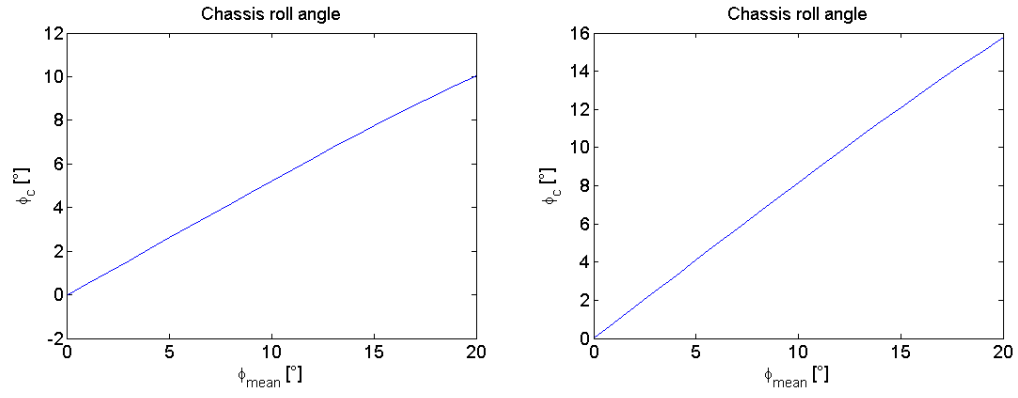

(a) (b)

Figure 3.29: Worst c_{3roll} score: chassis roll angle over φ_{mean} for (a) four-bar and (b) six-bar linkage mechanism

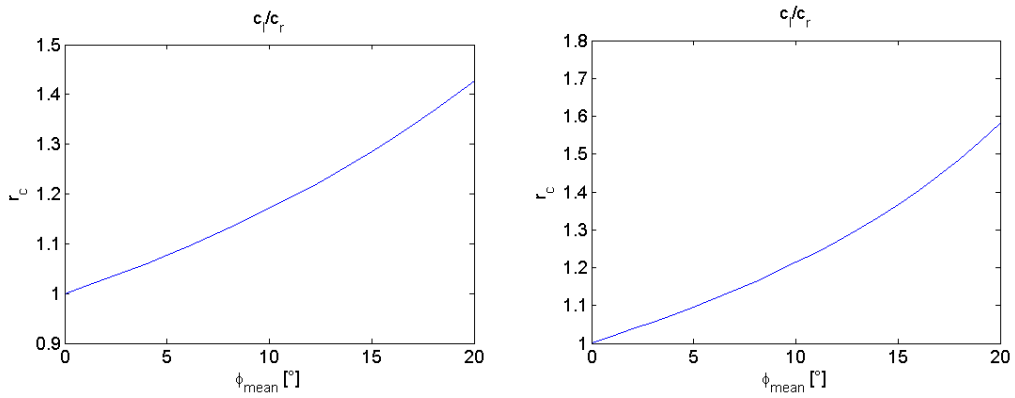

(a) (b)

Figure 3.30: Worst c_{3roll} score: $r_c = \frac{c_l}{c_l}$ ratio over φ_{mean} for (a) four-bar and (b) six-bar linkage mechanism

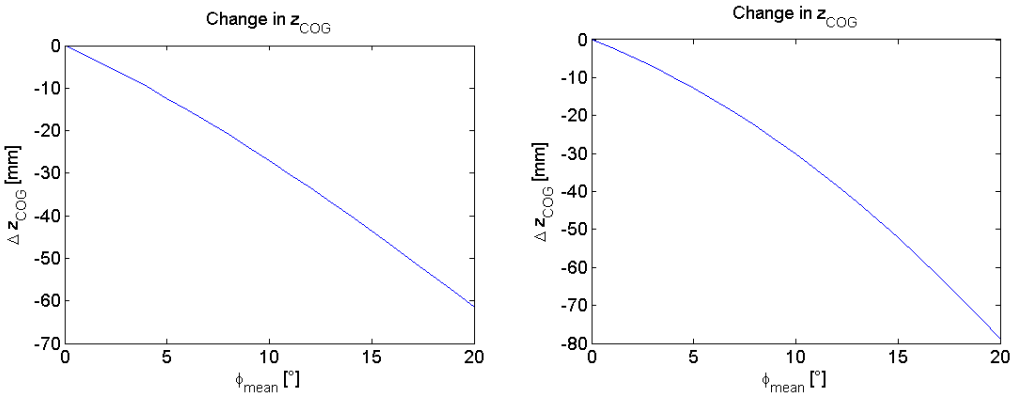

(a) (b)

Figure 3.31: Worst c_{3roll} score: change in z_{COG} over φ_{mean} for (a) four-bar and (b) six-bar linkage mechanism

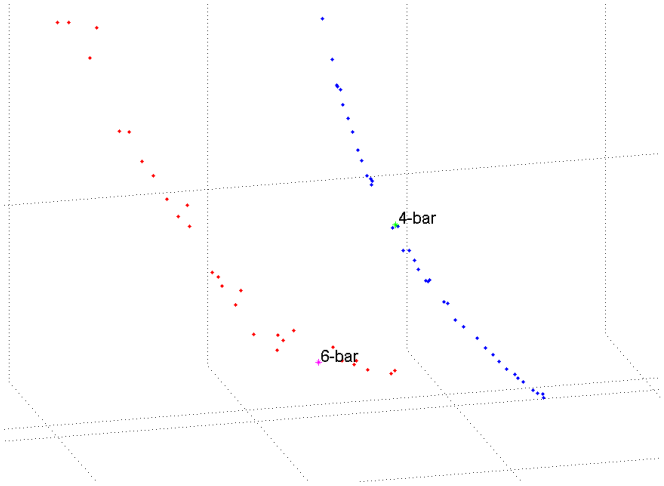

Figure 3.32: Similar maximum track change: compared mechanisms

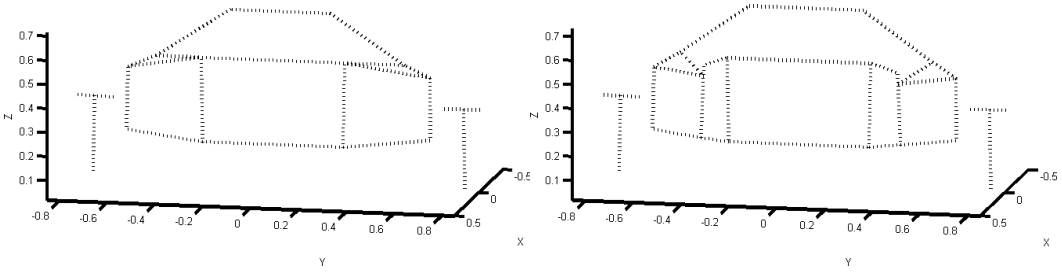

(a) (b)

Figure 3.33: Similar c_{3roll} score: (a) four-bar and (b) six-bar linkage mechanism

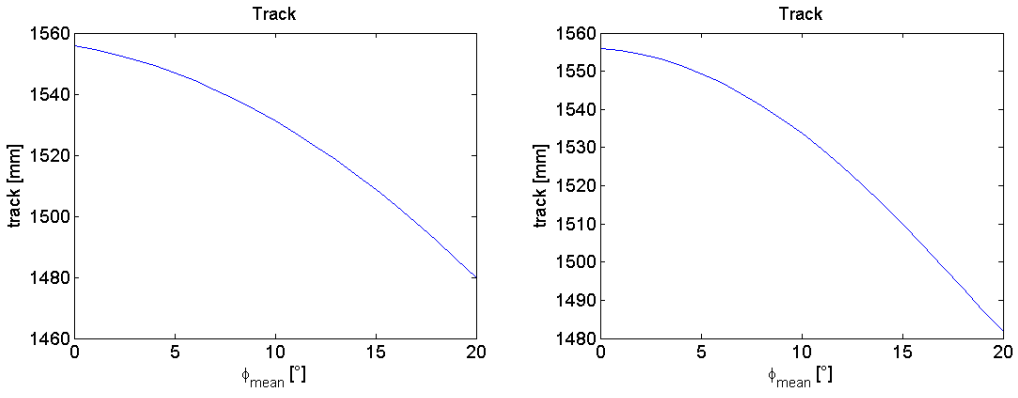

(a) (b)

Figure 3.34: Similar c_{3roll} score: track over φ_{mean} for (a) four-bar and (b) six-bar linkage mechanism

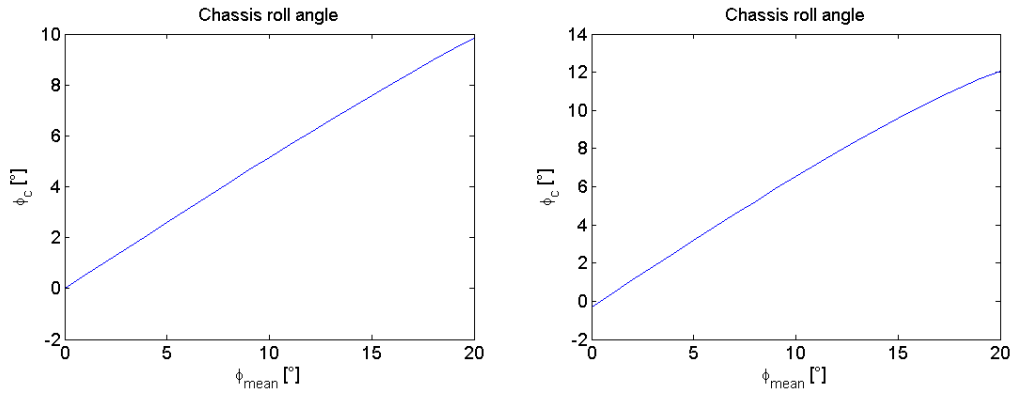

(a) (b)

Figure 3.35: Similar c_{3roll} score: chassis roll angle over φ_{mean} for (a) four-bar and (b) six-bar linkage mechanism

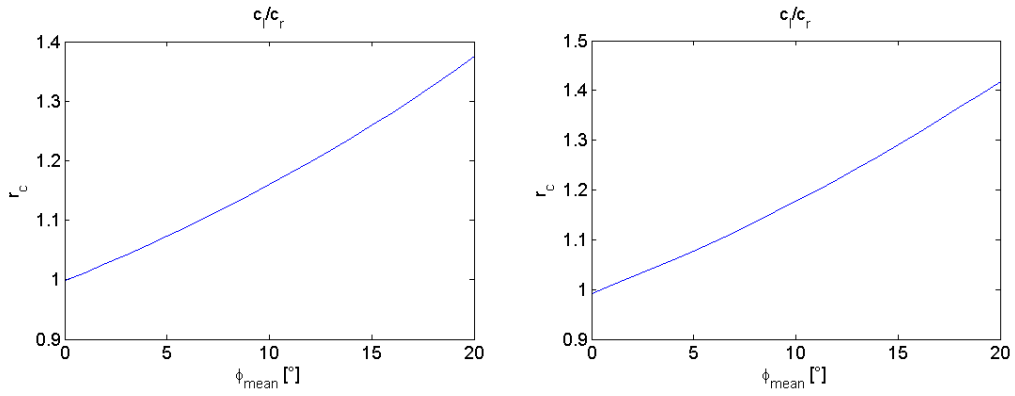

(a) (b)

Figure 3.36: Similar c_{3roll} score: $r_c = \frac{c_l}{c_l}$ ratio over φ_{mean} for (a) four-bar and (b) six-bar linkage mechanism

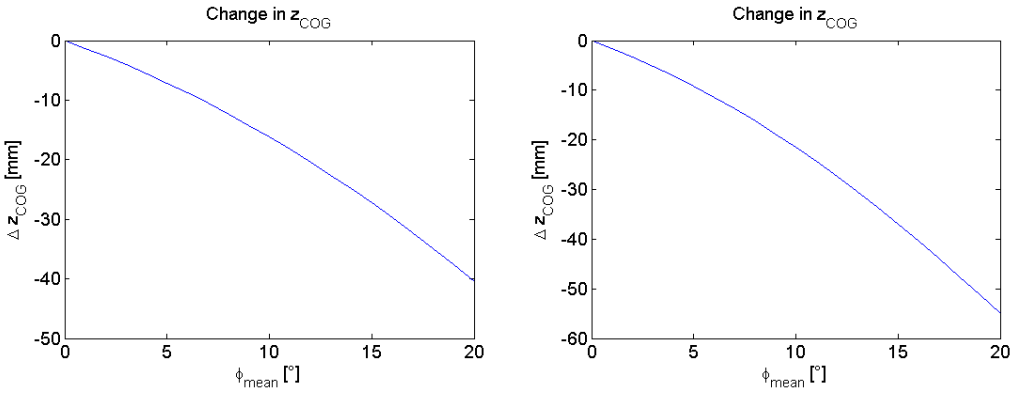

(a) (b)

Figure 3.37: Similar c_{3roll} score: change in z_{COG} over φ_{mean} for (a) four-bar and (b) six-bar linkage mechanism

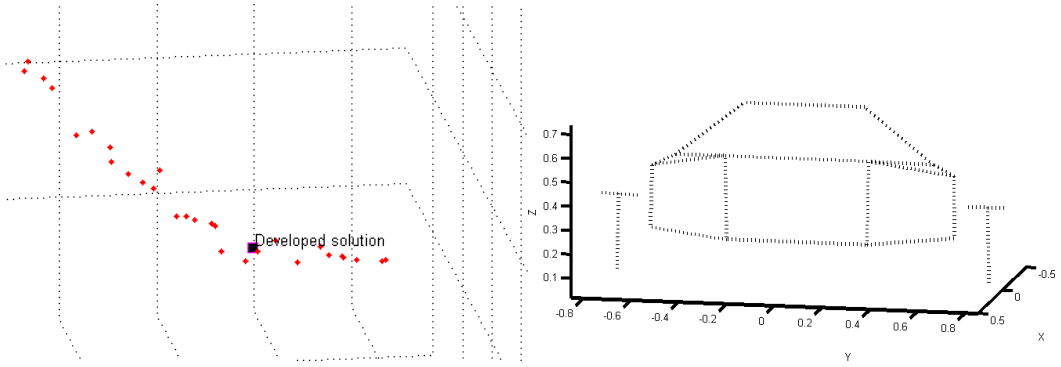

(a) (b)

Figure 3.38: Adopted solution: (a) position in the Pareto front and (b) mechanism

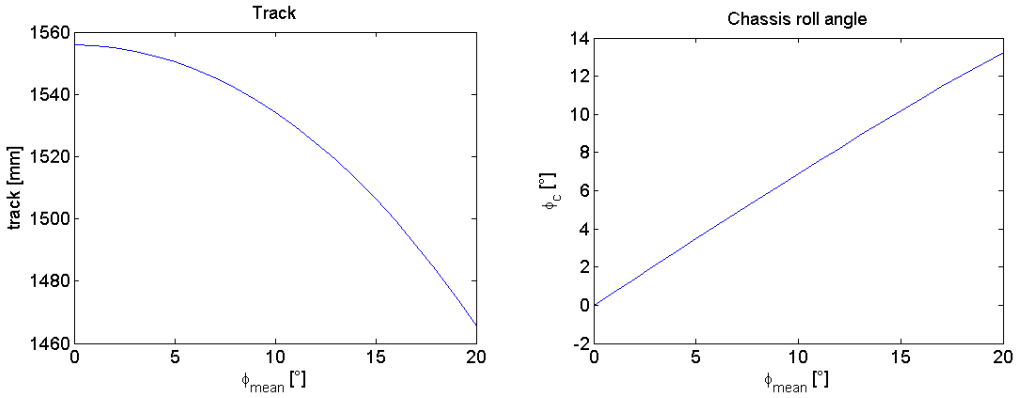

(a) (b)

Figure 3.39: Adopted solution: (a) change in track and (b) in chassis roll angle

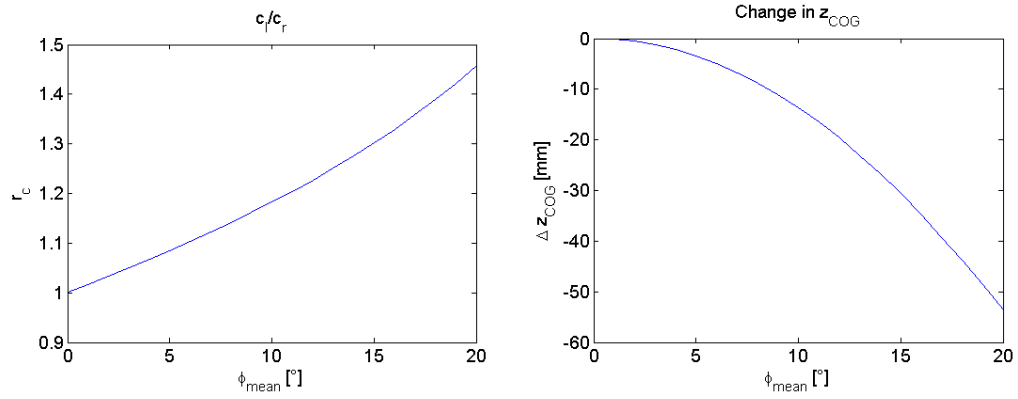

(a) (b)

Figure 3.40: Adopted solution: (a) $r_c = \frac{c_l}{c_l}$ ratio and (b) in z_{COG}

CHAPTER 4

The steer system

This Chapter describes the kinematic synthesis of the steer system. The chosen approach is very similar to the one described in Chapter 3 concerning the roll system. It essentially consists in:

1. Performing a preliminary analysis implemented in a commercial code, aimed at investigating the general behaviour of a set of possible solutions, obtained by manually changing geometrical parameters according to a trial and error approach. This phase proved to be very useful in the solution of this design problem, since it highlighted some specific aspects directly related to the particular concept of the prototype to be constructed.
2. Constructing a fully customized multibody model dedicated to solve the specific problems highlighted in the previous phase, by overcoming some limitations of the commercial code.
3. Performing a numerical optimization based on the custom model to obtain a solution which fulfills functional requirements.

In Chapter 2 some guidelines and their dynamical motivations were discussed. In detail, the steer system:

(a) should grant a good compatibility with Ackerman steering condition, so limiting scrub and drive to a motorcycle oriented use of tires;

(b) should feature a small correlation with roll system, so allowing for a profitable phase shift between camber and sideslip angles, found to be a good drive strategy in dynamical simulations addressed by the Optimal Maneuver Method. Additionally, a small correlation can reasonably result in a handling improvement, contributing to predictability of vehicle behaviour.

These functional requirements are used as targets.

4.1 Preliminary analysis

The target of this phase is to study the steering system layout providing information about possible kinematic problems and sensitivity to design parameters. As in roll system preliminary analysis, low testing time, ease and intuitiveness in definition and representation of outputs, and fast changes in the model to be tested are taken as requirements in methodology definition. This case study, however, differs from the previous one with regards to objectives: any purpose of evaluations about the topology to be adopted is missed, since it is determined according to technological considerations. Therefore, this analysis and the following modelling and optimizations are uniquely aimed to define the best performing solution.

The selected topology corresponds to a traditional rack and pinion steering system layout (Fig. 4.1) [9], composed by a steering rack, two tie rods and two steer (or track) arms fixed to uprights. In conventional cars, tie rods are generally connected to other bodies by spherical rod ends. In the present application, however, these bodies are considered to be coupled by means of a fully spherical joint at the inner side, and a universal joint at the outer side, in order to overcome the limitations on articulation angles typical of traditional rod ends, that could result in camber limitations. The choice of the rack and pinion technology is made for following reasons [4] [10]:

- High reverse efficiency, resulting in a better transmission of wheel dynamics to steering-wheel/handlebar; this is particularly suitable in this application case, due to the complex drive model which employs both sideslip and camber angles during the steer maneuver. According to safety, the driver must be provided with all possible information useful to produce right trajectory corrections.
- Design flexibility. Due to the presence of a variable camber, common steering system dimensions could not be employable in this particular application: the rack and pinion system is easy tunable by varying member lengths and the velocity ratio. Moreover, in case commercial solutions reveal to be suitable, a large amount of models are available at a reasonable cost.
- Both hydraulically and electrically actuated servo-systems can be easily implemented, if necessary.

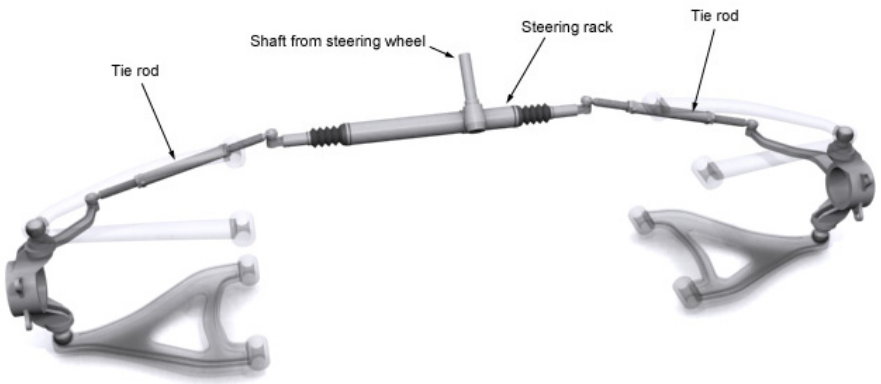

Figure 4.1: Conventional rack and pinion steering layout

The very first steps of this design stage revealed to be useful mainly in redefining the strategy and the parameters to be taken into account in the definition of the topology. This preliminary analysis can be divided in the following steps:

(a) Construction of a parametric multibody model based upon a commercial code (LMS Virtual.Lab); this model must contain both steer and roll systems, to be capable of reproducing a complete set of cornering maneuvers;

(b) Definition of a convenient test strategy, aimed at pointing out general aspects of the overall kinematic behaviour of the system;

(c) Evaluation of the particular configuration tested, on the basis of visual inspection of multibody animations and of computation of a first set of parameters;

(d) Generation of different candidate mechanisms by manually changing the values of geometrical parameters (i.e. varying member lengths, according to a trial and error heuristic approach);

(e) redefinition of test parameters and iteration of previous steps.

In the following paragraph the multibody model, the test strategy, the specific targets and the preliminary results are illustrated.

4.1.1 Parametric multibody model, test strategy and results

The preliminary multibody model is created in LMS Virtual.Lab environment, profiting of the capability of this software to be addressed by common data files through *Design Tables*: the generation of new candidate mechanisms to be tested and the storage of trial configurations and outputs can be managed through common spreadsheets, so obtaining the flexibility needed in this preliminary phase. The multibody model is represented in Fig. 4.2: the digital mock-up consists of the whole vehicle. Tires are modelled by a TNO tire superelement, which implements a complete Pacejka formulation. Rear wheels are blocked by fixing the transmission system to the chassis. Shock absorbers are substituted by rigid bodies, in order to avoid bump/rebound movements which are not considered in this analysis. The model features 62 bodies and 2 DOF's: steer slides and rack translations. The free parameters considered for kinematic synthesis are coordinates of points LN, RN, LO, RO; the symmetry constraint between left and right homologous points reduces design space dimensions to 6, i.e. x, y and z coordinates of points LN and LO with reference to the global frame (represented in Fig 4.2). By changing values of these parameters, all member lenghts, and rack positioning, can be modified. A first set of simulations was aimed to characterize possible spatial volumes suitable for point positioning, according to the following criteria:

- respect of constructive constraints;
- entity of camber/sideslip angle correlation;
- quality of kinematic behaviour, i.e. attitude of respecting the Ackerman condition.

Constructive constraints are given by chassis layout, volume occupied by pilot and other components: therefore, the four coloured A, B, C and D volumes reported in Fig. 4.3 were selected as suitable to contain points LO and RO; volume E of Fig. 4.4 was considered for LN point, at the same time. In addition, tie rods must not interfere with plates 1 and 2 during rack translations. To investigate the roll/steer correlation and the overall kinematic behaviour, the following strategy was defined: a rack/roll slide translation routine was imposed to the model, consisting in 20 evenly spaced translations from left to right side for both commands, in order

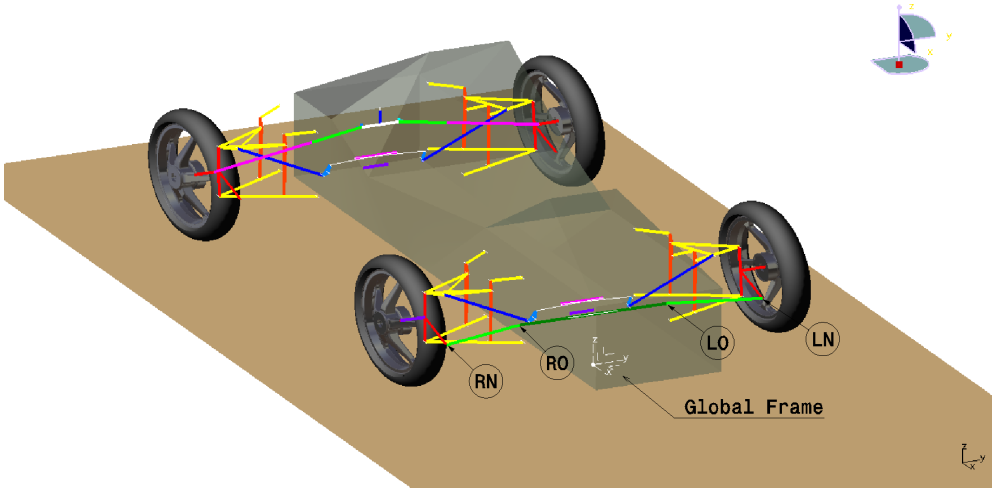

Figure 4.2: Multibody model in LMS Virtual.Lab, used in the preliminary analysis of the steer system

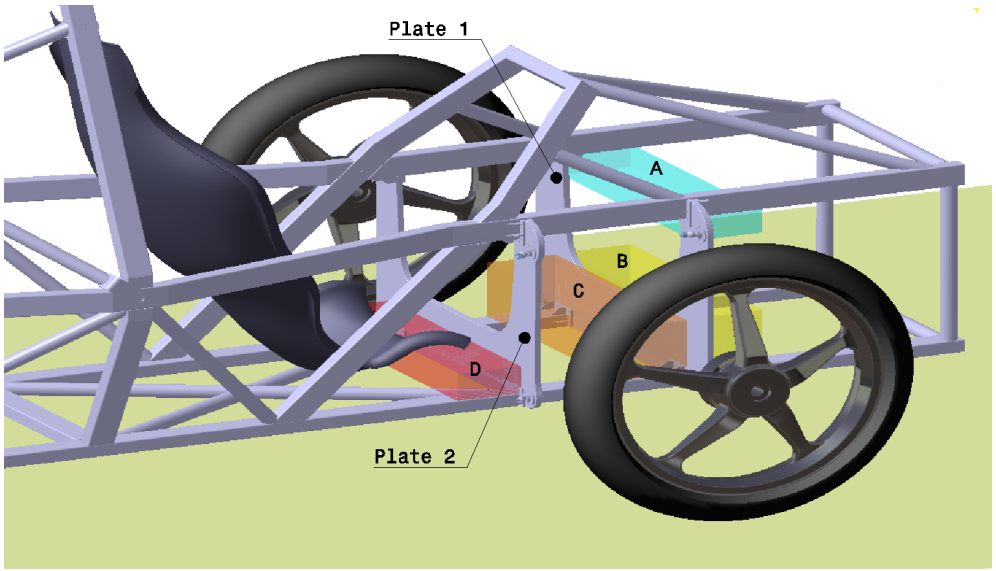

Figure 4.3: Suitable volumes for points LO and RO positioning

to test corresponding φ and δ angles, chosen as test parameters, in a complete grid composed by 400 points. Limits in translation magnitudes are differently chosen, for each mechanism, to obtain a maximum value of $30°$ both for camber and steer angle. In some cases, the grid was cut at corners to avoid singular configurations (Fig. 4.5). By adopting the described strategy, a series of 40 possible solutions were tested by choosing proportions commonly used in steer systems of small passenger cars and a trial and error approach in manually generating new candidates. The kinematic characterization was represented by diagrams of type reported in Fig. 4.6: each line represents or the variation in angle δ (left and right) induced by a change in roll slide position, or the variation in angle φ (left and right) induced by a change in rack position. By locally comparing left and right wheel steer angles, it is possible to obtain indications on the capability of reproducing a kinematic behaviour similar to Ackerman condition. This representation does not prove to be particularly handy for a quantitative comparison of mechanisms, but is useful to give information about effectiveness of test parameters: due to roll/steer interactions, the knowledge of both camber and steer angles provides a useful kinematic information only if two

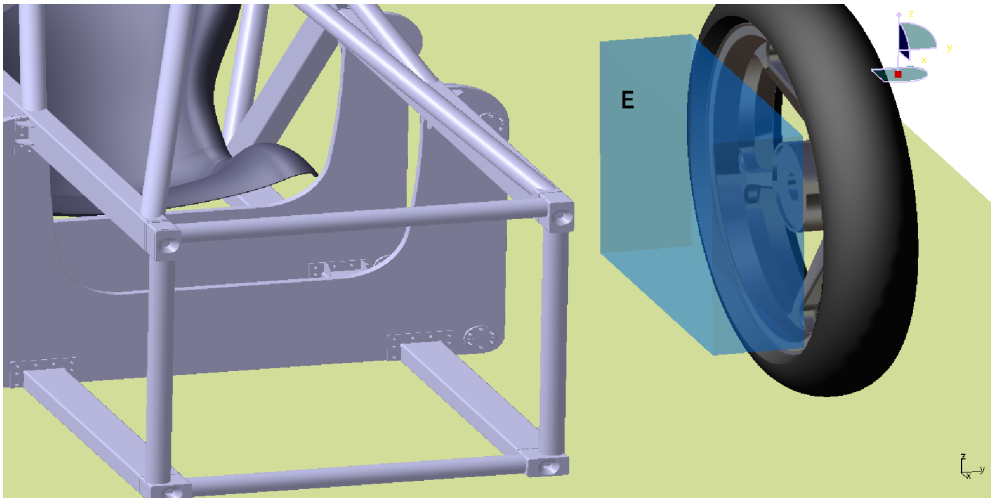

Figure 4.4: Suitable volumes for point LN

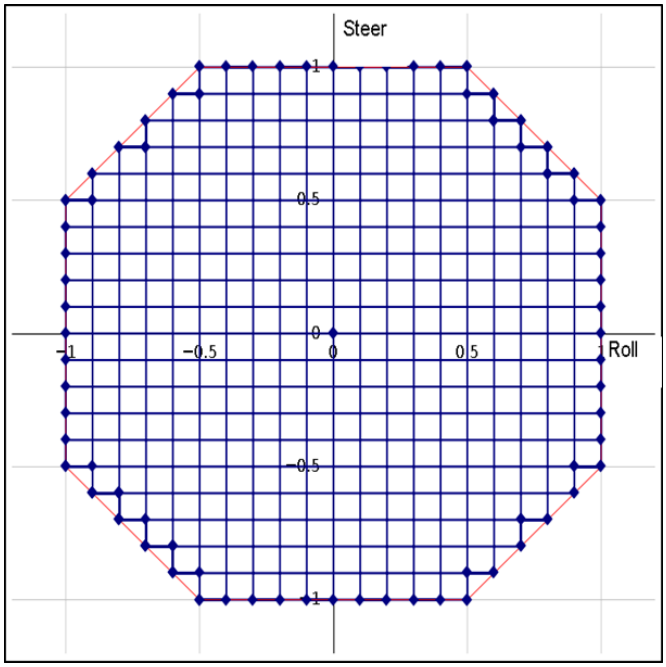

Figure 4.5: Rack/roll slide translation routine

angles are combined through Eq. 2.6, expressing the effective kinematic steer angle Δ. This consideration led to perform a second set of 70 multibody analyses, adopting both the mean Δ value between left and right wheel and the Ackerman ratio as test parameters; the latter one, for conventional cars (almost null camber) can be defined as [3]:

$$A_{conventional} = \frac{\delta_o - \delta_{mean}}{\frac{L}{\left[\frac{L}{\delta_{mean}} + \frac{t}{2}\right]} - \delta_{mean}} \tag{4.1}$$

where δ_{mean} and δ_o are the mean steer angle and the one of outer wheel, and L and t are wheelbase and track, as usual. In the present case, however, it can more conveniently be

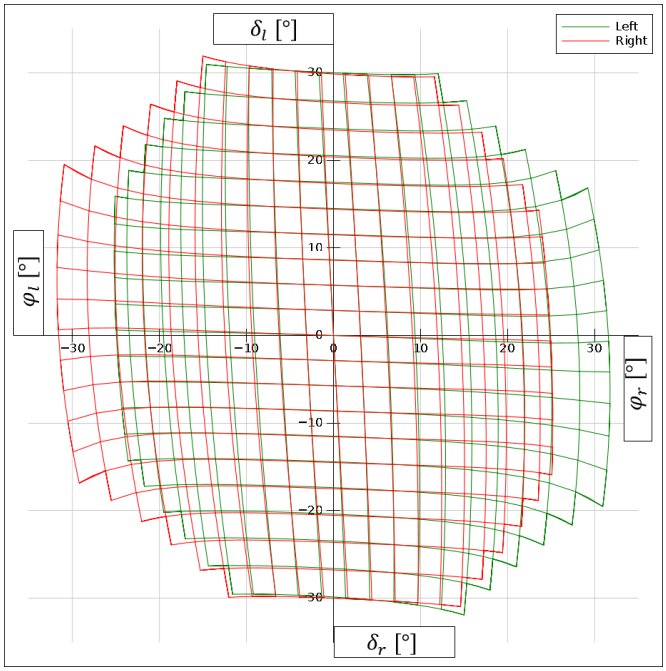

Figure 4.6: Roll/steer correlation: green line refers to left wheel, red line to right wheel

re-defined in terms of effective kinematic steer angle:

$$A = \frac{\Delta_o - \Delta_{mean}}{\frac{L}{\left[\frac{L}{\Delta_{mean}} + \frac{t}{2}\right]} - \Delta_{mean}} \tag{4.2}$$

with the same meaning of symbols. By this new definition, a change in camber is not only evaluated with regards to pure kinematic correlations (as in the previous set of simulations), but also, and more significantly, with regards to its effects in cornering kinematics. This second step of preliminary analyses could improve the knowledge of problems related to steer/kinematic correlation: a bad layout can emphasize its effect by producing bad kinematic configurations. For example, wheels can converge (Fig. 4.7(a)) or diverge (Fig. 4.7(b)) by excessive values; in addition, supposing a certain δ_{mean} value is imposed by setting a defined position to rack, an increment of camber in the same direction can make the mean effective steer angle Δ_{mean} to raise or decrease, due to roll/steer correlation, through a δ_{mean} increase or decrease. Fig. 4.8 - 4.16 depict three different layouts and respective diagrams reporting $A\%$ and Δ_{mean} fields over rack and roll slide translations. The first and the third configurations differs only in rack length, with a value of respectively 50 and 590 mm; the second one features slightly diversifies from the third in rack length (620 mm) and position (20 mm above). The Ackerman fields (reported in percent) of Fig. 4.9, 4.12 and 4.15 consist of all points between two limit values, arbitrarily set at -50% and 150%: all operative points (in terms of rack and roll slide translations) inside this field were considered as suitable. The third configuration offers the wider Ackerman field (Fig. 4.15) and, despite of a great difference in rack lenght, it features a behaviour which is similar to first configuration (Fig. 4.10 and 4.16) : a rise in camber early generates $A\%$ above 100%, so exhibiting a pro-Ackerman behaviour; additionally, in both configurations it produces a general decrease in Δ at low steer angles (even if not monotonic) , and an increase at high steer angles. The second configuration, very similar in member lengths to the third one, features a different behaviour: the $A\%$ field presents a set of points with negative values (not present in other configurations), and is generally prone to an anti-Ackerman behaviour. Additionally, a

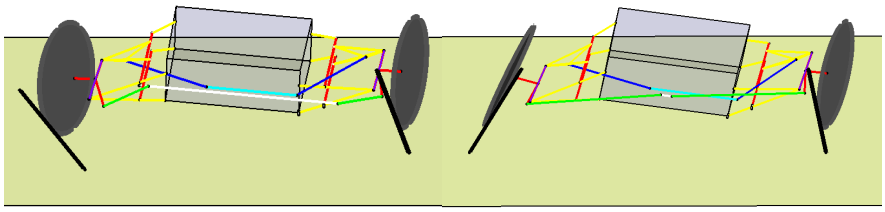

(a) (b)

Figure 4.7: Configuration with convergent (a) and divergent (b) wheels generated by roll slide translation, with rack fixed to chassis in symmetrical position (front view)

rise in camber leads to a decrease in Δ_{mean} in the whole field: this effect is obviously regarded as a strong drawback both by a kinematic and a handling point of view. It can be concluded

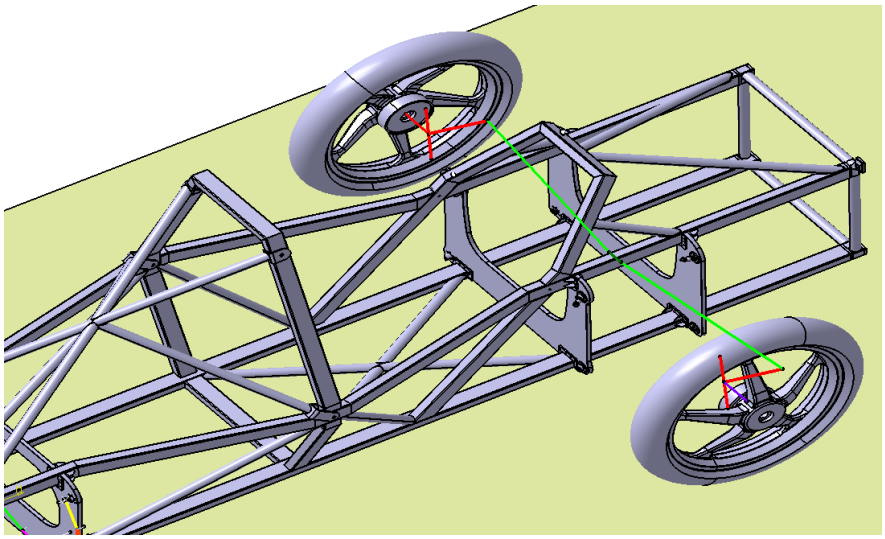

Figure 4.8: Layout of first configuration

that this analysis proved to be useful to highlight following aspects:

- Δ_{mean} and A can be chosen as test parameters both for an immediate evaluation and for a numerical optimization, since they represents in a direct, quantitative way both the conformity of the kinematic behaviour to the Ackerman condition and the entity of roll/steer correlation (which are taken into account in discussed guidelines);

- The number of design variables is too great to perform a non automatic enumerative optimization with a reasonably low step size; in addition, the sensitivity of test parameters on different design variables is not clearly determinable: in some cases, apparently similar candidate mechanisms (e.g. the second and third configurations above presented) feature a very different kinematic behaviour, while very different mechanism (first and second configurations) perform similarly;

- Despite of the large amount of simulations (110, accounting both steps), only trials in the volume C of Fig. 4.3 produced acceptable results in terms off $A\%$ field and correlation; however, the best among 110 configurations found (the third described configuration)

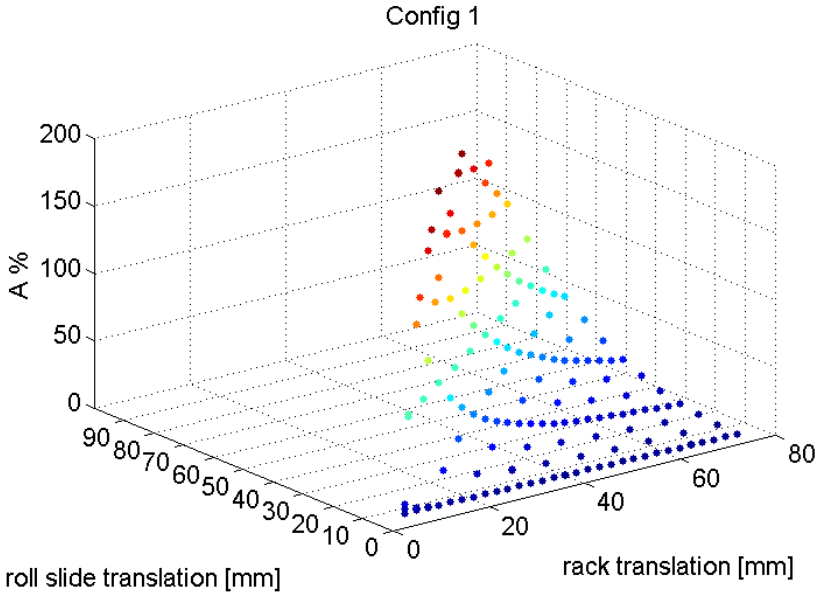

Figure 4.9: First configuration: $A\%$

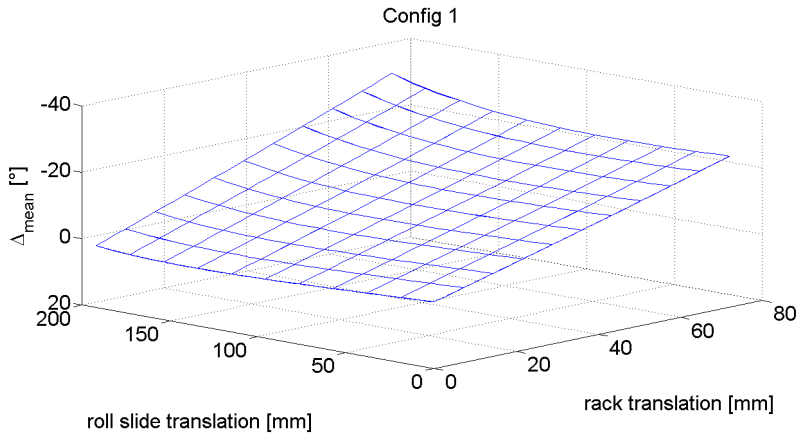

Figure 4.10: First configuration: Δ_{mean}

features a plateau at around 17% in the $A\%$ diagram: this value is considered to be too small to fully satisfy one of functional requirements. In addition, due to constructive restrictions, the best target volume to locate the rack is volume B of Fig. 4.3: in this zone, however, the heuristic approach could not produce any feasible solution.

This considerations motivate the choice of performing a numerical optimization adopting a fully dedicated multibody model. This preliminary analysis revealed to be useful also by a constructive point of view: in fact, the visual inspection of kinematic animations revealed that for $\varphi_{mean} > 20°$ some points of the chassis could collide with road during suspension bump movements. Therefore, in following phases, $\varphi_{mean} = 20°$ will be considered as a boundary condition.

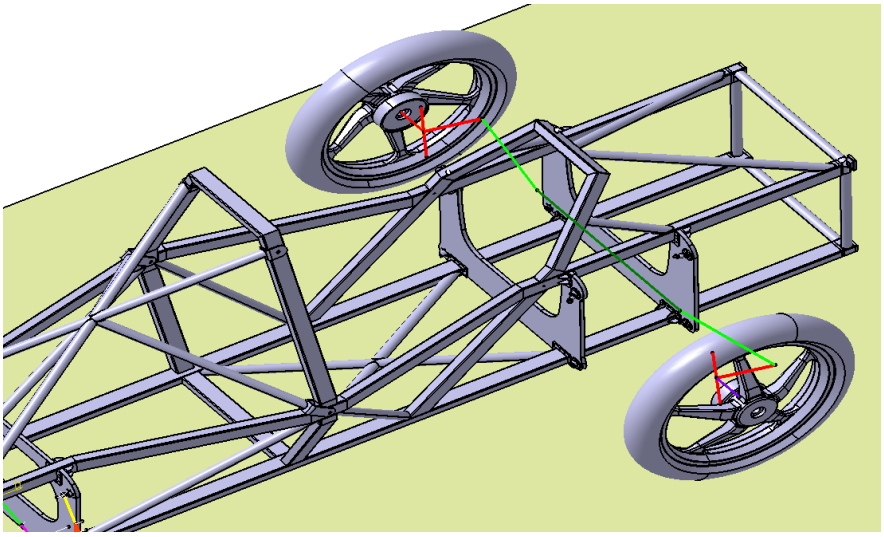

Figure 4.11: Layout of second configuration

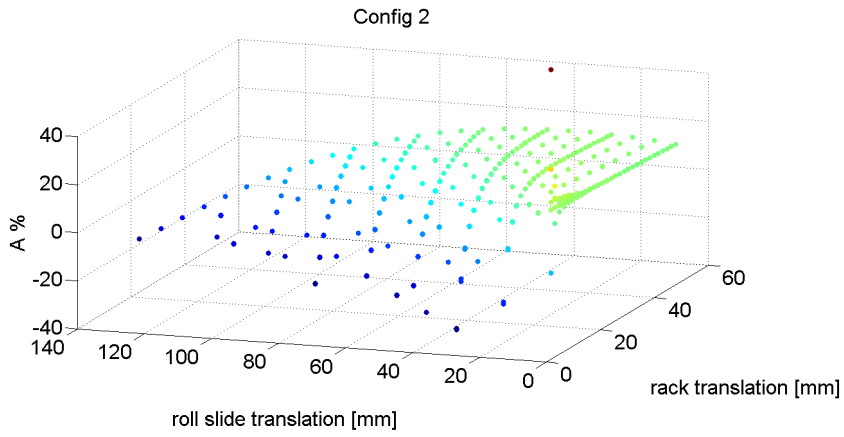

Figure 4.12: Second configuration: $A\%$

4.2 Dedicated multibody modelling

The preliminary analysis described in the previous paragraph highlights the necessity of a numerical optimization to define a performing solution for steering system. Methods adopted in this phase are very close to the ones used in roll system optimization: a fully dedicated multibody model is implemented in Matlab code to solve the kinematic problem, and then an optimization algorithm is used to define one (or some) optimal solution according to a chosen performance criterion (see Fig. 3.15). This paragraph describes the definition of the multibody model, which is based, like in roll system optimization case, on the Natural Coordinates Method. Both roll and steer systems must be taken into account, since they interact by means of the cited roll/steer correlation and are both involved in cornering maneuvers. Therefore, the steer system model is implemented in the multibody model described in Par. 3.2.2 to solve both roll and steer kinematic. This model is based upon the six-bar linkage mechanism selected for development on the basis of the previous kinematic optimization, and on the cited rack and pinion layout for steer system. Fig. 4.17 depicts chosen basic points. For roll system model description, please refer to Par. 3.2.2. The implementation of the steer system leads to an important difference between the previous model and the one in object: the movement of some basic points can

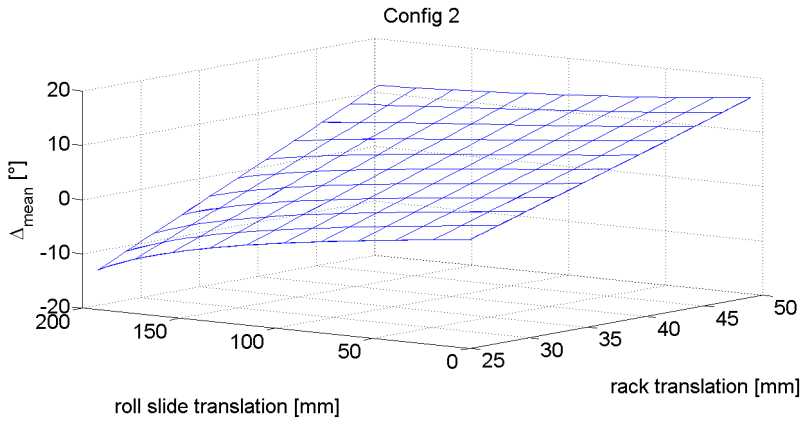

Figure 4.13: Second configuration: Δ_{mean}

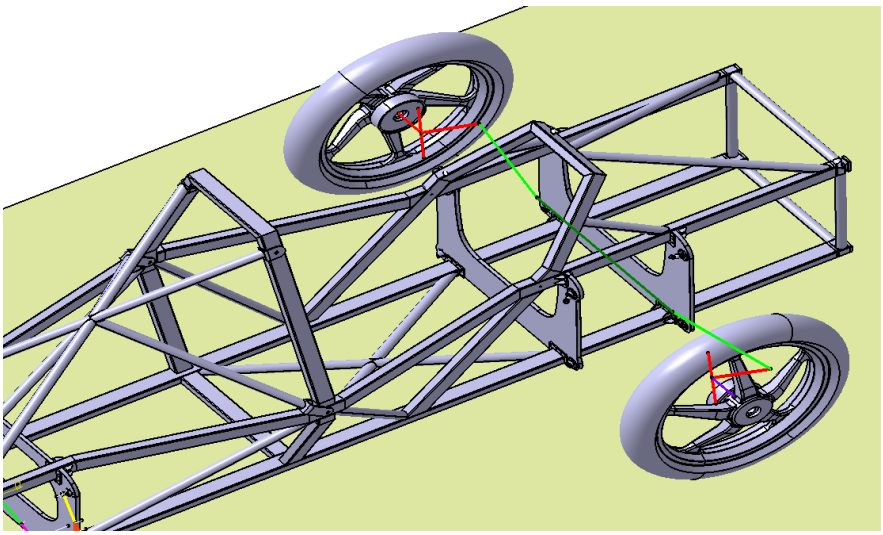

Figure 4.14: Layout of third configuration

no longer be considered planar, therefore two natural coordinates (being the third fixed to a constant value) are no longer sufficient. The steer system is composed by four basic points: LO, RO, whose movement is planar (they represent the rack, which can only move in transversal direction and roll together with the chassis), and LN, RN which can move in three dimensions. In addition, some integrations to wheel modelling are necessary: the introduction of the steer system requires points W and R and unit vectors w to be defined by a third natural coordinate, to make three-dimensional transformations possible. A total of 16 additionally natural coordinates are used, therefore at least 15 constraints must be imposed, since the subsystem features a single DOF. The congruency is imposed, like in roll system modelling, in two different ways: first, by the already described rigid body condition:

$$(y_P - y_Q)^2 + (z_P - z_Q)^2 - [(y_{P_0} - y_{Q_0})^2 + (z_{P_0} - z_{Q_0})^2] = 0 \tag{3.6}$$

which is applied to members $\overline{NO}$ (left and right) and to fictitious members $\overline{EN}$, $\overline{FN}$ and $\overline{WN}$, for 8 conditions total. Other conditions are directly implemented in the definition of the displacement vector of the rack, in the same way they were imposed to roll slide (Eq. 3.14):

$$\begin{aligned} y_P &= (y_{P_0} + \Delta y_{rack})u_{z_c} - z_{P_0}u_{y_c} \\ z_P &= \Delta z_c + (y_{P_0} + \Delta y_{rack})u_{y_c} + z_{P_0}u_{z_c} \end{aligned} \tag{4.3}$$

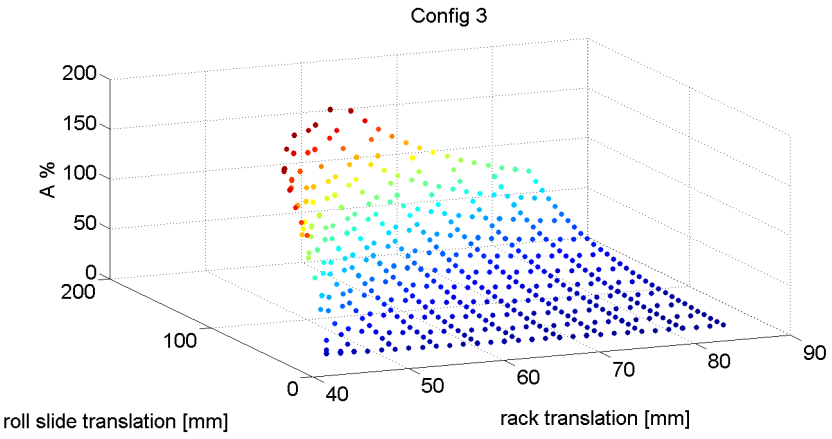

Figure 4.15: Third configuration: $A\%$

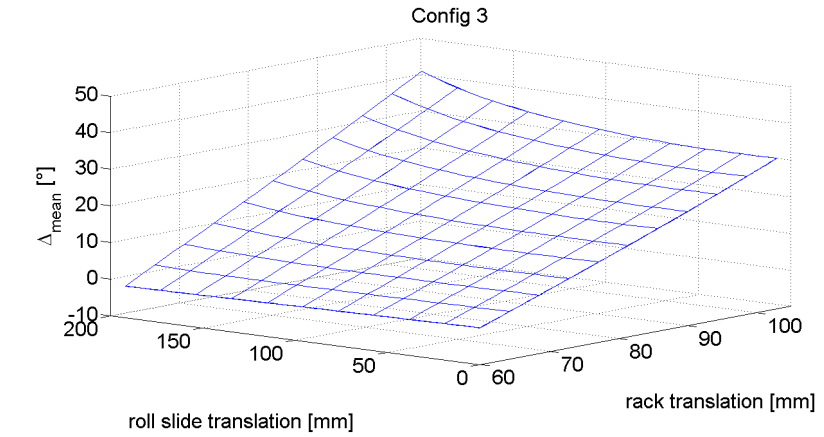

Figure 4.16: Third configuration: Δ_{mean}

adopting the components of displacement Δz_c, u_{y_c} and u_{z_c} already defined for the chassis and the new one Δy_{rack} which represents rack lateral translation; the latter one requires an additional condition. Therefore, 4 constraints are expressed by means of Eqns. 4.3 and other 4 are still required. The orientation of unit vectors w with respect to uprights is fixed only during roll movements by first of Eqns. 3.8: an analogous formulation must be adopted with regards to steer movements:

$$w \cdot (F - N) - w_0 \cdot (F_0 - N_0) = 0 \tag{4.4}$$

where w, with the same symbolism of roll system model, is the unit vector which defines wheel axis direction, and 0 subscript indicates the starting configuration, as usual, which corresponds to null rack and roll slide translations. Eq. 4.4 introduces two of four conditions needed. Last two constraints concern bodies represented by lines $\overline{WR}$ which join wheel centers with contact points, and must be parallel to YZ plane (as defined in Chapter 3):

$$x_{u_{wheel}} = 0 \tag{4.5}$$

where $u_{wheel} = w \times (R - W)$. All needed constraints are defined: the whole system is described by means of 69 variables (5 of which are introduced in constraint definitions); the 16 equations above described, together with the 51 conditions reported in Par. 3.2.2 produce 67 total conditions. Therefore, the system features 2 DOF's, as needed: one is related to roll, the other one to steer movements.

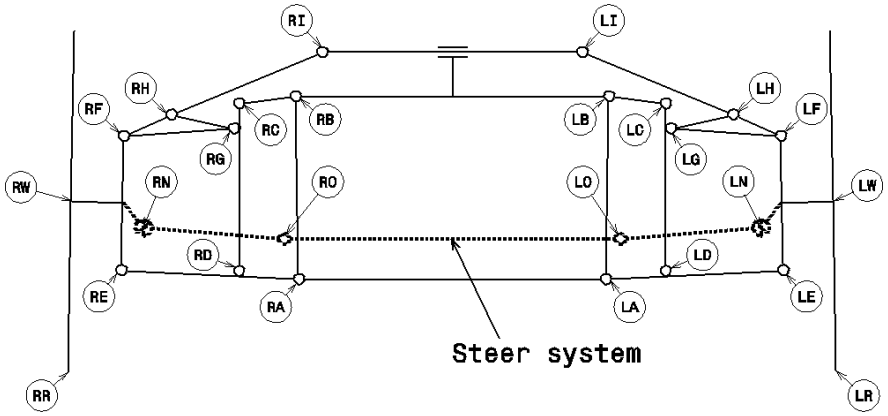

Figure 4.17: Steer mechanism: basic points

4.3 Steer system optimization

This section is dedicated, first, at the description of the specific implementation of the optimization of the steer system, and then at presenting the results obtained.

4.3.1 Specific implementation

The optimization dedicated to the steering system follows the same general scheme used in roll system optimization, discussed in Par. 3.3.1 and depicted in Fig. 3.15. Being the kinematic solver discussed in Par. 4.2, the Kinematic Parameters upon which to define the Performance Criterion, the Design Space and the Optimization Algorithm must be chosen. As usual, optimization targets are considered as the first input in this process; the optimal solution must consist in a steer system granting:

1. a good compatibility with Ackerman steering condition, in order to limit scrub and perform a motorcycle-like use of tires.

2. a correlation with the defined roll system as small as possible, allowing for timeshifts between camber and steer angle and a predictable kinematic behaviour;

These functional requirements must be first translated in measurable kinematic parameters to be computed in convenient test states and used to calculate performance indices. According to information acquired in the preliminary analysis described in Par. 4.1, two kinematic parameters are chosen as:

(a) the Ackerman ratio A defined in Eq. 4.2 (or the corresponding percent value $A\%$);

(b) the mean effective kinematic angle:

$$\Delta_{mean} = \frac{\Delta_L + \Delta_R}{2} = \frac{\arctan\left(\frac{x_{w_L}}{y_{w_L}}\right) + \arctan\left(\frac{x_{w_R}}{y_{w_R}}\right)}{2} \tag{4.6}$$

with the usual meaning of symbols.

The Performance Criterion can be formulated by following equations:

$$\begin{cases} c_{1steer} = (obj_A(s) - A)^2 \\ c_{2steer} = (obj_\Delta(s) - \Delta_{mean})^2 \\ c_{steer} = \sum w_A c_{1steer} + w_\Delta c_{2steer} \end{cases} \tag{4.7}$$

where $w_A c_{1steer}$ and w_Δ are scale factors used to homogenize the magnitude of two components, and $obj_A(s)$ and $obj_\Delta(s)$ are chosen objective values. In this case, a single final cost component c_{steer} is defined: in fact, the target is to obtain a good behaviour (according to cited criteria) over the full range of [Δy_{rs}, Δy_{rack}] (or [δ_{mean}, φ_{mean}]) couples; however, due to considerable computational time, only a few operative points must be contained in the state vector r which defines the positions to be tested. The effectiveness of the optimization strategy (and, in particular, of the vector r) and of the cost function should therefore be tested tested and tuned by a first phase, composed by fast optimization cycles followed by deeper kinematic analyses: doing so, a set of states s which can represent the behaviour over the whole operative field or, at least, capable of producing good results, could be determined. After this step, a more effective and time intensive algorithm could be adopted. The same "tuning process" should be done with scale factors, before obtaining good results. The adoption of a vectorial cost function and the search for a set of optimal solutions is not suitable to be coupled with this approach, in terms of computational time. Additionally, the only target of this optimization is the determination of a well performing solution (or, in case, a set of few good candidate mechanisms): each purpose of topology investigation is missed, as above cited. Therefore, the algorithm chosen in this optimization is based on the gradient method, traditionally prone in fast pointing out the best solution inside a small and regular optimization domain; however, these two conditions should not be reasonably respected, due to the strong non linear nature of the problem to solve: this does not represent an issue in the first "tuning phase", and can be overcome in the second one by adopting a multi-start approach.

The last aspect to be defined is the choice of the Design Space D_S and relative constraints: in this case the basic points subject to optimization are LN, LO, RN and RO (black points of Fig. 4.18), since all other basic points are defined in the roll system optimization phase. Therefore, taking into account the symmetry condition between points LN, RN and LO, RO,

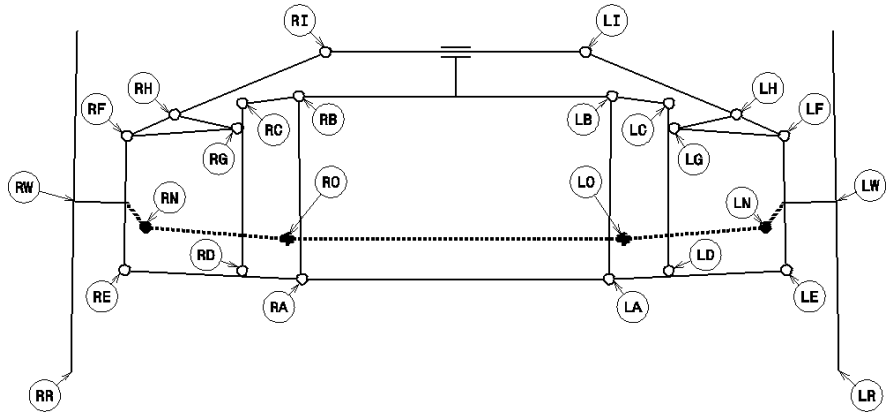

Figure 4.18: Design space points for steer system

the Design Space features 6 dimensions:

$$D_S = \{[x_{LN}]\,;[y_{LN}]\,;[z_{LN}]\,;[x_{LO}]\,;[y_{LO}]\,;[z_{LO}]\} \tag{4.8}$$

where brackets indicate that design variables are defined inside a range specified by limits of Table 4.1. In this case, no dynamic constraints are added. The D_S imposes points O to lie in the volume B of Fig. 4.3 and points N are in the forward half of volume E of Fig. 4.4: the choice of limiting the Design Space to these zones is made with the aim of pursuiting an optimized solution which simplifies constructive aspects, too. In fact, by this D_D definition, all possible collisions between tie rods and the plates of the chassis are intrinsically avoided.

	x_{LN}	y_{LN}	z_{LN}	x_{LO}	y_{LO}	z_{LO}
max [mm]	76.5	570	264	100	300	224
min [mm]	220	634	450	276.5	400	450

Table 4.1: P_0 basic points and their static ranges for steer mechanism

4.3.2 Results

In this section the results of the numerical optimization are presented. All evaluations are made on the basis of the roll system mechanism chosen to be developed. Some optimized solutions are described, with the purpose of highlighting some aspects pointed out during the "tuning process" cited in the previous paragraph, with particular regards to the influence of scale factors and vector state chosen to address the optimization. Two DOF's of the system can be constrained, as highlighted in Par. 3.3.2, by imposing values either to one (or more) variables directly defined in the multibody model, or to one (or more) indirect parameters. In this application, both approaches are used, according to the kinematic parameter to be evaluated:

1. second approach, by specifying a couple of values for δ_{mean} and φ_{mean} angles: this choice is used to evaluate $A\%$ values in some points inside the operative field $[\delta_{mean}; \varphi_{mean}]$, allowing for a more homogeneous evaluation of candidate mechanisms: in fact, if the particular state (i.e. the motion requirement specified by one or more components of r vector) to be evaluated by performance criterion is specified in terms of rack and roll slide translations (which are directly defined in the multibody model), any comparison between different mechanism is distorted, since kinematic parameters are computed at different values for δ_{mean} and φ_{mean}. In addition, by commanding the whole system through these two mean angles, the operative range in which to perform any evaluation can be bounded in a convenient range: i.e. limits for δ_{mean} and φ_{mean} can be directly chosen;

2. first approach to specify the rack translation Δy_{rack}, and second approach to specify the mean camber φ_{mean}. This method is adopted in the evaluation of the Δ_{mean} induced by roll movements: in fact the evaluation of the roll/steer correlation can be made only if the steer command is fixed, by measuring the change in Δ_{mean} induced by a change in φ_{mean}.

At this stage, the evaluation of kinematic parameters is restricted to the range range $[0; 20°]$ for both δ_{mean} and φ_{mean} angles, for two reasons: first, this range is considered wide enough to evaluate steer in common usage; second, camber is limited to a max value of $\sim 20°$ due to constructive restrictions, as explained in Par. 4.1.1.

The choice of w_Δ and w_A values and of vector r used to impose conditions 1 and 2 is arbitrary, however it must be made according to a defined criterion: in this case study, some

trials ($\sim$ 20) were made to test the effect of these variables in optimization results. During this "tuning phase", a local gradient-based optimization algorithm, fmincon, is used. The best solutions, according to functional requirements, were obtained by imposing:

1. defining a target of type obj_A (Eq. 4.7) in two different states of type $[\delta_{mean} = \delta_{m_1}; \varphi_{mean} = 0]$ and $[\delta_{mean} = \delta_{m_2}; \varphi_{mean} = 0]$ (where subscripts indicate a chosen constant value);

2. defining two targets, one of type obj_A and the other one of type obj_Δ (Eq. 4.7), in a single state of type $[\Delta y_{rack} = 0; \varphi_{mean} = \varphi_{m_1}]$ (with the same notation).

The first trial configuration used in the optimization process is represented in Fig. 4.19: this layout is generated by choosing a rack length equal to a commercial model and placing it at the same height of six-bar linkage center of rotation with respect to the chassis, in the desired volume B; other member lengths and position on XY plane are inspired by common proportions of commercial steer systems, too. The kinematic behaviour of this first trial solution is represented by Fig. 4.20 and 4.21: the first one shows the distribution of $A\%$, the second one of Δ_{mean}, over the specified operative field; please note that angles φ_{mean} and δ_{mean} were substituted by Δy_{rs} and Δy_{rack}, more meaningful by a handling point of view. This solution is not well

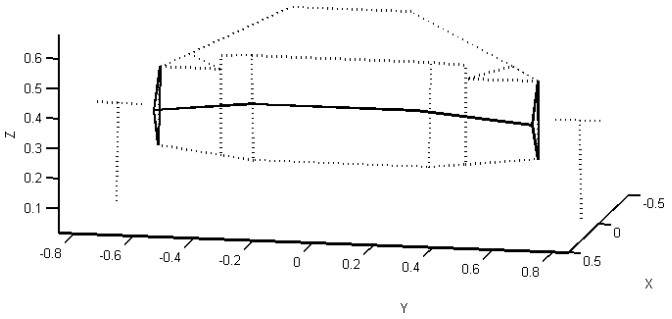

Figure 4.19: First trial solution

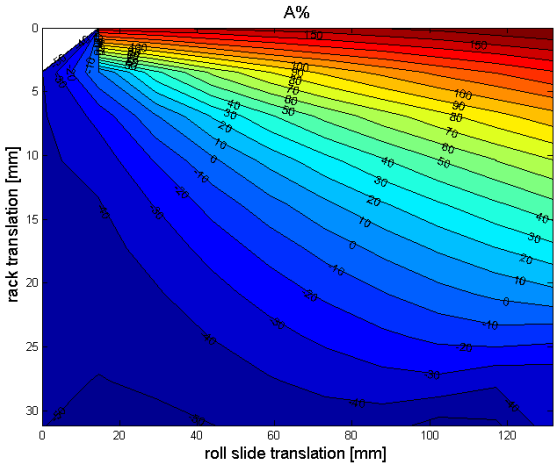

Figure 4.20: $A\%$ field for first trial solution

performing: the $A\%$ field presents negative values in the lower, left area, so wheels are toed in a considerable part of the operative field. In addition, Fig. 4.21 depicts an improvable roll/steer

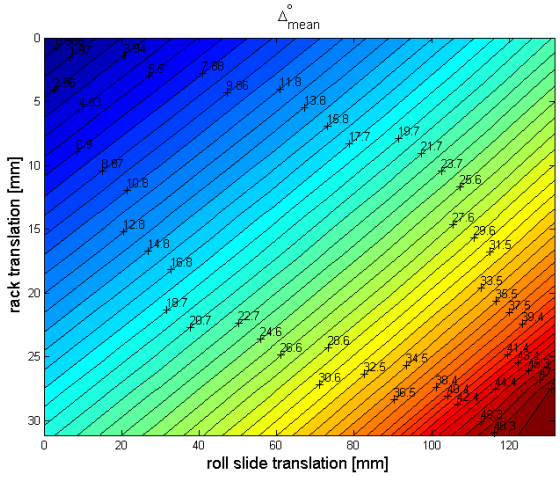

Figure 4.21: Δ_{mean} field for first trial solution

correlation, due to the high slope of curves: being the rack fixed in symmetrical position, a 20° mean roll angle φ_{mean} induces a Δ_{mean} of $\sim 20°$. The first "tuning phase" of optimization revealed some key aspects. The first one is the importance of imposing a target obj_A in a rolled position: Fig. 4.23 and 4.24 refer to two conditions obj_A on two non rolled positions ("Case 1", Table 4.2); Fig. 4.26 and 4.27, instead, depict the results obtained by a single condition obj_A on a rolled configuration with null rack translation Δy_{rack} ("Case 2", Table 4.3). The optimal configurations obtained in two cases are reported in Fig. 4.22 and 4.25, respectively.

state	**condition**	**scale factors**
$[\varphi_{mean} = 0; \delta_{mean} = 1°]$	$obj_A = 1$	$w_A = 1$
$[\varphi_{mean} = 0; \delta_{mean} = 20°]$	$obj_A = 1$	$w_A = 1$

Table 4.2: States and conditions imposed on Case 1

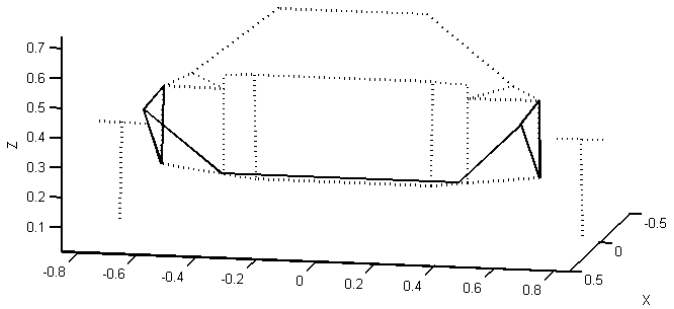

Figure 4.22: Case 1: optimal solution layout

Case 2 features a better behaviour concerning both the A field distribution and the roll steer correlation: in fact, Case 1 exhibits acceptable $A\%$ values only at low camber values, see Fig. 4.23; the white zone is characterized by $A < -0.5$, i.e. wheel toe angle is very high. At the same time, camber has a contrasting effect on Δ_{mean}, Fig. 4.24: imposing a fixed value to rack translation Δy_{rack}, a raise in roll slide translation causes an irregular decrease in Δ_{mean} value, with apparent issues in terms of handling and safety. On the contrary, Case 2 presents a regular A field distribution (except for high left corner, in which A raises toward an infinite

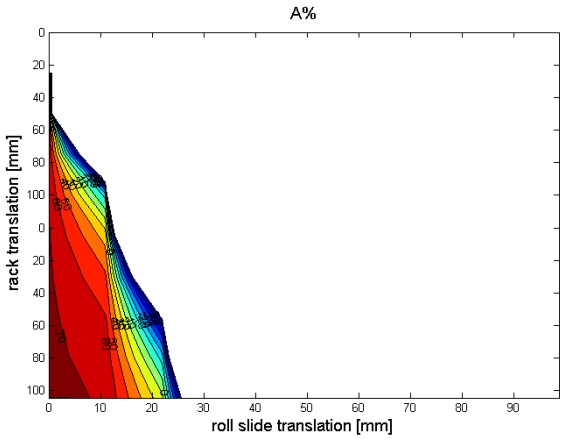

Figure 4.23: $A\%$ field for Case 1

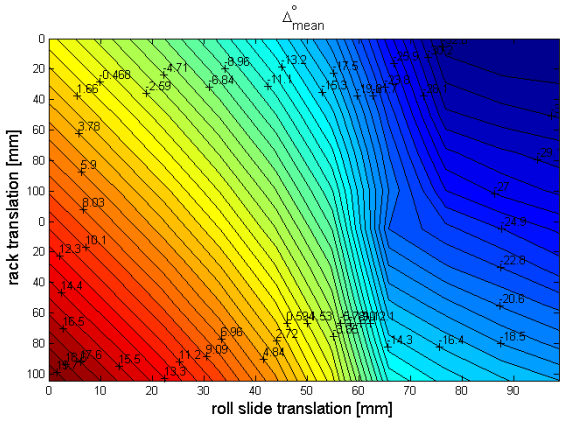

Figure 4.24: Δ_{mean} field for Case 1

state	condition	scale factors
$[\varphi_{mean} = 1°; \Delta y_{rack} = 0]$	$obj_A = 1$	$w_A = 1$

Table 4.3: State and condition imposed on Case 2

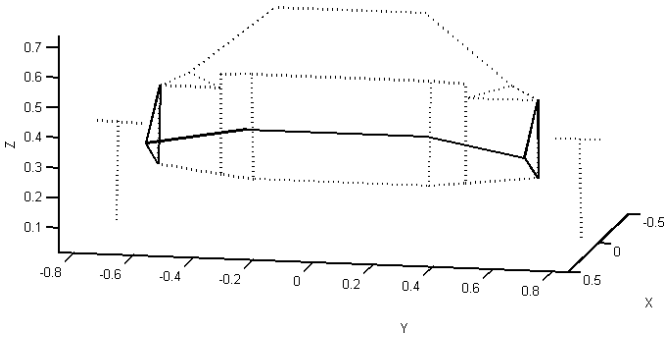

Figure 4.25: Case 2: optimal solution layout

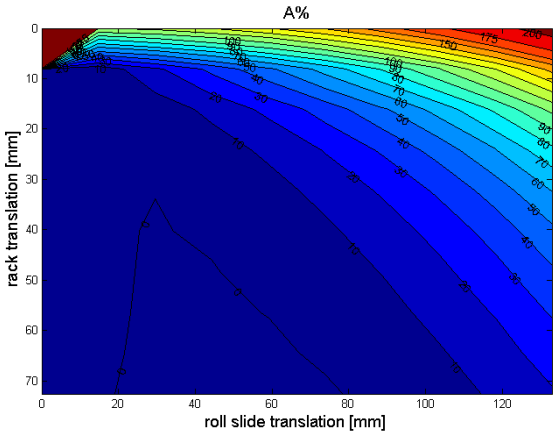

Figure 4.26: $A\%$ field for Case 2

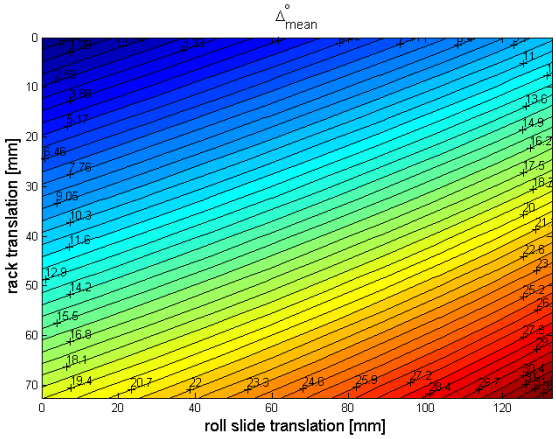

Figure 4.27: Δ_{mean} field for Case 2

value, but this behaviour is to be considered common, due to A formulation and small Δ values), Fig. 4.26. Also the roll/steer correlation is improved, Fig.4.27: a regular, enhancing effect of roll over Δ_{mean} value is observed, even if of very high entity. For example, with null rack translation, a roll angle of $20°$ corresponds to an induced Δ_{mean} of about $11°$. A second key

state	**condition**	**scale factors**
$[\varphi_{mean} = 0; \delta_{mean} = 1°]$	$obj_A = 1$	$w_A = 3$
$[\varphi_{mean} = 0; \delta_{mean} = 20°]$	$obj_A = 1$	$w_A = 3$
$[\varphi_{mean} = 1°; \Delta y_{rack} = 0]$	$obj_A = 1; obj_\Delta = 1°$	$w_A = 1; w_\Delta = 100$

Table 4.4: States and conditions imposed on Case 3

aspect is related to relative magnitude of scale factors w_A and w_Δ: Fig. 4.29, 4.30 and Fig. 4.32, 4.33 refer to solutions of Fig. 4.28 (”Case 3”) and 4.31 (”Case 4”), respectively, obtained with parameters of Table 4.4 and 4.5. It can be observed that the only change in w_A and w_Δ proportions lead to totally different solutions. Two examples of effects of changes in r vector definition are reported. Case 4 and 5 (Table 4.6) differ only in the definition of the first point on which a target of type obj_A is imposed: in particular, in Case 5, a higher value of δ_{mean} is used. However, the local optimization produced an identical result, finding the same local minimum.

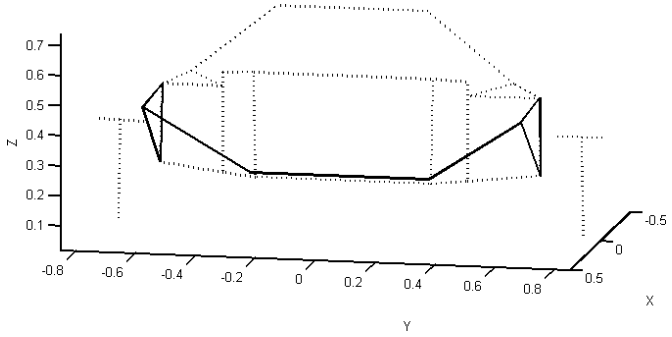

Figure 4.28: Case 3: optimal solution layout

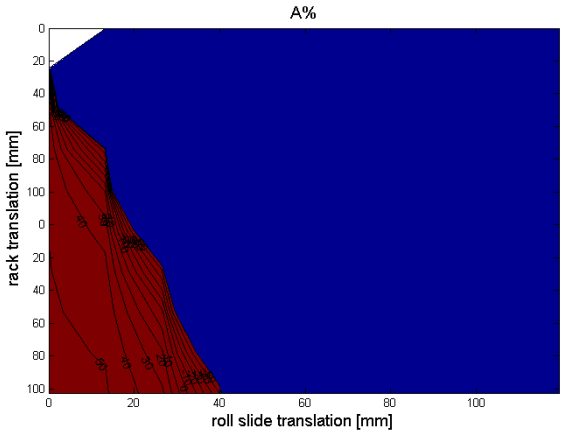

Figure 4.29: $A\%$ field for Case 3

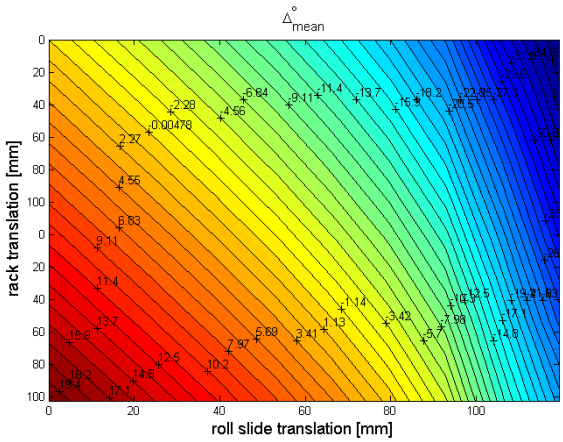

Figure 4.30: Δ_{mean} field for Case 3

state	**condition**	**scale factors**
$[\varphi_{mean} = 0; \delta_{mean} = 1°]$	$obj_A = 1$	$w_A = 1$
$[\varphi_{mean} = 0; \delta_{mean} = 20°]$	$obj_A = 1$	$w_A = 1$
$[\varphi_{mean} = 1°; \Delta y_{rack} = 0]$	$obj_A = 1; obj_\Delta = 1°$	$w_A = 1; w_\Delta = 1000$

Table 4.5: States and conditions imposed on Case 4

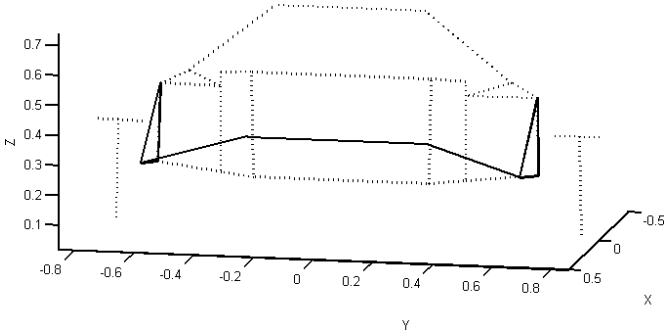

Figure 4.31: Case 4: optimal solution layout

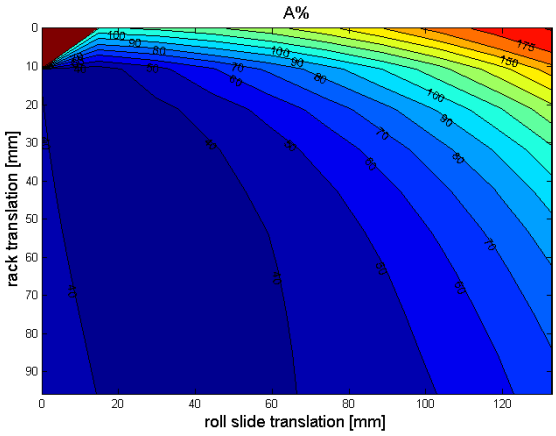

Figure 4.32: $A\%$ field for Case 4

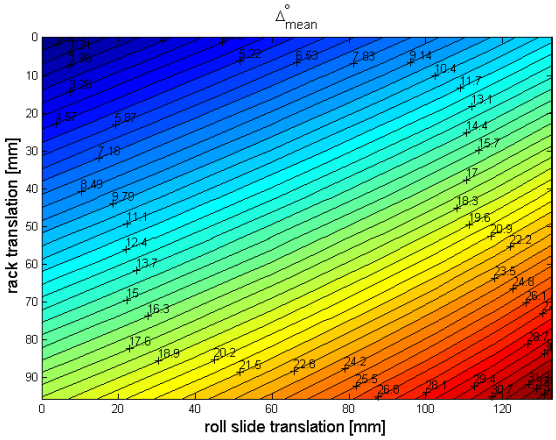

Figure 4.33: Δ_{mean} field for Case 4

On the contrary, a similar change in the definition of the operative point with the target condition

state	condition	scale factors
$[\varphi_{mean} = 0; \delta_{mean} = 5°]$	$obj_A = 1$	$w_A = 1$
$[\varphi_{mean} = 0; \delta_{mean} = 20°]$	$obj_A = 1$	$w_A = 1$
$[\varphi_{mean} = 1°; \Delta y_{rack} = 0]$	$obj_A = 1; obj_\Delta = 1°$	$w_A = 1; w_\Delta = 1000$

Table 4.6: States and conditions imposed on Case 5

of type obj_Δ (Case 6, Fig. 4.35, 4.36, 4.34 and Table 4.7) produces, with respect to Case 4, again, a worsening effect on $A\%$ distribution (lower values), paired with a positive, but small, reduction in roll/steer correlation. It can be concluded that parameters used in Case 4 (Table 4.5) can be used as a reference for the final step of optimization. Therefore, they are used to address a global optimization by using the GlobalSearch algorithm embedded in Matlab [11] [12] this gradient-based method differs from the previous one by the generation of multiple starting points by a scatter algorithm, so producing a series of candidate optimal solutions, among which the best is selected. Even if this algorithm is dedicated to the search for the global minimum, the final solution can coincide with it or not, depending on the position of starting points and their number. In this case, a total of 64 starting points are taken into account; 29 local minima are found, according to the selection criteria used by the algorithm. Fig. 4.37, 4.38 and 4.39 report the layout and the $A\%$ and Δ_{mean} distributions of the final optimal solution. It can be noticed that the overall behaviour represents a further improvement over the best local optimal solution, Case 4: the $A\%$ field presents a plateau at around 40% value in the middle-left zone, and higher values between 50% and 100% in a greater range of operative points. Similarly, Fig. 4.39 highlights a small, enhancing roll-steer correlation: only the Δ_{mean} field of Fig. 4.36 depicts a better behaviour. In the end, the solution found by the GlobalSearch algorithm can be considered as the best performing one among the presented optimal solutions.

state	condition	scale factors
$[\varphi_{mean} = 0; \delta_{mean} = 1°]$	$obj_A = 1$	$w_A = 1$
$[\varphi_{mean} = 0; \delta_{mean} = 20°]$	$obj_A = 1$	$w_A = 1$
$[\varphi_{mean} = 15°; \Delta y_{rack} = 0]$	$obj_A = 1; obj_\Delta = 1°$	$w_A = 1; w_\Delta = 1000$

Table 4.7: States and conditions imposed on Case 6

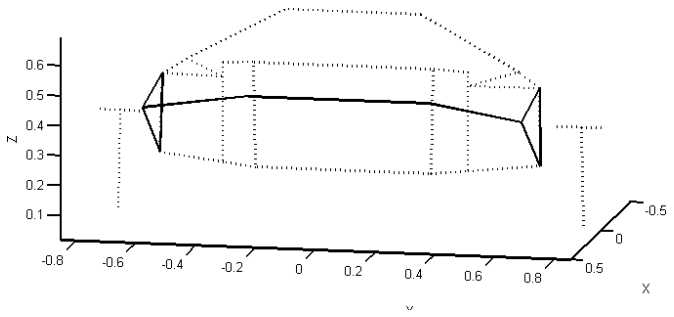

Figure 4.34: Case 6: optimal solution layout

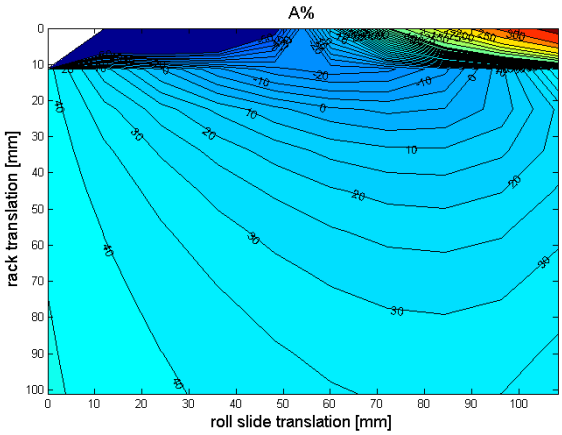

Figure 4.35: $A\%$ field for Case 6

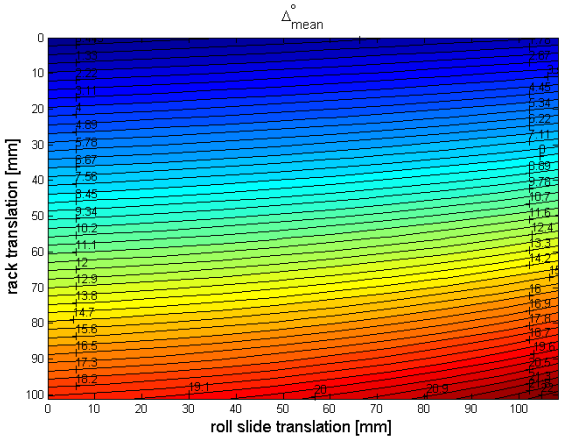

Figure 4.36: Δ_{mean} field for Case 6

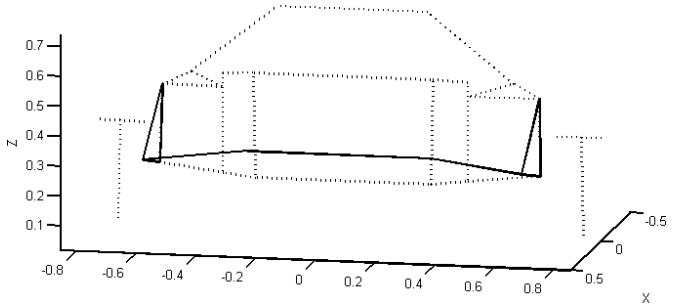

Figure 4.37: Final optimal solution layout

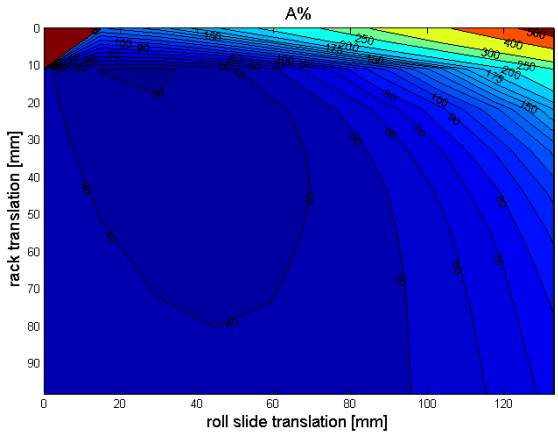

Figure 4.38: Δ_{mean} field for final optimal solution

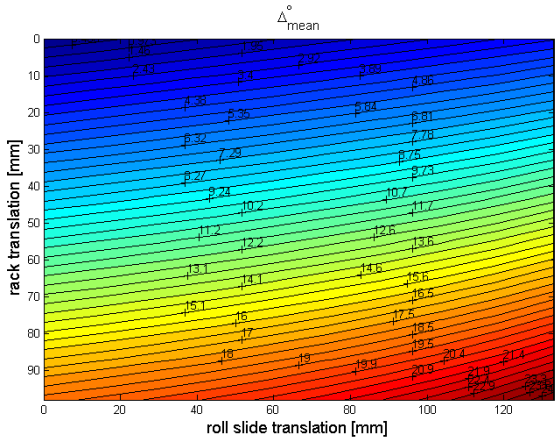

Figure 4.39: Δ_{mean} field for final optimal solution

4.4 Conclusions

The present Chapter presents the kinematic synthesis of the steer system. This process considers the roll system layout chosen for the development as a starting point: in fact, both subsystems must cooperate during cornering. Therefore, the target, in this case, is focused only on pointing out a well performing solution to be adopted in the specific analyzed case. The synthesis process was composed of two main steps: the first one aimed to highlight some critical aspects and based upon an empirical approach, supported by the use of a multibody model implemented in a commercial code. This phase proved to be useful to investigate the general behaviour of some candidate mechanisms and to address the following phase by an improvement in the definition of test parameters, but not performing enough to lead to the definition of a final result. The second step was based on a numerical optimization based upon a fully dedicated multibody model implemented in Matlab code. The optimization strategy required to perform a set of trials to be fully defined: the final optimal solution, even if found by a global optimum search algorithm, depends on chosen input parameters and on the specific implementation of the performance criterion. There is no guarantee that such a solution fully coincides with the best optimum, but it proved to be the best performing candidate among all solutions found, and completely fulfills functional requirements. The target of the kinematic synthesis is so reached.

CHAPTER 5

The suspensions

The design of suspensions presents, in this case study, a degree of correlation with other subsystems higher than usual. In fact, the six-bar linkage mechanism provides both the roll movement and the suspensive effect. The layout of this mechanism is defined in Chapter **??** according to targets expressly dedicated to satisfy functional requirements related to the roll movement. However, the subsystem composed by the roll slide, the rockers and the shock absorbers is still undefined: therefore, this sub-assembly can be studied to promote a satisfying suspensive behaviour. The geometrical layout is represented in Fig. 5.1. The scheme follows

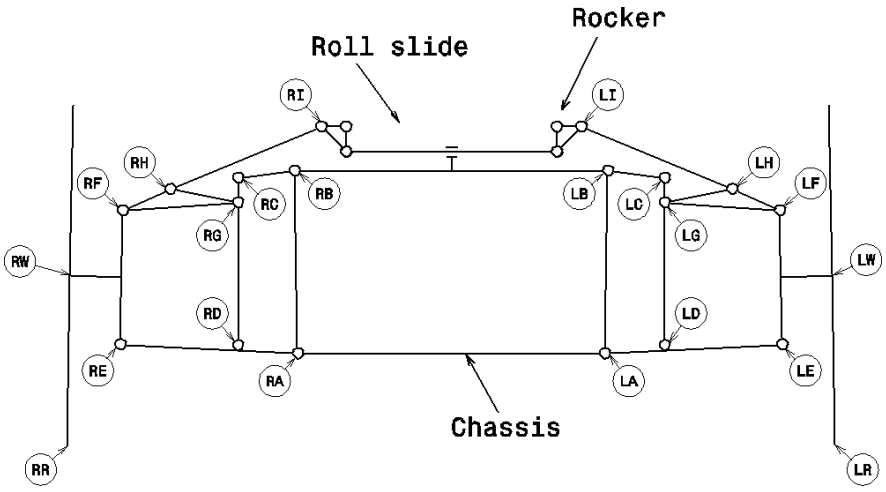

Figure 5.1: Layout of the suspension system

the model of Fig. 3.7, however all the roll slide subsystem is positioned on the top of the chassis, due to the constructive reasons discussed in Chapter 1. Points I are already fixed according to the chosen roll system layout, therefore the only geometrical points which can be set at this stage coincide with rotational joints which link rockers to roll slide and shock absorbers.

The process adopted for this kinematic synthesis differs a bit from previous ones: this case is characterized by a smaller amount of variables, and the interpretation of the problem is done without the empirical, trial and error based preliminary analysis adopted in roll and steer

system synthesis. Additionally, constructive constraints are limited with respect to previous cases. The definition of test parameters, however, is not fully conventional: common criteria can be used to test the suspensive behaviour of this subsystem, but other ones must be defined to grant a good correlation between roll and suspensive actions: the integration of the roll and suspension subsystems should provide a damping effect on roll movements, without precluding performances of suspensive effect. In particular, the following functional requirements are set:

1. the compression or extension of shock absorbers should not substantially modify the balance in static, rolled positions;

2. suspensive capability should not significantly change when the chassis is rolled.

These requirements can be achieved if shock absorber travel induced by roll actuation is minimal. Since conventional suspension design guidelines does not cover the fulfillment of this particular requirement, a dedicated solving strategy must be defined: similarly to previous chapters, a kinematic optimization is performed on rockers, with the aim to obtain an acceptable interaction between roll movement an suspensive behaviour.

5.0.1 Multibody modelling for kinematic optimization

The kinematic multibody model described in Chapter 3 can be adjusted to be used in rocker optimization, by introducing basic points L, M and L' depicted in Fig. 5.2. To describe

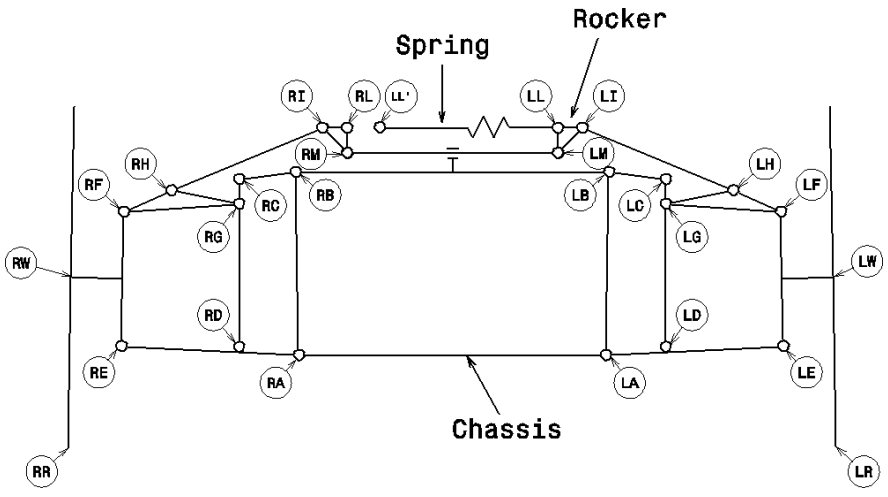

Figure 5.2: Basic points of the adopted kinematic multibody model

constraint definition, the optimization strategy must be first discussed. As usual, the whole optimization process can be referred to the general scheme of Fig. 3.15. The functional requirements listed in the previous paragraph must be translated in kinematic parameters upon which the performance criterion can be defined. Fig. 5.3 illustrates the lateral equilibrium in a generic rolled configuration. Referring to a single axle, the lateral load transfer is composed by two components, ΔF_{zc} and ΔF_{zg}, caused by the centrifugal force F_c and by the gravity force F_g, which can not equally distribute on two wheels since the actual center of gravity G' is not in symmetrical position. Neglecting the component due to F_c, and defining $F_{zl} = \frac{F_g}{2} + \Delta F_{zg}$ and

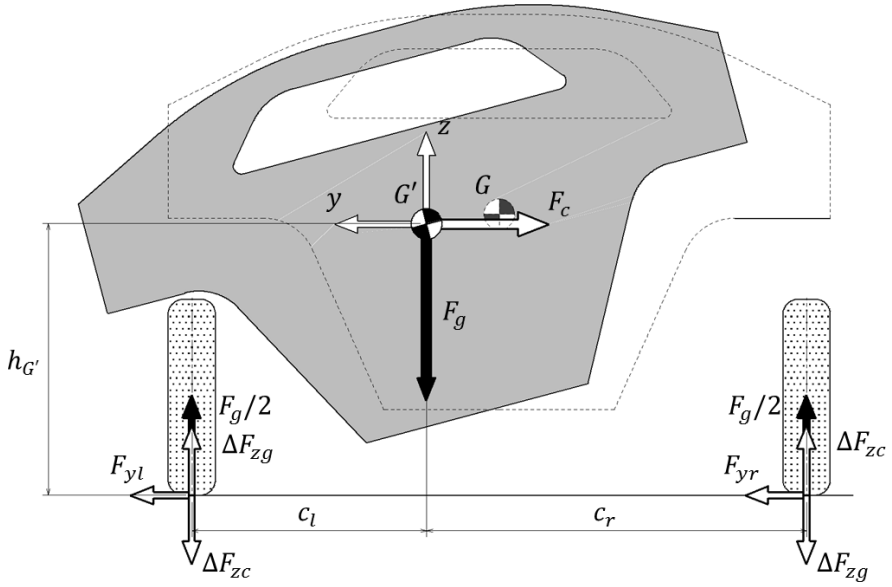

Figure 5.3: Lateral equilibrium in a generic rolled configuration

$F_{zr} = \frac{F_g}{2} - \Delta F_{zg}$, the rotational equilibrium results in:

$$\begin{cases} F_{zl} = F_g \dfrac{c_r}{c_l + c_r} \\ F_{zr} = F_g \dfrac{c_l}{c_l + c_r} \end{cases} . \tag{5.1}$$

To fulfill the above cited first and second functional requirements, in ideal conditions the force acting on both left and right spring is identically the same, in each configuration (i.e. at each roll angle): in fact, if this condition is satisfied, spring travel induced by a roll position (in static conditions) is null. Even if the fulfillment of this condition cannot be identically achieved, the error can be minimized. Ideally:

$$\frac{F_{el}}{F_{er}} = 1 \tag{5.2}$$

for each roll angle. Introducing velocity ratios τ_l and τ_r between spring travel and vertical displacement of wheel contact point (on left and right side, respectively), vertical forces acting on two wheels can be expressed as:

$$\begin{cases} F_{zl} = F_{el}\tau_l \\ F_{zr} = F_{er}\tau_r \end{cases} \tag{5.3}$$

where F_{el} and F_{er} are the elastic forces acting on left and right spring, respectively. It is basic to note that, in this case, the defined velocity ratios change not only during suspension travel, but also as a consequence of a change in the imposed roll angle, since it induces an overall displacement of the mechanism. By combining Eqns. 5.1, 5.2 and 5.3:

$$\frac{\tau_l}{\tau_r} = \frac{c_r}{c_l} \tag{5.4}$$

which represents the final condition, and can be used as a target in the optimization phase. The implementation could consist in adopting Eq. 5.4 as an objective in a limited set of system states defined, as usual, by a vector r; for this specific evaluation, r contains a first array r_1 of

mean camber angles (between left and right wheel) at which the target defined by Eq. 5.4 can be imposed. A first component of the objective function can be chosen as:

$$c_{1susp} = \sum_{r_1} \left(1 - \frac{r_\tau}{r_c}\right)^2 \tag{5.5}$$

where $r_\tau = \frac{\tau_l}{\tau_r}$ and $r_c = \frac{c_r}{c_l}$. The minimization of this first objective function component is aimed at limiting the interaction between roll actuation and suspensive effect, therefore at least one additional condition should be used to address the synthesis of rockers according to damping performances: for example, a progressive behaviour could be desirable. However, in the present optimization, another objective is chosen: the maximization of the magnitude of the velocity ratio τ_l (and τ_r), defined as the mean value between a set of evaluations computed in different system states, which coincide with the same roll angles specified by vector r_1. The second component of the objective function is therefore:

$$c_{2susp} = -\sum_{r_1} \left(\tau_l^2 + \tau_r^2\right) \tag{5.6}$$

This second criterion aims at maximizing, being chosen the spring stiffness, the total force calculated at the contact points (Eq. 5.3), so allowing shock absorbers to be selected among a greater set of commercial (or dedicated) solutions: in particular, softer springs can be adopted, and a wider range of equivalent force applied to contact points can be obtained, so providing a greater flexibility in the final tuning phase. However, a so defined optimization strategy suggests to test the progressive behaviour of produced optimal solutions before choosing the one to be developed.

The kinematic parameters needed to evaluate Eq. 5.5 and 5.6 are τ_l, τ_r, c_l and c_r, and need to be defined in the kinematic multibody model. Velocity ratios are defined by computing the spring axial travel caused by a unitary vertical displacement imposed on wheel contact point. This displacement is assumed to be symmetrical with respect to the position to be tested. By an operational point of view, this means that first, a rolled configuration must me computed, which is used as reference. Then, two different additional displacements must be imposed, corresponding to two additional system states: the first one is applied to the contact points (left and right) on z direction, and has negative sign (State 1); the second one is similar, except for the positive sign (State 2). At the same time, the distance between points L and L' (Fig. **??**) is calculated on both sides, for each of two additional system states. Since the total vertical displacement imposed on contact points is unitary, the difference between $\overline{LL'}$ length calculated in State 2 and State 1 on both sides coincides with velocity ratios τ_l and τ_r:

$$\begin{aligned} \tau_l &= \left|\overline{LL - LL'}\right|_{State2} - \left|\overline{LL - LL'}\right|_{State1} \\ \tau_r &= \left|\overline{RL - RL'}\right|_{State2} - \left|\overline{RL - RL'}\right|_{State1} \end{aligned} \tag{5.7}$$

with the usual notation of symbols. The imposition of both State 1 and State 2 can be applied by introducing a second state array r_2: therefore, the complete state of the system is imposed by a vector state $r = [r_1; r_2]$. Last, the computation of kinematic parameters c_l and c_r is performed in the same system states, by using following expressions:

$$\begin{aligned} c_l &= y_L R - y_{COG} \\ c_r &= y_{COG} - y_R R \end{aligned} \tag{5.8}$$

which require the definition of center of gravity position.

Being the optimization strategy discussed, the constraint equations to be applied to the multibody model can be defined. As aforementioned, the state vector r is used, in this case, to impose two types of motion requirements to the system: the first one consists in a mean camber angle φ_{mean} to be applied to wheels; the second one is a pair of vertical displacements Δz_R to be applied on both contact points (left and right side), with the same value. Therefore, a single state of the system is theoretically defined by a couple of values of type $[\varphi_{mean}(r); \Delta z_R(r)]$. In the adopted implementation, however, the kinematic problem is solved in two sequential steps: first, a roll position is imposed and taken as reference (State 0) for the calculation of the above mentioned two additional states State 1 and State 2. The solution of State 0 is carried out by an algorithm similar to the one used in the roll system optimization, implementing the constraint equations described in Par. 3.2.2: in this case, points L, M and L' are added, and constrained to be fixed to the roll slide with conditions, embedded in the displacement vector, of type:

$$\begin{aligned} y_P &= (y_{P_0} + \Delta y_{rs})u_{z_c} - z_{P_0}u_{y_c} \\ z_P &= \Delta z_c + (y_{P_0} + \Delta y_{rs})u_{y_c} + z_{P_0}u_{z_c} \ . \end{aligned} \tag{3.14}$$

Then, the solution of State 1 and 2 is performed: it requires a dedicated set of conditioning equations. All points that belong to chassis and roll slide does not undergo to any transformations, since at this computation stage they are fixed: therefore, values of their natural coordinates are not modified by the displacement vector ΔP, and congruency is intrinsically respected. On the contrary, the rigid body condition must be imposed on all members of six-bar linkages and to bodies $\overline{IL}$, $\overline{IM}$ and $\overline{LM}$ which compose rockers, by the already described expression:

$$(y_P - y_Q)^2 + (z_P - z_Q)^2 - [(y_{P_0} - y_{Q_0})^2 + (z_{P_0} - z_{Q_0})^2] = 0 \ . \tag{3.6}$$

The imposition of motion requirements does not need the definition of indirect kinematic parameters, since it is directly applied on existing natural coordinates z_{LR} and z_{RR}.

The multibody model used in State 0 solution features a single DOF (φ_{mean}), while the model used in State 1 and 2 solutions has two DOF's (z_{LR} and z_{RR}), even if they are imposed to be identical by specifying the same motion requirement. Kinematic parameters c_l and c_r are computed in State 0, while τ_l and τ_r are calculated after determining the State 1 and 2.

5.0.2 Implementation and results

The use of the performance criterion defined in previous paragraph needs the specification of COG coordinates: in this case, it can be determined only by an estimation of weights distribution. However, the relative error is considered to be small enough to allow for obtaining reliable results, in relation to targets to be obtained. The optimization is performed by adopting a mean roll angle φ of $6°$, $12°$ and $18°$, therefore three states are tested. Vertical translations of both contact points are set to be equal to $-0.5\ mm$ and $0.5\ mm$ on additional State 1 and 2, respectively. Like in roll system optimization, the multi-objective genetic algorithm embedded in Matlab code is chosen, aiming, in this case, at providing a set of possible solutions which grant a flexible selection of shock absorbers. This last process can be profitably done only when precise data on overall inertial properties of the vehicle will be available.

The Design Space is in this case defined by variables of Table 5.1: it features four dimensions, being z_M fixed and $z_{L'}$ set to be equal to z_L:this means that the center line of shock absorber must be horizontal in initial configuration. The condition on $y_{L'}$ imposes an acceptable range in total spring length.

	LL	LM	LL'
y [mm]	190^{200}_{180}	180^{190}_{170}	$y_L{}^{-270}_{-280}$
z [mm]	700^{700}_{695}	660	z_L

Table 5.1: P_0 basic points and their limits for rocker optimization

Results are represented by the Pareto front of Fig. **??**. As for roll system optimization,

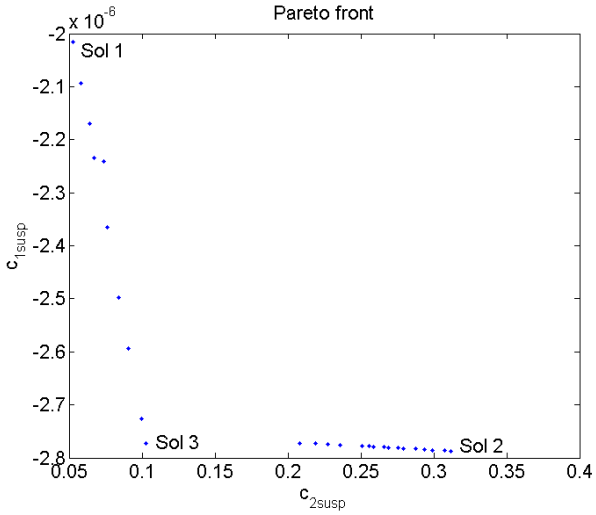

Figure 5.4: Pareto front produced by rocker optimization

objective function components c_{1susp} and c_{2susp} must be regarded as synthetic indices. In addition, as mentioned in previous paragraph, the effective trend of velocity ratios τ_l and τ_r must be analyzed: three solutions are proposed, corresponding to labeled points of Fig. 5.4. Fig.

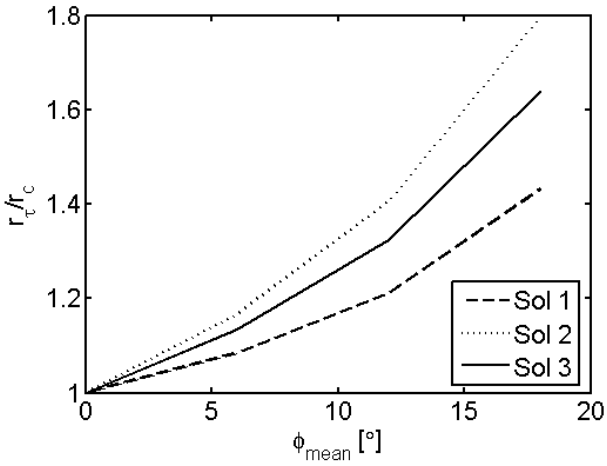

Figure 5.5: $\frac{r_{tau}}{r_c}$ values over mean roll angle φ_{mean} for three selected solutions

5.5 reports ratio $\frac{r_{tau}}{r_c}$ c_{1rock} values over φ_{mean} angles imposed by the state vector r_1 for three selected solutions. Fig. 5.6-5.8 report trend of $\tau_l = \tau_r$ over contact point vertical translations $\Delta z_{lc} = \Delta z_{rc} = \Delta z_R$ in symmetric position ($\varphi_{mean} = 0$). The comparison of three trends

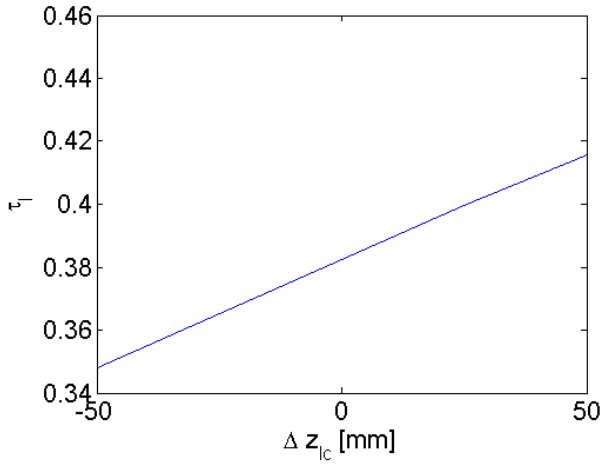

Figure 5.6: Trend of τ_l and τ_r Solution 1, $\varphi_{mean} = 0$

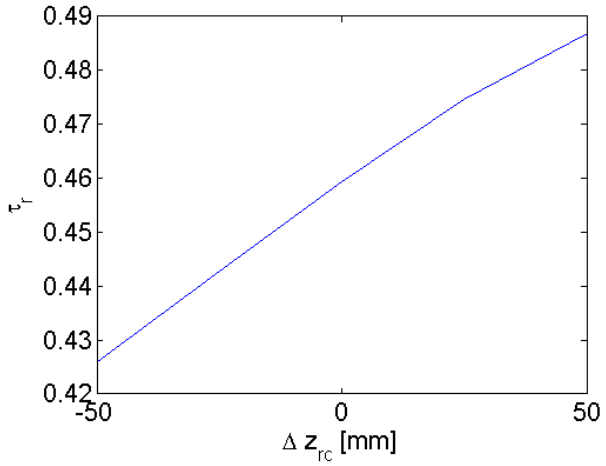

Figure 5.7: Trend of τ_l and τ_r Solution 2, $\varphi_{mean} = 0$

confirms the position of three solution along the Pareto front, demonstrating the effectiveness of $c1susp$ index. Fig. 5.9-5.17 depict the same indices in rolled positions ($6°$, $12°$ and $18°$). It can be observed that, even if in symmetric position all solutions present a progressive behaviour, the ones featuring higher velocity ratios are more prone to exhibit a regressive behaviour in rolled configurations, especially in the wheel at the outer side of curve. In addition, inner side suspension generally features higher velocity ratios. Both these behaviour are more marked at high roll angles. However, Solution 1 appears to be the less affected by these trends, and the loss of the progressive behaviour, in real cases, could be only theoretical: in fact, the regressive behaviour is exhibited in most cases at high values of spring extension. It can be concluded that none of these solution can be rejected at first glance: a solution should be chosen taking into account the characteristics of shock absorbers. Table 5.2 reports position of points for three solutions, with reference to an arbitrary global frame with plane XZ coincident with the longitudinal plane of symmetry of the vehicle.

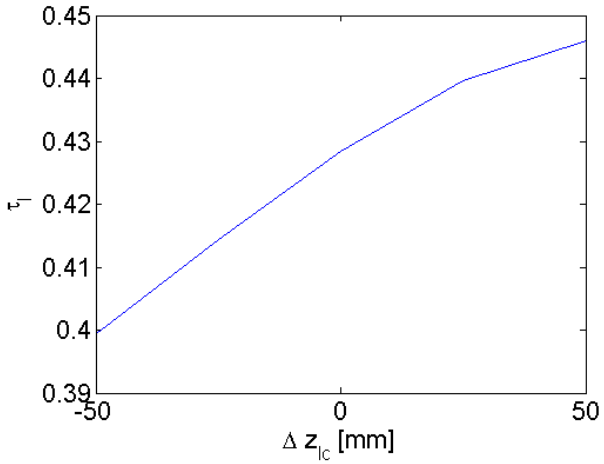

Figure 5.8: Trend of τ_l and τ_r Solution 3, $\varphi_{mean} = 0$

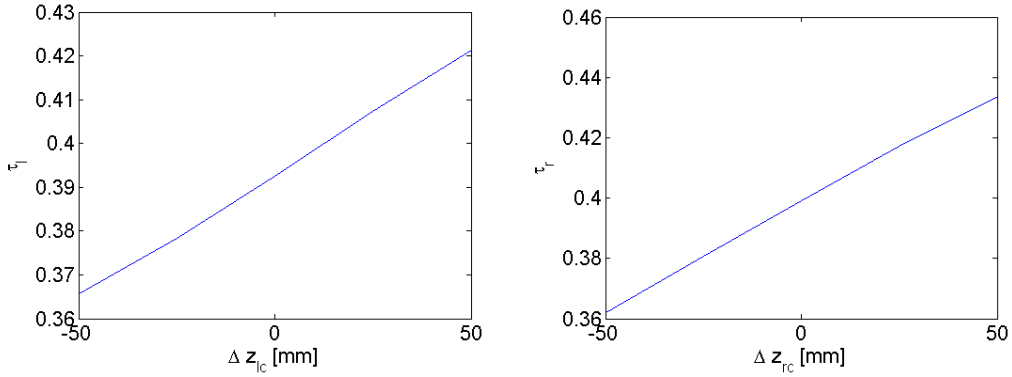

(a) (b)

Figure 5.9: Trend of (a) τ_l and (b) τ_r for Solution 1, $\varphi_{mean} = 6°$

	y_L	z_L	y_M	z_M	$y_{L'}$	$z_{L'}$
Solution 1	180	740	170	655	271.3	740
Solution 2	186.2	740	190	635.4	278.7	740
Solution 3	184.7	740	190	655	277.5	740

Table 5.2: Basic point coordinates of presented solutions [mm]

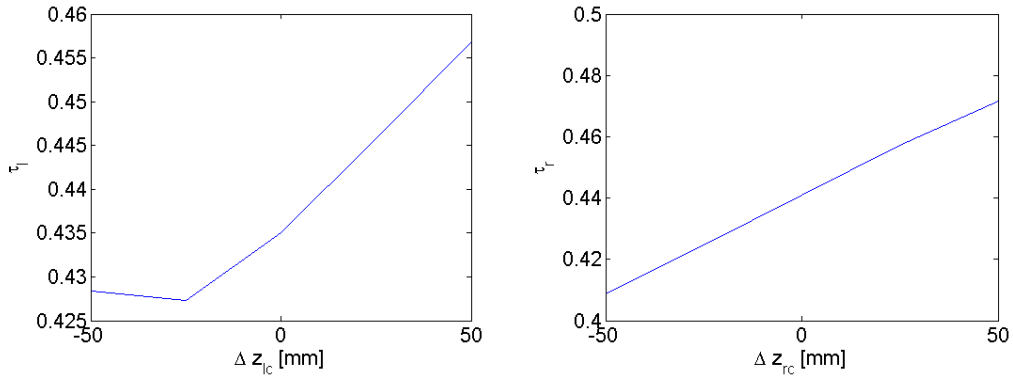

(a) (b)

Figure 5.10: Trend of (a) τ_l and (b) τ_r for Solution 1, $\varphi_{mean} = 12°$

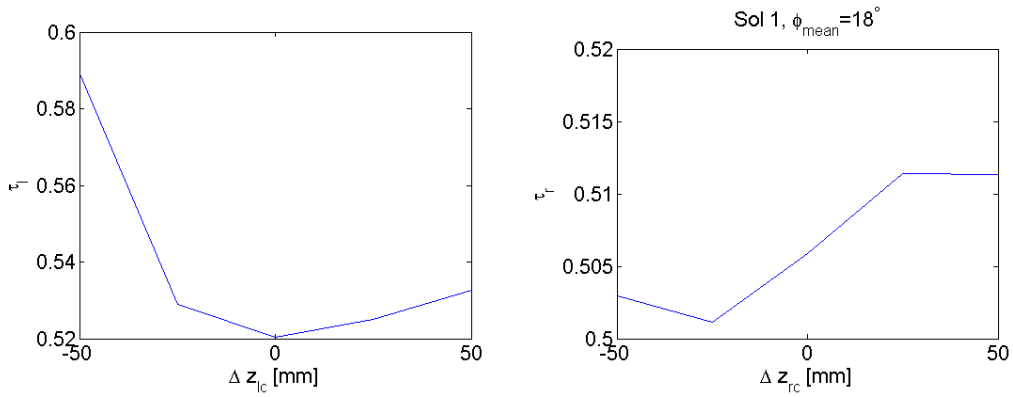

(a) (b)

Figure 5.11: Trend of (a) τ_l and (b) τ_r for Solution 1, $\varphi_{mean} = 18°$

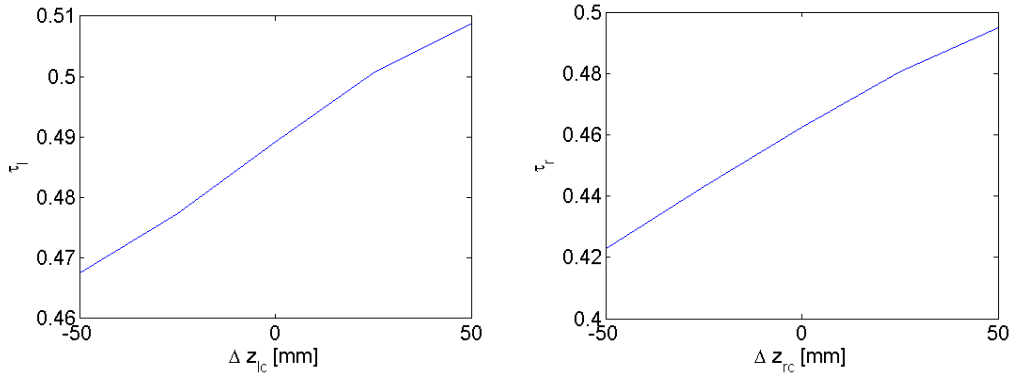

(a) (b)

Figure 5.12: Trend of (a) τ_l and (b) τ_r for Solution 2, $\varphi_{mean} = 6°$

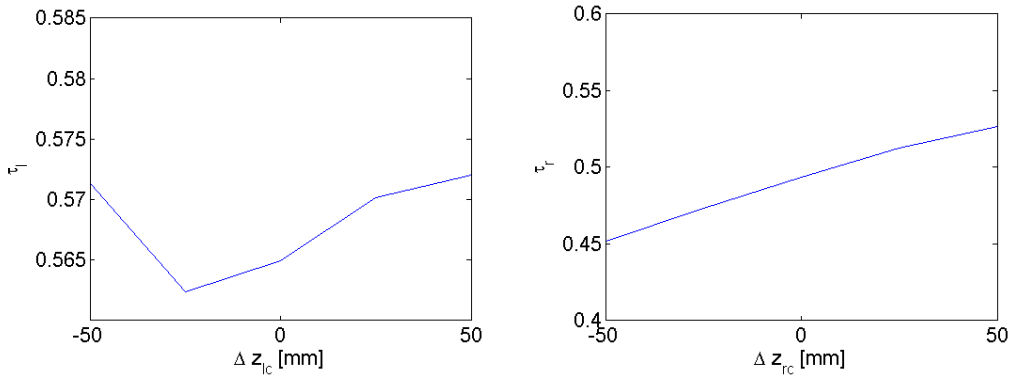

(a) (b)

Figure 5.13: Trend of (a) τ_l and (b) τ_r for Solution 2, $\varphi_{mean} = 12°$

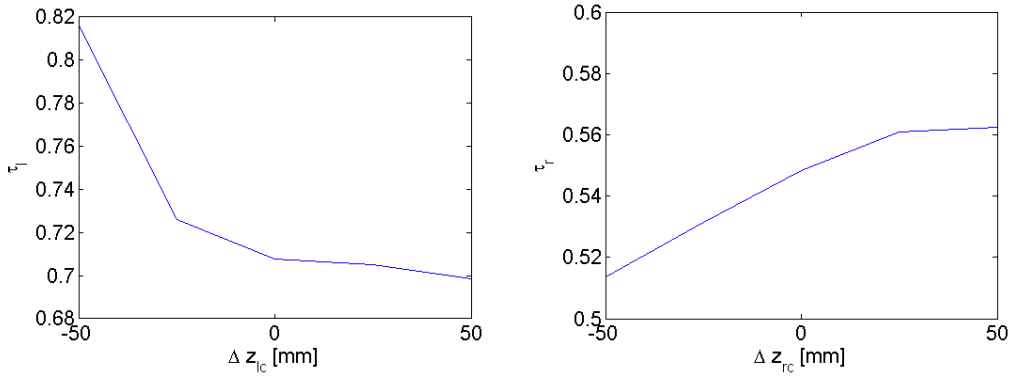

(a) (b)

Figure 5.14: Trend of (a) τ_l and (b) τ_r for Solution 2, $\varphi_{mean} = 18°$

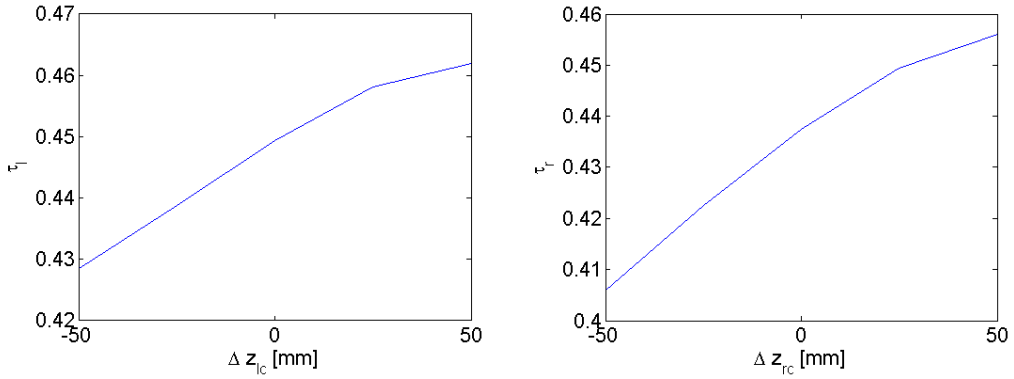

(a) (b)

Figure 5.15: Trend of (a) τ_l and (b) τ_r for Solution 3, $\varphi_{mean} = 6°$

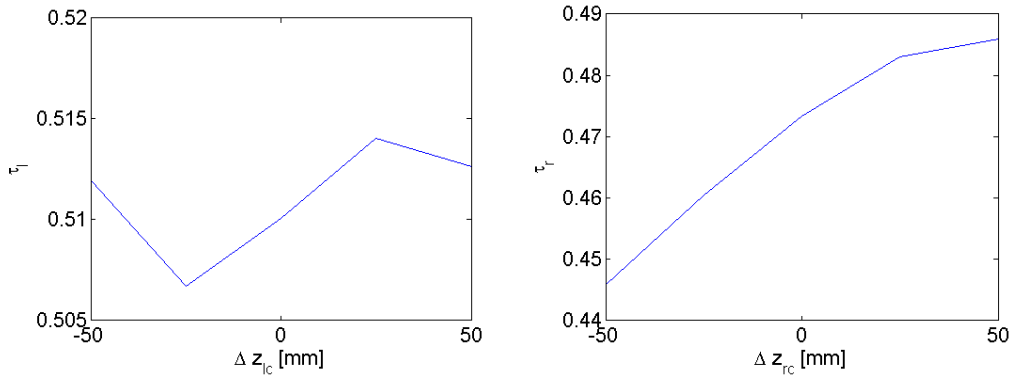

(a) (b)

Figure 5.16: Trend of (a) τ_l and (b) τ_r for Solution 3, $\varphi_{mean} = 12°$

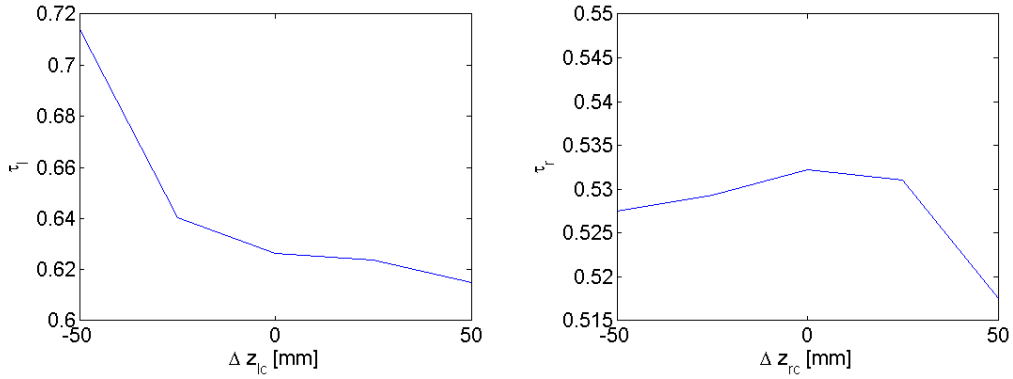

(a) (b)

Figure 5.17: Trend of (a) τ_l and (b) τ_r for Solution 3, $\varphi_{mean} = 18°$

CHAPTER 6

Constructive design of main subsystems

This chapter describes the main aspects related to the constructive design and production of chassis, suspension linkages and steer system. Then, an overall description of the final layout is provided. The general purpose is not to provide a deep insight in constructive problems, but rather highlighting peculiarities due to the particular car concept.

6.1 Chassis

The chassis was the first element to be defined and constructed. The development of this component presents a clear serial approach, characterized by several successive refinements in technical requirement definition. As cited in Chapter 1, the first target to be analyzed consisted in providing a layout which could grant a rational subsystem integration, in particular, by allocating enough room for roll subsystem, without limiting ergonomics. A symbolic master geometry (Fig. 1.2) was used in order to provide the model with the flexibility needed in this phase, aiming at establishing first volumes and measures. Then, a first concept was defined (Fig. 1.3), characterized by a segmented volume partitioning: the key aspect of this solution is related to the adoption of four Ergal plates, which can grant:

- the definition of volumes to be addressed at roll system positioning;
- an increase in stiffness in zones where linking points to suspensions are located;
- an increase in precision of linking points position, by numerically controlled fabrication;
- a smart assembling/disassembling procedure, particularly useful in this prototype, which could require frequent adjustments and modifications. Not only plates can be easily removable, but they can be used as reference for positioning of other components.

The last point could be satisfied also by adopting a patented technology of one of technical sponsors: this consists in producing triangular cuts on pipes of square or rectangular section, involving only three of four edges. This way, the pipe can be bended by using the unique edge as reference, and then be welded. Since cuts are done by laser technology, not only ”bending

pockets" can be produced, but also "assembly pockets". Fig. **??** depicts a pipe prepared for bending. The advantage of this technology resides in an improvement in precision and in time to be dedicated to the assembly phase. The decision of using bending pockets, assembly

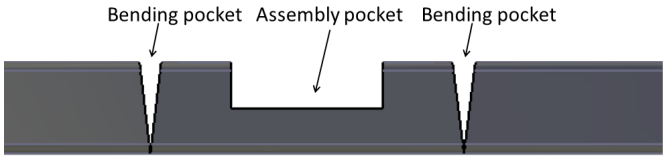

Figure 6.1: Bend and assembly pocket

pockets and described plates completes the preliminary definition of the chassis. The next phase consisted both in the detailed definition of the assembly phase and geometrical properties, and in performing a detailed structural design, coupled with weight containment. This required the combination of two CAE methods, geometrical modelling and structural F.E.A., the first one carried out in Catia V5 environment, the second one in Ansys code. To obtain the functional solution, several iterations and refinements were necessary.

Finite element analyses [13] were aimed at finding out a well performing layout based on the preliminary result obtained by considerations on subsystem integration and ergonomics. Only in a second stage, the detailed geometry was defined. The definition of the topology requires a procedure which can produce fast and reliable results with reference to the overall structural behaviour of the chassis. Processing time and ease in model modifications are two main requirements of the methodology to be adopted. Therefore, the model at this stage was based on $1D$ and $2D$ finite elements: in particular, *beam44* was used for pipes, while *shell63* for plates. Fig. 6.2 depicts one of model revisions. Structural requirements were fixed in:

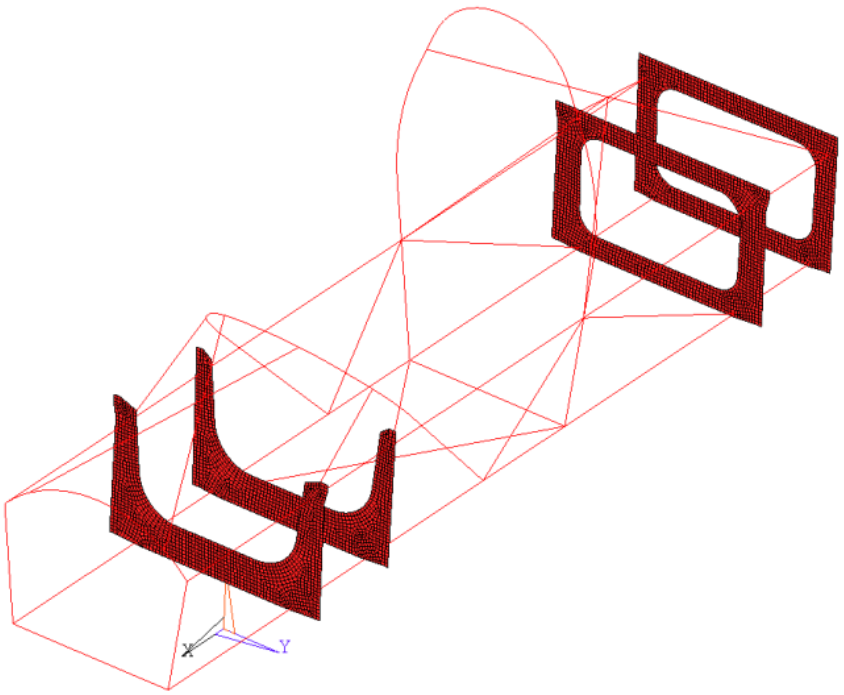

Figure 6.2: $1D$ and $2D$ element based model

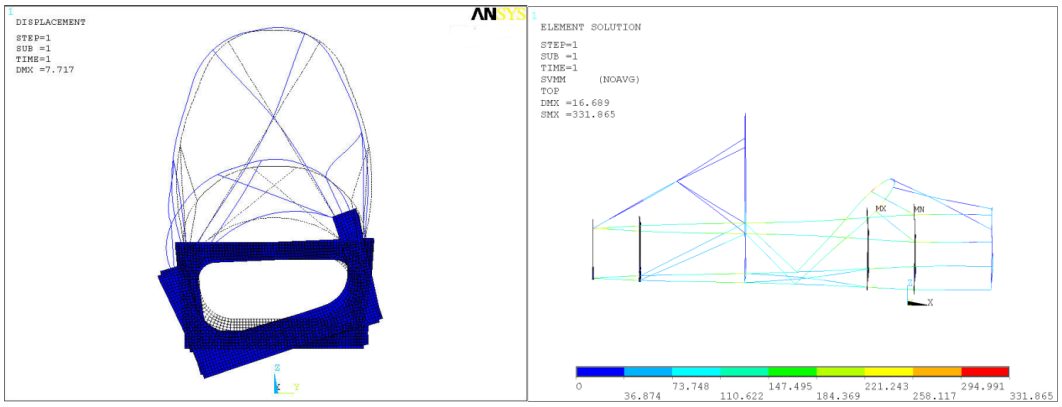

(a) (b)

Figure 6.3: Example of torsional test results: (a) displacements and (b) Von Mises stress distribution

- overall torsional stiffness $K_T = 1300 Nm/°$;
- overall flexural stiffness $K_F = 400 N/mm$.

To fulfill these requirements, several trial configurations were compared by performing both torsional and flexural tests: in both cases, all DOF's of linking points of the rear plate were constrained, while forces were applied in four linking points of the first, front plate. Forces were all applied in the same direction for flexural tests, and in opposite direction in couples for torsional test. Design parameters were:

- section, thickness and material of pipes;
- material of plates
- layout

At the same time, different solutions were compared in weight. Fig. 6.3 reports an example of results of torsional test. This step resulted in pointing out a topology which fulfills structural requirements, with an estimated weight of $67 kg$. The definition of detailed geometry was carried out by geometrical modelling in Catia V5 environment, with the aim of coupling the defined layout with the functional assembly opportunities provided by the particular solutions above discussed. Fig. 6.4 and 6.5 depict the assembling sequence and the final result.

6.2 Suspensions

In this case, the term "suspension" refers to the integrated roll/suspension system. Due to the particular functions provided by this subassembly, constructive aspects must be studied carefully, with the aim of satisfying the following functional requirements:

1. capability in reproducing desired roll maneuvers, without collisions between members;
2. structural compliance;
3. ease in adjustment of member lengths;

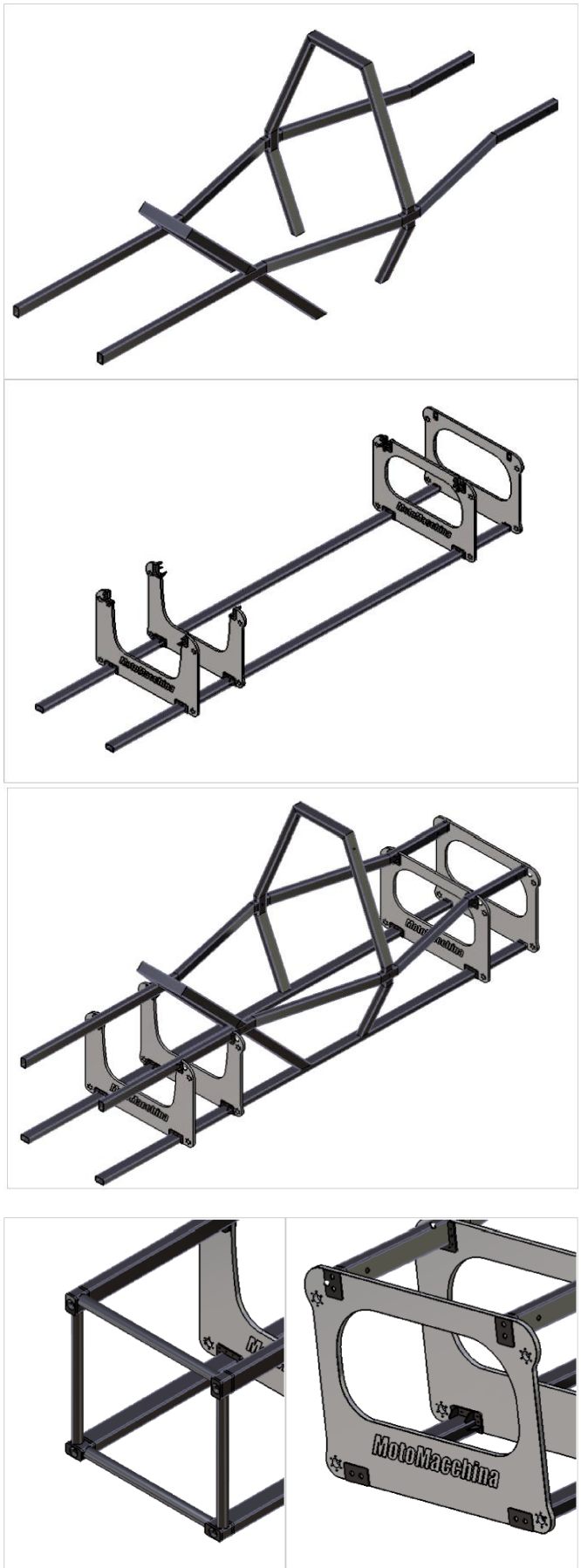

Figure 6.4: Assembling sequence of the chassis

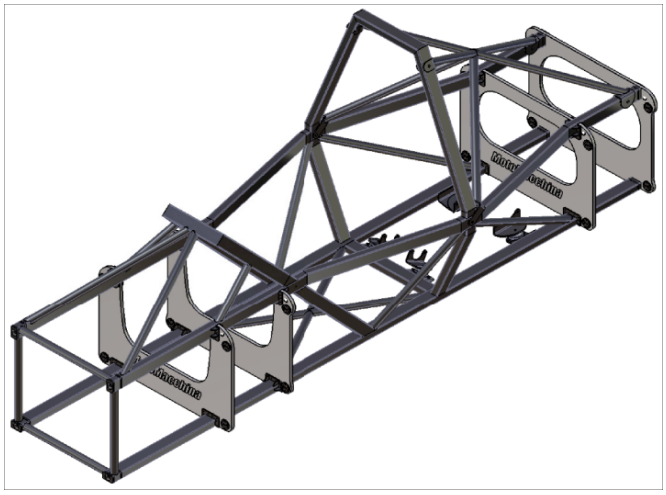

Figure 6.5: Final chassis model

4. lightness.

In this specific case, the last requirement is less important than in conventional race vehicle: in fact, the aim of this prototype is not to be as fast as possible, but to propose innovative drive model and dynamics. On the contrary, the solution of collision problems reveals to be particularly significant, due to the large magnitude of displacements needed to actuate the roll movement. At the same time, the possibility of system adjustments must be granted to allow for testing different suspension configurations or, if necessary, for compensating lacks in tolerance compliance. The constructive scheme illustrated in Fig. 6.6 is common to both front and rear suspensions (except for uprights). The six-bar linkage topology is chosen for development: the

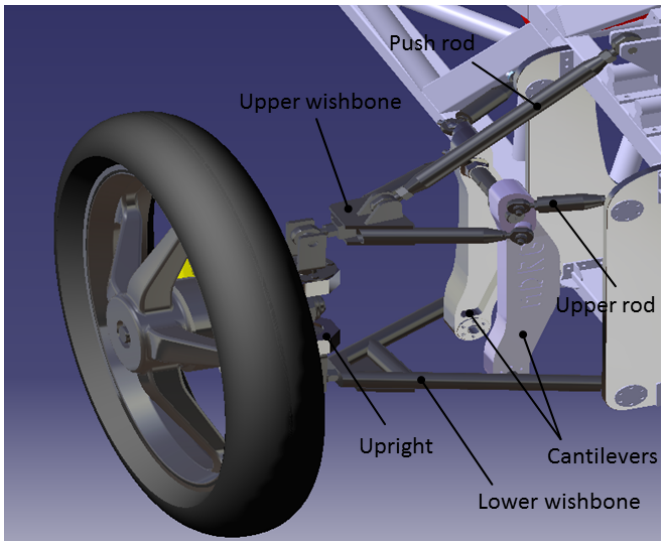

Figure 6.6: Constructive scheme of suspensions

layout of the mechanism is set according to results of the kinematic optimization of the roll system discussed in Chapter 3. The subassembly is composed by a lower wishbone, an upper wishbone, two cantilever arms and two upper beams. Fig. 6.7 illustrates two configurations, in fully symmetrical and in rolled position. Some constructive details are inspired by common race car suspension layout, in particular wishbone shape: angle between rods should be as small

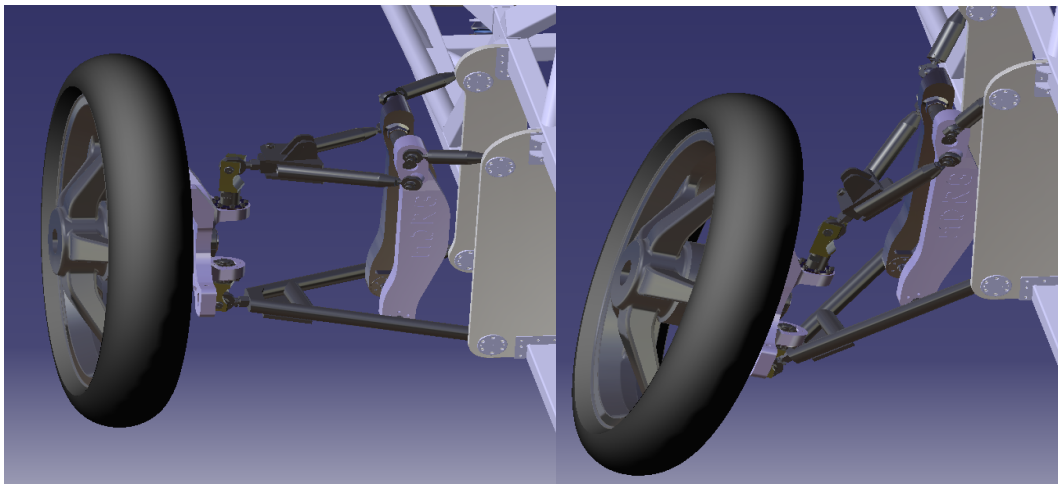

(a) (b)

Figure 6.7: Example of (a) fully symmetrical and (b) rolled configuration

as possible, thus granting a sufficient stiffness in forward direction (i.e parallel to the forward velocity of the vehicle). The possibility to adopt different set-up making adjustments in rod length is granted by coupling, when possible, left and right-handed rod ends.

Two main problems consist in obtaining a compliant mechanism with regard to structural aspects, and capable of avoiding possible collisions during roll maneuvers. No guidelines can be adopted to solve these problems, due to the peculiarity of this application: therefore, specific methods must be studied.

Differently from common suspensions, in structural design the roll actuation must be considered during the estimation of solicitations. Additionally, to avoid member collisions, the symmetric position cannot be the unique configuration taken as reference during geometrical modelling. Therefore, both problems require the definition of a detailed, CAD-integrated multibody model of the car, to provide the calculation of specific solicitations applied to members during typical maneuvers, and to perform fitting simulations. This multibody model is defined in LMS Virtual.Lab environment: in fact, it adopts the Catia V5 solid geometrical environment, which is used for geometrical modelling, so allowing for a total integration of geometry definition and kinematical/dynamical analyses. The model is represented in Fig. 6.8: it basically features only the symbolic elements, which constructive geometry can be attached to. First, the CAD-integrated multibody model is used to solve collision problem: in this case,

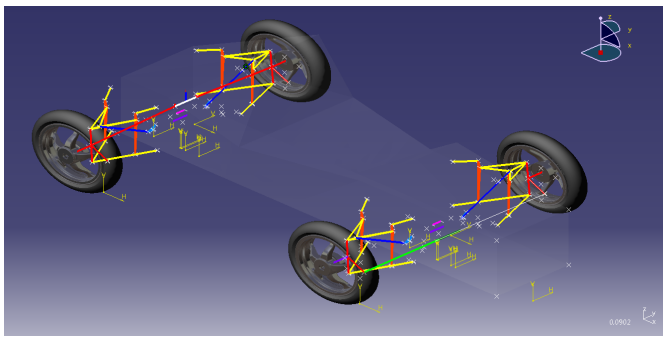

Figure 6.8: Multibody model developed on Virtual.Lab

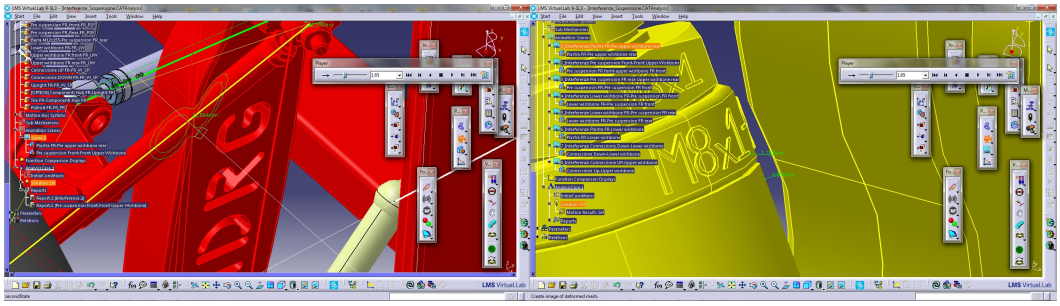

(a) (b)

Figure 6.9: Collision detector: (a) collision detection example and (b) proximity detection example

a complete geometrical mock-up must be used. In simulations, the functionality of collision detection provided by the software is used: proximity and collisions can be highlighted by a change in color (e.g. yellow for proximity and red for collisions); a threshold can be defined to set the minimum acceptable clearance between bodies. By successive refinements, a kinematically correct shape of component is found. Then, the multibody model is used to calculate forces applied to suspension linkages, with particular regards to cantilevers and wishbones, solicited both by axial and transversal forces. Fig. 6.10 depicts an example of simulation outputs: the magnitude of the force transmitted by push rod to upper wishbone. These results are then used to perform F.E.A. on constructive geometry (Fig. 6.11 [14]). In some cases, an iterative process

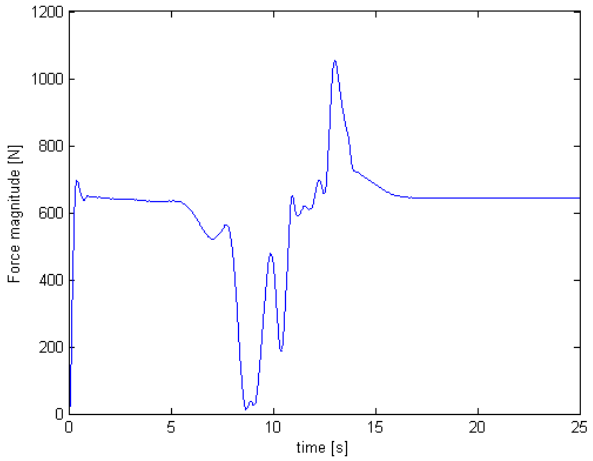

Figure 6.10: Total force transmitted from push rod to upper wighbone in a chicane maneuver, 35 km/h

between two phases is needed. The concurrent adoption of different methodologies (kinematic and dynamical multibody modelling, geometrical modelling, structural F.E.A.) revealed to be fundamental in the constructive design of this subsystem. Finally, two different materials are adopted:

- $25CrMo4$ steel for wishbones and upper rods;
- Ergal 7075 for cantilevers and upright assembly.

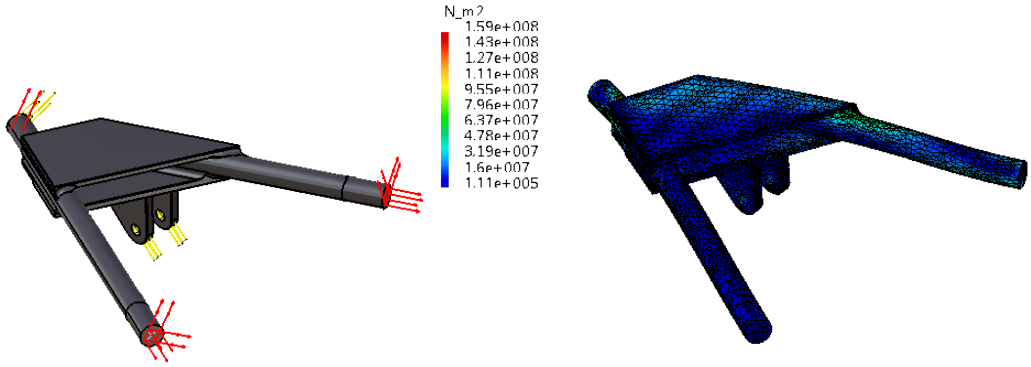

(a) (b)

Figure 6.11: Example of F.E.A. for structural validation: (a) constraints and (b) Von Mises stress distribution

6.3 Steer system

As discussed in Chapter 4, the steer system layout was optimized to achieve dedicated kinematic requirements, particularly related to the interaction with the roll system. Results are taken as an input to the constructive design phase, which must grant the right functioning of the system both by a structural and a kinematic point of view. Even if chosen type and topology (system composed by rack and pinion, tie rods and steer arms) are conventional, the proportions and the operative conditions of this specific implementation are indeed unusual: in particular, angles developed between members are out of range for common steer systems. The constructive geometry of the developed solution is reported in Fig. 6.12. Two main problems were considered during the constructive design:

1. granting the required kinematic capability;
2. providing an acceptable ratio between handlebar and rack displacements.

Both targets can be pursuit by, first, obtaining numerical inputs from a dedicated multibody simulation. In particular:

- articulation angles between track rods and tie rods, and between tie rods and rack were calculated: in the most critical condition, the joint between track and tie rods must be capable of articulation angle of about $43°$;
- the maximum force acting along rack axis was computed, consisting in about $500N$. As reference maneuver, a complete steer travel (full left-full right) was imposed in one second, with null forward velocity and wheel camber at maximum value: the force acting on the rack is mainly due to the rise in COG position. The knowledge of this value can be translated in a handling issue: in fact, the maximum angle imposed by pilot on the handlebar can be estimated in $45°$. This means a high ratio between rack translation and handlebar rotation is expected: as a consequence, a great effort could be necessary to actuate steering. Therefore: the steer ratio must be great enough to grant the possibility of imposing high steer angles with limited handlebar rotation, without necessiting of an uncomfortable steer effort.

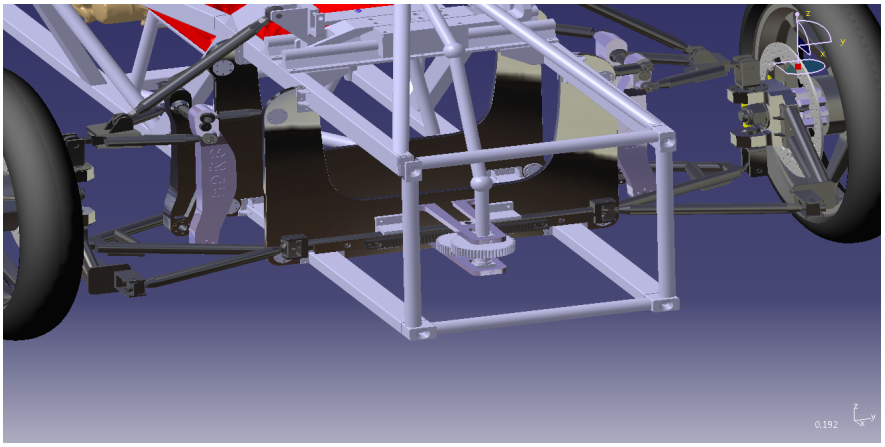

Figure 6.12: Adopted constructive scheme

The problem of high articulation angle was solved by designing specifically dedicated spherical joints and cardan joints, Fig. 6.13 and 6.14, respectively, capable of unconstrained rotation around axes indicated in figures. The problem of steer ratio was solved as follows. Fig. 6.15

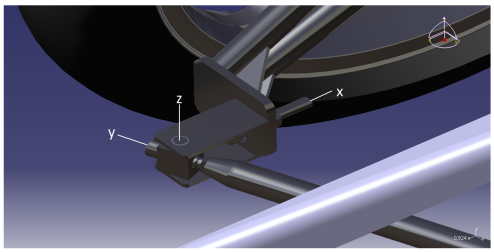

Figure 6.13: Dedicated spherical joint

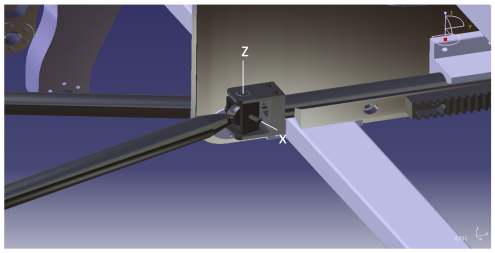

Figure 6.14: Dedicated cardan joint

depicts the dedicated implementation of steer system: the choice of a custom scheme was made to provide a better flexibility in the solution of the discussed problem. The system is composed by three gears 1, 2 and 3: 1 and 3 are supposed to feature the same number of teeth. A routine was developed in Matlab code to obtain a set of feasible solutions. The input data are:

- target steer ratio;

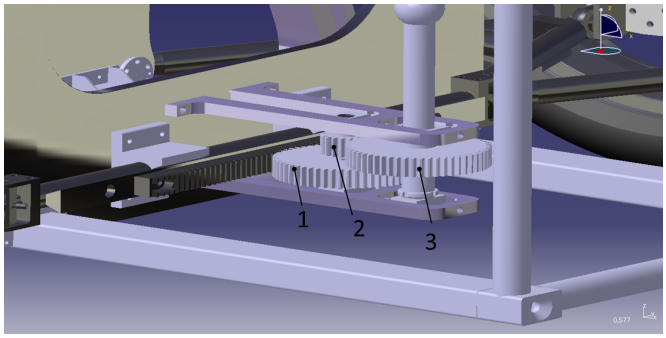

Figure 6.15: Steer gears

- a range of acceptable max handlebar torque (calculated with reference to the above described steer maneuver;
- geometrical standardised properties of a set of gears;
- selected gear modulus.

Outputs of program are all solutions which respect the above conditions and, in addition:

- are structurally compliant, i.e. resistance of shafts on which gears are mounted is tested by common analytical formulation;
- are compliant with Lewis and Hertz criteria [15].

Results, in terms of number of teeth for each gear ($Z1$,$Z2$,$Z3$) and total handlebar angle tha (full handlebar rotation) over the maximum required handle bar torque, are reported in Fig. 6.16 and 6.17.

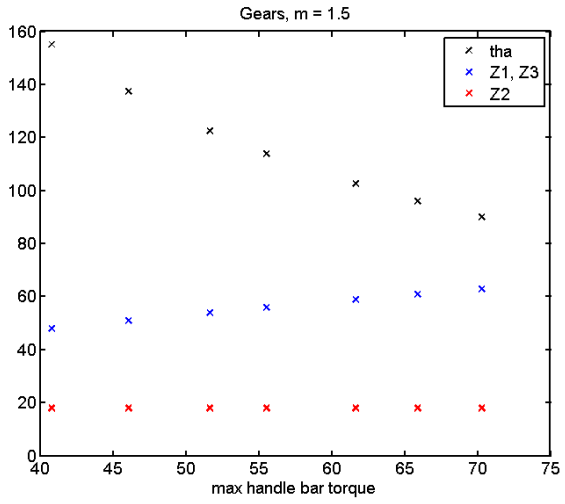

Figure 6.16: Set of solutions for modulus $m = 1.5$

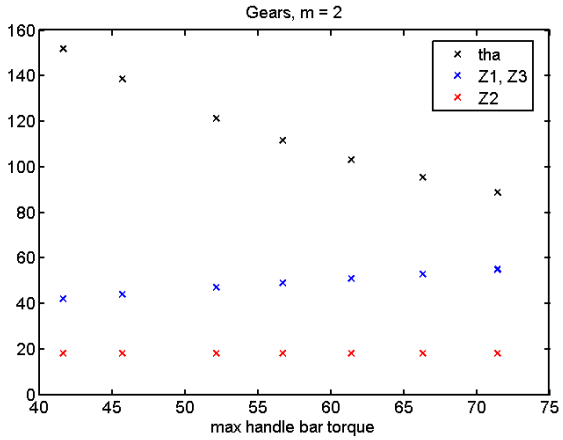

Figure 6.17: Set of solutions for modulus $m = 2$

6.4 Final layout

The final layout is schematized in Fig. 6.18. A few, important changes are introduced with

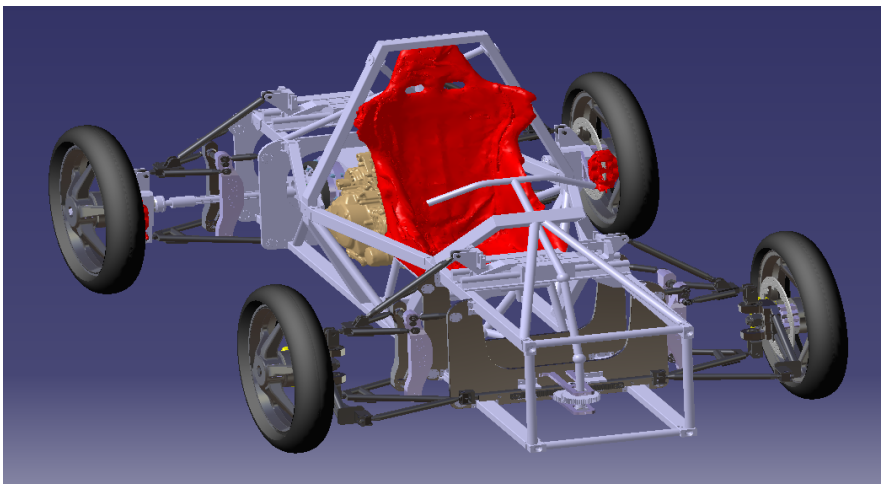

Figure 6.18: Final layout

respect to the preliminary layout: first, this result is addressed by kinematic optimizations presented in Chapters 3, 4 and 5, so providing a better behaviour according to chosen performance criteria. Second, a safer and more effective mechanic steer system is adopted. Third, roll slides are moved to the top of the chassis: at first glance, this is not a remarkable aspect, but at a deeper analysis this choice results fundamental. In fact, it allows for a better positioning of transmission, in order to solve the highlighted problem of unacceptable angles at CV joints (Fig. 6.20), especially in non rolled configurations (which could fast lead to failure). In symmetrical position, in fact, old solution featured about $15°$, while in new one this value is pair to $1°$; max values in rolled configurations are about $43°$ and $34°$, respectively. Finally, some pictures of produced components and of the partial assembly are reported in Fig. 6.21-6.23.

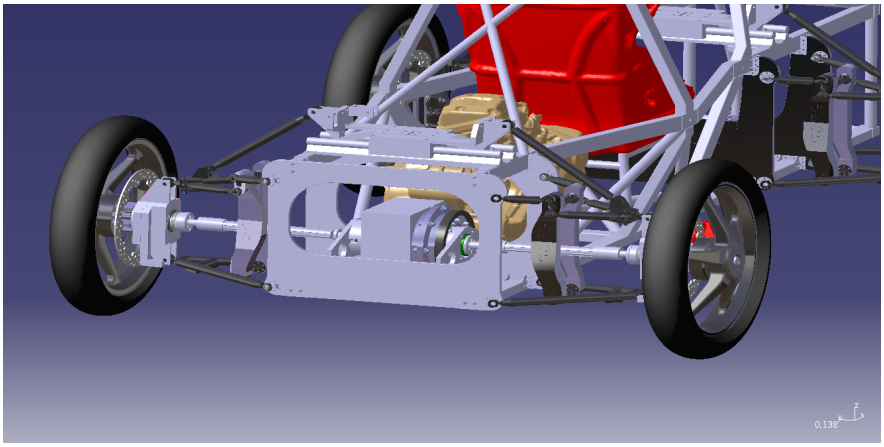

Figure 6.19: New positioning of transmission

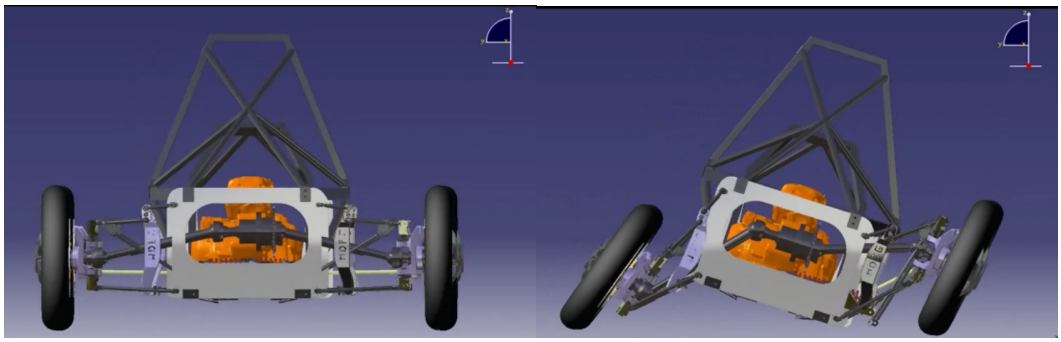

(a) (b)

Figure 6.20: Previous layout: problem of high angles in transmission joints in (a) symmetrical position and (b) in rolled configuration

Figure 6.21: Produced partial assembly

Figure 6.22: Suspension and track rod

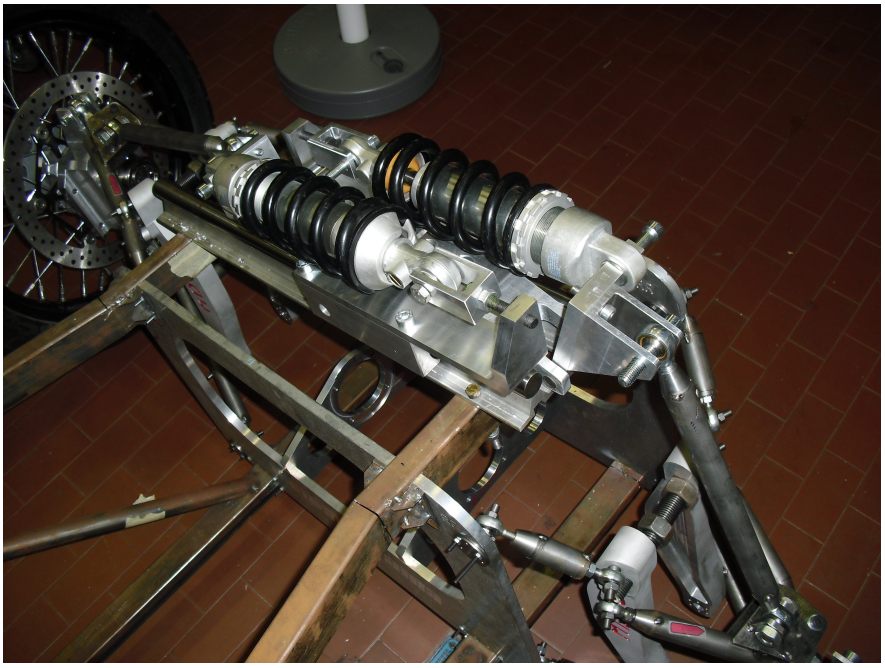

Figure 6.23: Roll slide and trial shock absorbers

Conclusions

Aim of this work is the design and development of a tilting four-wheeled vehicle. The peculiar aspects of this car like proportions, similar to small race cars, and the particular driving system, with steer and roll separately actuated, make this prototype different from most already presented tilting vehicles. In addition, developing a such innovative prototype inside the departmental facility represents a real challenge for the Motorcycle Dynamics Research Group. The absolute lack in design guidelines, consolidated literature and dedicated methodologies, force the designer first to develop a case knowledge, and then to self-construct specific models. In this case, the first phase of design was inspired by a trial and error approach, with the aim of highlighting critical aspects and develop sensitivity to significant variables. At this stage, general purpose methods were chosen, with the target of producing the larger amount of test cases and set first technical requirements. Then, a most methodical approach was used, developing specifically dedicated models to solve problems pointed out in the previous phase. In particular, some lacks in general layout and subsystem concepts required to reconsider roll, steer and suspension systems. The first target was to define a roll system capable of profiting of the particular dynamical definition of this vehicle: a theoretical confrontation between two and four- wheeled vehicles first, and results of a preliminary multibody model addressed by the *Optimal Maneuver Method* then, were used to traduce general objective in specific kinematic targets. The obtained results not only consisted in the determination of a profitable solution to the specific problem, but also improved general knowledge by a numerical confrontation of different candidate topologies. A second step consisted in the kinematic definition of the steer system, aimed at limiting all possible bad interactions between roll and steer actuation. Again, specific targets were pointed out by results produced by the preliminary design phase and by multibody modelling. The creation of a dedicated model oriented to optimization allowed, in this case too, to perform a rational definition of the solution to be adopted. The same systematic approach was applied to suspension design: in this case, however, intrinsic limitations of internal manufacturing did not allow the complete definition of the system. Therefore, the study was limited to rocker design, with the aim of pointing out a set of good performing solutions which could fulfill different requirements, to be defined in a later stage of production. Last, an overview of constructive aspects is presented: the aim is not to produce a deep description, but to highlight some unusual aspects related to the particular concept of the prototype.

Bibliography

[1] V. Cossalter, *Motorcycle dynamics*, 2nd ed. Lulu, 2006.

[2] J. Y. Wong, *Theory of ground vehicles*, 3rd ed. Wiley, 2001.

[3] M. Blundell and D. Harty, *The Multibody System Approach to Vehicle Dynamics*, 1st ed. Elsevier Butterworth-Heinemann, 2004.

[4] W. F. Milliken and D. L. Milliken, *Race Car Vehicle Dynamics*, 1st ed. SAE, 1995.

[5] D. Tavernini, "Studio del veicolo motomacchina mediante il metodo della manovra ottima," Master's thesis, Università degli Studi di Padova, Dipartimento di Ingegneria Industriale, Italy, 2010.

[6] J. G. de Jalón and E. Bayo, *Kinematic and Dynamic Simulation of Multibody Systems*, 1st ed. Springer-Verlag, 1994.

[7] M. Da Lio, V. Cossalter, and R. Lot, "On the use of natural coordinates in optimal synthesis of mechanisms," *Mechanism and Machine Theory*, vol. 35, pp. 1367–1389, 2000.

[8] *Global Optimization Toolbox - User's Guide*. The MathWorks, Inc., 2013.

[9] The steering bible. [Online]. Available: http://www.carbibles.com/steering_bible.html

[10] H. Heisler, *Advanced vehicle technology*, 2nd ed. Butterworth-Heinemann, 2002.

[11] Z. Ugray, L. Lasdon, J. Plummer, F. Glover, J. Kelly, and R. Martí, "Scatter search and local nlp solvers: A multistart framework for global optimization," *INFORMS Journal on Computing*, vol. 19, pp. 328–340, 2007.

[12] F. Glover, "A template for scatter search and path relinking," *Lecture Notes in Computer Science*, no. 1363, pp. 13–54, 1998.

[13] G. Stefani, "Il progetto motomacchina: Telaio e meccanismo di sterzo," Master's thesis, Università degli Studi di Padova, Dipartimento di Ingegneria Industriale, Italy, 2012.

[14] M. Guidolin, "Progettazione del veicolo innovativo a quattro ruote rollanti denominato motomacchina," Master's thesis, Università degli Studi di Padova, Dipartimento di Ingegneria Industriale, Italy, 2011.

[15] P. Andreini, *Manuale dell'ingegnere meccanico*, 2nd ed. Hoepli, 2013.

Acknowledgements

First, I'd like to thank all the Motorcycle Dynamics Research Group, above all Prof. Vittore Cossalter, for giving me the opportunity to get involved in such an amazing project, and for the consistent technical and personal growth I developed. I also want to thank Prof. Gianmaria Concheri and the Laboratory in Design Tools and Methods in Industrial Engineering, for other activities carried out together and all the training I received.

I cannot forget all colleagues of the Ph.D. course for all funny moments we shared.

I want to thank all sponsors and in particular Emanuele Zanardo and Filippo Pirotta of Nadella, and Friedrich Feichter for the willingness they demonstrated.

Last, an important auto-quote:

Ringrazio infine chi ha saputo aspettare.